Relativistic accretion onto compact objects

Dem Fachbereich Physik und Elektrotechnik
der Universität Bremen

zur Erlangung des akademischen Grades eines
Doktor der Naturwissenschaften (Dr. rer. nat.)
vorgelegte Dissertation

von

Dipl.-Phys. Pavel Efremov (Paul Jefremov)

wohnhaft in Bremen

1. Gutachter: PD Dr. Volker Perlick
2. Gutachter: Prof. Dr. Domenico Giulini
Eingereicht am: 29.V.2018
Datum des Promotionskolloquiums: 10.VII.2018

Bremen 2018

Annotation

The present PhD thesis summarises results on analytical accretion models obtained during my PhD studies in 2014—2018. I present the new ansatz for specific angular momentum-angular velocity dependence obtained in (Witzany & Jefremov 2018) for perfect fluid in circular motion around a Kerr black hole. With this ansatz new solutions for toroidal configurations were obtained. I discuss here in detail the dynamical properties of these configurations and results of their application as initial conditions for accretion simulations with 2-D HARM code.

For the case of circular motion in the NUT spacetime I present our results (Jefremov & Perlick 2016) on characteristic circular geodesics radii in it. These results are further used for modelling perfect fluid tori with constant specific angular momentum (Polish Doughnuts). Characteristic changes in the patterns of circular motion of perfect fluid due to presence of the NUT parameter are discussed.

The last part of the work presents a pre-study for accretion of spinning particles/fluids onto Kerr black holes. I discuss the results of our work (Jefremov et al. 2015, Tsupko et al. 2016) on spin-induced advance in last stable orbits and its relevance for accretion models.

Contents

Acknowledgements

I should like to express my deep gratitude to all those who made my stay and studies in Germany possible and fruitful. I am especially grateful to Volker Perlick for his supervision of my work, his lectures that I had a pleasure to attend and the discussions on physics that we had that allowed me to deepen my understanding of what a black hole really is and how it can be described in modern mathematical language.

I am very grateful to my fellow PhD students from the University of Bremen in particular to Dennis Philipp for his help in administrative and housing issues especially in the first months of my stay in Germany, for helping me to overcome a language barrier and for the time we spend together in discussions, at conferences and at summer schools.

I am grateful to Ms Kris Schroven who was a constant counterpart in discussions and arguments that we had and from whom I learnt so many things about life and mentality of the country where I stayed.

I express my gratitude to Vojtěch Witzany for our close scientific collaboration and help in orientation in the scientific world. Our scientific discussions allowed me to understand the field of research I was working upon better than any handbook that I read could do and our discussions "about life" helped me to figure out my further path in life.

I am grateful to Efthimia Deligianni,whom for her kindness and readiness to help me I could almost call my elder sister.

I should also thank my former colleague from Space Research Institute of R.A.S. Oleg Tsupko for collaboration and his lively interest in my work.

Last but not least I should express my deep gratitude to Dharma Light Buddhist Monastery in Finsterwalde and to Zen-Kreis Bremen e.V. for encouraging me to practise meditation that helped me among other things to overcome stress during my studies and accomplish this work.

This work and my stay in Bremen could not have been possible without financial support from Erasmus Mundus Joint Doctorate in International Relativistic Astrophysics (EMJD IRAP) and the German Research Foundation (DFG) within Research Training Group "Models of Gravity" that I kindly acknowledge.

Author's publications during the PhD studies

During my PhD studies I was involved in 4 fully-referred journal publications: Jefremov et al. (2015), Tsupko et al. (2016), Jefremov & Perlick (2016), Witzany & Jefremov (2018) and 2 conference proceedings: Jefremov (2016) and Jefremov et al. (2017).

My first journal article: Jefremov, P. I., Tsupko, O. Yu., Bisnovatyi-Kogan, G. S. (2015) *Innermost stable circular orbits of spinning test particles in Schwarzschild and Kerr space-times*, Physical Review D **91**(12), 124030 – summarised the results of my diploma work further developed during my PhD studies. In this article we obtained linear in spin corrections to the circular orbits of a spinning test particle, advance in parameters of circular orbits and an exact solution for a spinning particle in the extreme Kerr background. My contribution was in literature research, derivation of analytical expressions for the spin corrections, obtaining the exact solution for extreme Kerr black hole and writing the text.

My second journal article: Tsupko, O. Yu., Bisnovatyi-Kogan, G. S., Jefremov, P. I. (2016) *Parameters of innermost stable circular orbits of spinning test particles: Numerical and analytical calculations*, Gravitation and Cosmology **22**(2), 138—147 compared numerically obtained characteristics of circular orbits of spinning particles with results from our linear approximation from the previous article. In this paper accretion efficiency for a thin disk of spinning particles was computed in the extreme Kerr spacetime using our analytical solution for this case and found to exceed its maximal value for perfect fluid accretion. My contribution was in checking correctness of the formulae and editing the text.

The results of these two papers in context of accretion models were summarised and discussed in the Chapter 7.

My third journal article: Jefremov, P. I., Perlick, V. (2016) *Circular motion in NUT space-time*, Classical and Quantum Gravity **33** (24), 25014 – presented our work on NUT spacetime. We discussed different interpretations of the NUT metric and conditions under which the space-times with different values of Manko-Ruiz constant are isomorphic to each other. For the circular geodesics we obtained correct expressions for their position in the space-time outside of the equatorial plane and characetristical radii, such as marginally stable orbit. We also investigated the influence of Manko-Ruiz constant on the von Zeipel cylinders with respect to zero-angular-momentum observers (ZAMOs) and those with respect to the stationary observers. For

the general case of a stationary and axisymmetric spacetime we obtained connection between these two types of von Zeipel cylinders in the limit when the rotation velocity approaches the velocity of light. Further, we investigated the behaviour of Polish Doughnuts in this space-time and found that they no longer lie in the equatorial plane of the black hole. My contribution was in deriving the analytical expressions, producing plots, partially writing the text and editing it. Note that this article contained some mistakes which we noticed while working on the present PhD thesis and the Corrigendum will soon be published (Jefremov & Perlick 2018). The results of this work are used here in the Chapters 3 and 6.

My fourth journal article: Witzany, V., Jefremov, P. (2018) *New closed analytical solutions for geometrically thick fluid tori around black holes: Numerical evolution and the onset of the magneto-rotational instability*, Astronomy and Astrophysics **614** A75. The paper centred around the new analytical solutions for perfect fluid in circular motion that we obtained and their application in accretion simulations. We analysed different forms of the Euler equation for perfect fluid in circular motion and presented alternative ways of derivation of complete analytical solutions for perfect fluid in circular motion in Schwarzschild and of the Komissarov's magnetised tori. The main analytical result of the paper was the new ansatz for the specific angular momentum–angular velocity dependence that allowed us to obtain a new class of analytical toroidal solutions out of which the known ones: Polish Doughnuts (with constant specific angular momentum) and Fishbone-Moncrief tori can be obtained as special cases. We compared the resulting toroidal solutions by positioning their edges between 2 radii in the Kerr space-time and varying one parameter that remained free. For the 24 new tori solutions obtained in this manner we ran an accretion simulation within the 2-D HARM code using them as initial configurations for it. We found that deviation of angular momentum distribution in the resulting solutions from the Keplerian one which appeared to monotonously depend on our free parameter plays the key role in development of Rayleigh-Taylor and magnetorotational instabilities. This difference between solutions however gets weaker with the simulation time and is no longer identifiable in its later stages. We assumed the reason for this is non-linear MRI mode in which the disks enter at those stages. Using our new tori ansatz we found that unlike it had been believed the accreted specific energy within HARM code set-up can be essentially bigger than 1 which suggests strong advection in the simulated flow. My contribution was in deriving part of the analytical formulae,

producing pictures, processing the output of the simulation and editing the text. The paper constitutes the skeleton of the present work with its results used mainly in the Chapters 4 and 5.

During my studies short proceedings articles from the major conferences with my participation were published summarising results given in the aforementioned journal papers:

Jefremov, P. I., Tsupko, O. Yu., Bisnovatyi-Kogan G. S. (2017) *Spin-induced changes in the parameters of ISCO in Kerr spacetime* in Proceedings of the 14th Marcel Grossman (MG14) Meeting on General Relativity, University of Rome "La Sapienza", Italy, 12 – 18 July 2015 – dealt with the results on spinning particles published in Jefremov et al. (2015)

Jefremov, P. I. (2016) *Circular motion and Polish Doughnuts in NUT spacetime*, Proceedings of the International Astronomical Union **12**(S324), 353–354 presented our results on Polish Doughnuts in the NUT spacetime in detail published in (Jefremov & Perlick 2016).

1 Introduction

The very name of the objects that will be the main subject of the present work – "black holes" – presupposes that unlike those more conventional objects of astronomy: planets, stars and galaxies – they cannot be observed by detecting electromagnetic radiation ("light") produced or reflected by them.[1] This circumstance distinguishes black-hole astronomy from that of the baryonic-matter objects and forces one to look for some other ways for obtaining observational evidences of their physical existence. Along with another highly compact objects, neutron stars in the first place, black holes are the subject of *relativistic astrophysics* that studies them in the generally relativistic framework.

Probably not the full but currently mostly applied list of the astrophysical processes which lead or are expected to lead in the near future to observational evidences of existence of black holes includes accretion, test-particle geodesics analysis, recently discovered gravitational-waves emission and detection and gravitational lensing with black hole shadow as its most vivid manifestation. In the present work I shall consider the first of them, accretion, the oldest and one can say the most classical process, in the sense that apart from however relevant additional effects arising from generally-relativistic treatment of the problem similar structures are produced also around non-relativistic objects e. g. around stars and planets and can be described by Newtonian physics.

***

In what follows we adopt the following conventions. All Greek indices run from 0 to 3 and throughout the paper Einstein's summation convention is assumed. The spacetime metric has signature -2. We work in the geometrised units with velocity of light c, gravitational constant G and Boltzmann constant k set equal: $c = G = k = 1$.

1.1 Black holes

Speaking physically and – as physicists usually like – not very precisely black holes (BH) are regions of spacetime separated from the rest of it by

[1] We shall speak here only about astrophysical black holes for which Hawking radiation (Hawking 1974) is of no relevance at least for us observers on the Earth.

a sort of causal membrane which lets everything in and nothing out: any object that crosses this membrane called *event horizon* will be forever lost for the rest of the world with no signal including light being able to come from it. What remains from it for us is its more and more slowed down and red-shifted picture approaching the event horizon.[2] A more precise mathematical definition of a black hole can be found at (Wald 1984, pp. 299–300). Black-hole spacetimes as we shall treat them in the present work are solutions to the vacuum Einstein's Field Equation, which in the absence of the cosmological constant can be written

$$R_{\mu\nu} = 0, \tag{1}$$

where $R_{\mu\nu}$ is the Ricci tensor characterising spacetime curvature, that possess the so-called trapped surfaces, the event horizon(s). The solutions to this equation are given in terms of *metrics* representing interval between two infinitesimally close *events*, points of given time and space coordinates that together constitute the *spacetime*. Among all the black hole solutions one especially distinguishes those asymptotically flat, i. e. having asymptotically Minkowskian metric given in the spherical coordinates as

$$\eta = \mathrm{d}t^2 - \mathrm{d}r^2 - r^2 \left(\mathrm{d}\theta^2 + \sin^2\theta \mathrm{d}\phi^2\right). \tag{2}$$

These metrics are subject to the *black-hole uniqueness theorem* (also know as "no-hair theorem") according to which all the vacuum solutions of the Einstein-Maxwell Field Equation that are asymptotically flat and free from singularities outside of the event horizon, i. e. with the singularities that, even if they are present, are still invisible for the observers in the *domain of outer communication* (see Figure 1), are described only by 3 parameters: black hole mass M, black hole proper angular momentum J_{BH} and its electric charge Q.

The first black hole solution was obtained by Karl Schwarzschild (1916) and described a spherically symmetric and static black hole characterised only by its mass M. This metric given in the so-called Schwarzschild coordinates reads as

$$g = \left(1 - \frac{2M}{r}\right) \mathrm{d}t^2 - \left(1 - \frac{2M}{r}\right)^{-1} \mathrm{d}r^2 - r^2 \left(\mathrm{d}\theta^2 + \sin^2\theta \mathrm{d}\phi^2\right) \tag{3}$$

[2]See Misner, Thorne & Wheeler (1973, pp. 872–875) for an amusing and elucidating discussion of the properties and the name of these objects and Taylor & Wheeler (2000) that gives in the author's view the best representation of how a black hole would look like for different observers.

and is singular at $r = 0$ and $r = 2M$ which obviously motivated its author to present his solution actually in a slightly different coordinate set with the second singularity being pushed to the origin of the coordinates. The character of this second singularity was obscure for as long as 40 years, since unlike at $r = 0$, at $r = 2M$ the space-time curvature, and hence the *tidal forces* that an in-falling body would experience at this radius remain finite and could be even very mild if one chooses a big enough value for the mass M of the gravitating centre. In the meantime it was also shown that the singularity at $r = 2M$ is indeed merely a coordinate singularity connected with the choice of the observer and can be got rid of once one chooses a more appropriate one. The character of it was understood in the works of Finkelstein (1958) and others around that time who analysing the light-like geodesics in the Schwarzschild space-time realised that at this radius the spacetime has an *event horizon* a (light-like) surface, a "unidirectional membrane" as Finkelstein called it, that divides the space-time into two major domains: *the domain of outer communication* with the observers being able to move towards coordinate infinity ($r = \infty$) and the region inside horizon where all the observers are bound or one can say doomed to reach the "true", curvature singularity at $r = 0$ in a finite interval of their *proper time* (i. e. that they measure on their own clock) and be eventually destroyed by the infinite tidal stresses. This membrane thus lets signals and observers pass through it in only one direction: from without to within, with everything what happens inside it being completely isolated from the observers outside. The structure of the black hole is illustrated on the Penrose diagramme on Figure 1 constructed in such a way that both ingoing and outgoing light rays move on straight lines.

The most general black-hole solution of (1) along with Maxwell equations to take electromagnetism into account that satisfies the uniqueness theorem is the Kerr-Newman metric which has all 3 above-mentioned possible black-hole parameters with all other solutions being some limiting cases of it (see Table 1). From the black hole solutions presented in the Table 1 of astrophysical interest is mainly the Kerr one, since in the process of evolution of astrophysical objects (stars, neutron stars) they are expected to have non-zero angular momentum and only a very small charge that otherwise would be neutralised. We shall give a more detailed description of the Kerr solution with the view on the main topic of the present research later (see Section 3.1). It remains to add that once one assumes presence of some fields beyond electromagnetism (i. e. Yang-Mills fields) or relaxes the requirements of the

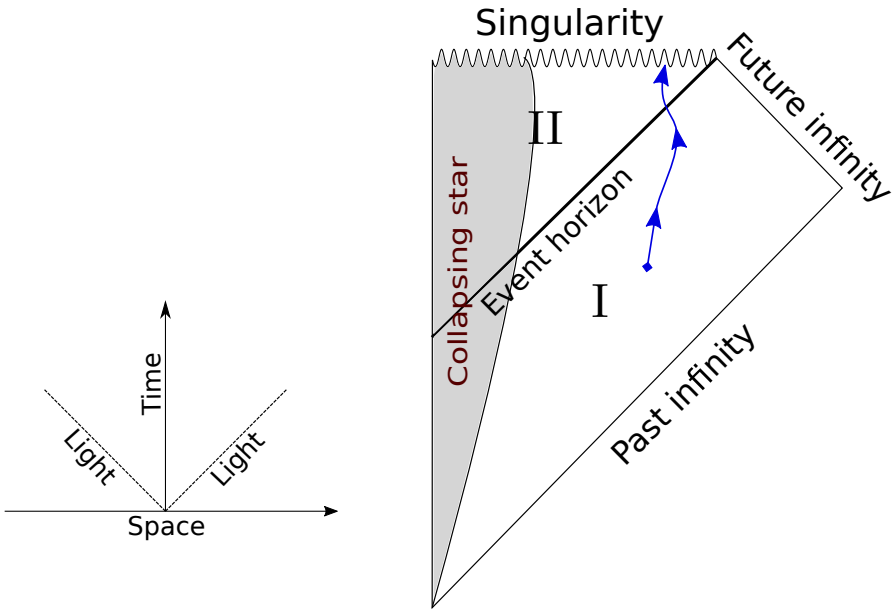

Figure 1: Penrose diagramme of a Schwarzschild black hole originating in a stellar collapse. Region I denotes the domain of outer communication from where it is possible to move and send signals towards future infinity $r = \infty$, region II lies inside the event horizon. The light cone on the left has the opening angle $\pi/4$ and defines the causal structure of the space-time: all physical (massive, time-like) observers can move only forward in time within the bounds of the light cone at each point. For any such observer represented by the blue line on the picture after crossing the event horizon at $r = 2M$ singularity ($r = 0$) lies in his future and he will inevitably reach it in a finite proper time.

Table 1: The black hole types satisfying the uniqueness theorem. The varying black-hole parameters are its spin parameter a and charge Q. We assume that the black hole has mass $M \neq 0$, otherwise the spacetime is Minkowskian for any value of a or Q.

BH parameters	$a \neq 0$	$a = 0$
$Q \neq 0$	Kerr-Newman	Reissner-Nordström
$Q = 0$	Kerr	Schwarzschild

uniqueness theorem, one can obtain multitudes of different solutions of the equation (1), however in the latter case almost all of them will have some undesirable properties like various types of singularities visible for the observers outside of the horizon or closed time-like curves in the domain of outer communication. These facts however do not exclude the physical relevance of these solutions *per se*, since some of them may be good candidates for description of gravitational field of objects other than classical black holes. One may argue in some cases that the singularities are of no relevance because they are localised below the surface of the object and thus the metrics describe only the external gravitational field of a star or that, as it is generally assumed in discussions about the central singularity within the black hole, the singularities outside also denote some unknown physics which cannot be described properly within the general theory of relativity. One example of such black holes, the NUT solution, will be extensively treated in this work (see Section 3.2).

1.2 Astrophysics and astronomy of black holes

The astrophysical black holes are classified by the value of their mass parameter in four groups:

- stellar-massive black holes with $M \sim 1 - 10 M_\odot$,
- intermediate black holes, with $M \sim 10^2 - 10^5 M_\odot$, and
- supermassive black holes, with $M \sim 10^5 - 10^9 M_\odot$,
- primordial black holes, mass from Planck mass M_{Pl} to $10^2 M_\odot$

As yet the intermediate black holes and primordial black holes remain only hypothetical, with the latter being believed to be produced by quantum

matter fluctuations in the early Universe and probably already evaporated due to Hawking radiation if their mass was not sufficiently big and no clear astrophysical mechanism known for the formation of the former ones even though there seem to be observational evidences in favour of their existence.

The stellar-massive black holes are a product of gravitational collapse of stars and collisions of neutron stars. After a star exhausts its "fuel": mainly hydrogen and helium which are "burnt" in thermonuclear reactions taking place in its inner regions, the equilibrium of its layers can no longer be maintained. The less massive stars $M \lesssim 8M_\odot$ (Bisnovatyi-Kogan 2010) will reach the stage of *red giant* with its volume increasing and get rid of their outer layers which gradually expand forming *planetary nebula* (which has nothing to do with planets) and dissolve forming the interstellar medium. The remaining core of $\approx 1M_\odot$ in turn becomes a faintly luminous *white dwarf* supported by degenerate electron gas pressure. The more massive stars end their stellar existence phase more violently: after nuclear synthesis in the core stops and there is no longer radiative pressure enough to compensate the gravitational pool towards the centre the outer layers start falling in, which comprises the stellar gravitational collapse. The result of the collapse is defined by parameters of the star, mainly by its mass. If the core of the star which under the conditions present during collapse is supported by degenerate *neutron* gas pressure is able to stabilise, the result of the collapse will be a *supernova explosion* which sways away the outer layers of the passed away star and its core survives in a form of a neutron star. The densities in some neutron stars are expected to exceed the nuclear ones ($\rho \sim 10^{14}\mathrm{g/cm}^3$) which leads to unknown states of matter and produces uncertainties in the estimate of the upper boundary of the neutron star mass. It is believed however that this limit cannot be much bigger than $\approx 3M_\odot$. If the core mass exceeds this limit no pressure can withstand the collapse and the star will proceed to shrink forming a black hole. The scheme on the Figure 2 summarises the stellar evolution of lighter and heavier stars.

Stellar black holes can also be born in the process of collision of two massive stars or neutron stars. In the latter case depending on the angular momentum of the colliding stars a short-lived hypermassive neutron star can be formed which then collapses to a black hole. The remnants of the collision are partially reused by the new-born black hole forming its accretion disk.

The supermassive black holes are found in the nuclei of galaxies and are believed to be present in almost all of them. For the present day there is no consensus as to the mechanism that lead to their formation during the

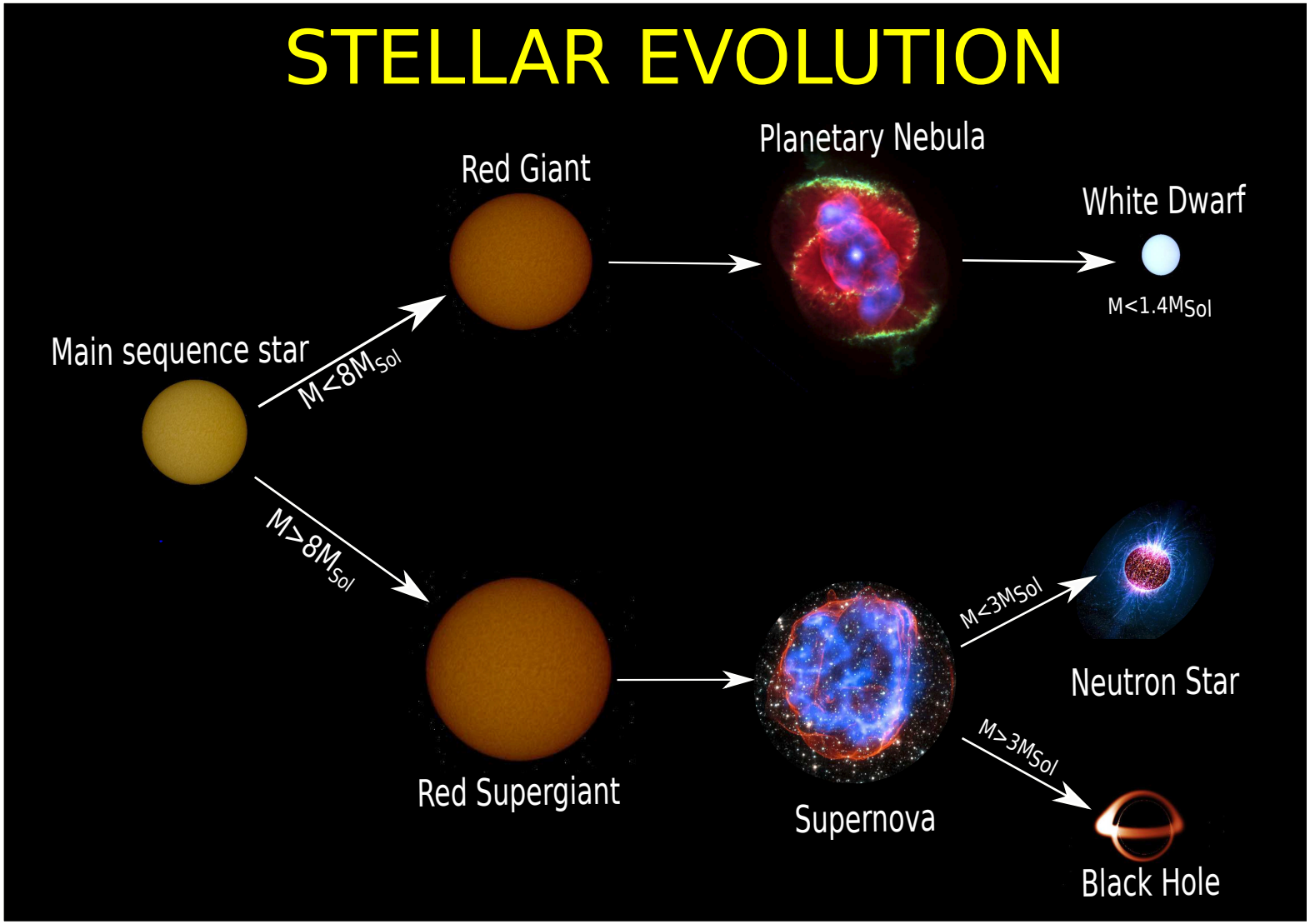

Figure 2: Evolution of stars of different mass (see explanation in the text)

evolution of galaxies. Main hypotheses for it range from collapse of dense hydrogen clouds without forming a star, accretion of matter onto primordial black holes acting as seeds with their subsequent merger and collisions of stellar black holes born from densely distributed very massive stars of first generation with masses $\sim 10^{2-3} M_\odot$ densely distributed in star clusters around galactic centres. One of the major restrictions on these models comes from the fact that the black holes must have reached their extremely high masses very rapidly, within already only several hundred million years from the Big Bang according to recent observational data (Bañados et al. 2018).

We now come to the observational effects from the black holes. The first observational evidences in favour of their existence were obtained from *X-ray binary systems* consisting of a stellar-massive black hole and a stellar companion whose matter is then accreted onto it. The first and currently the best-studied such X-ray source is Cyg X-1 discovered in 1964. It was identified as a black hole in 1970 when analysis of the period and mass of the system obtained from its spectra showed that its mass considerably exceeds that of a neutron star. With some uncertainties the black hole is currently estimated to have mass $10-16 M_\odot$. The structure of an X-ray binary is given on the Figure 3.

Accretion processes play the key role in the observations of super-massive black holes in the *active galactic nuclei* (AGN). Here the black hole is surrounded by a star cluster and the matter in its accretion disk comes mainly from tidal disruption of the nearby stars when they are passing too close to the black hole. As a result of accretion spectra deviating from those of normal stars and in the case of *quasars* having enormous luminosities are produced. Some of the active galactic nuclei produce *jets*: almost perpendicular to the accretion disk, highly collimated matter outflows believed to be caused by magnetic fields in the near-horizon regions of Kerr black holes. The observational image on Figure 4 presents an example of a galaxy (Hercules A) having an active nucleus and a jet reaching far beyond its size in the galactic plane.

The evidences for black holes in the galactic nuclei can also be obtained from observations of the stars orbiting them. So far these data are available only for the centre of our Galaxy Milky Way (Figure 5). Parameters of stars trajectories allow one to constrain the mass of the object to be $\approx 4 \times 10^6 M_\odot$ with its radius being less than 45 AU. No known astrophysical object other than black hole can comply with these restrictions.

A chapter in the astronomy of black holes became recent direct observa-

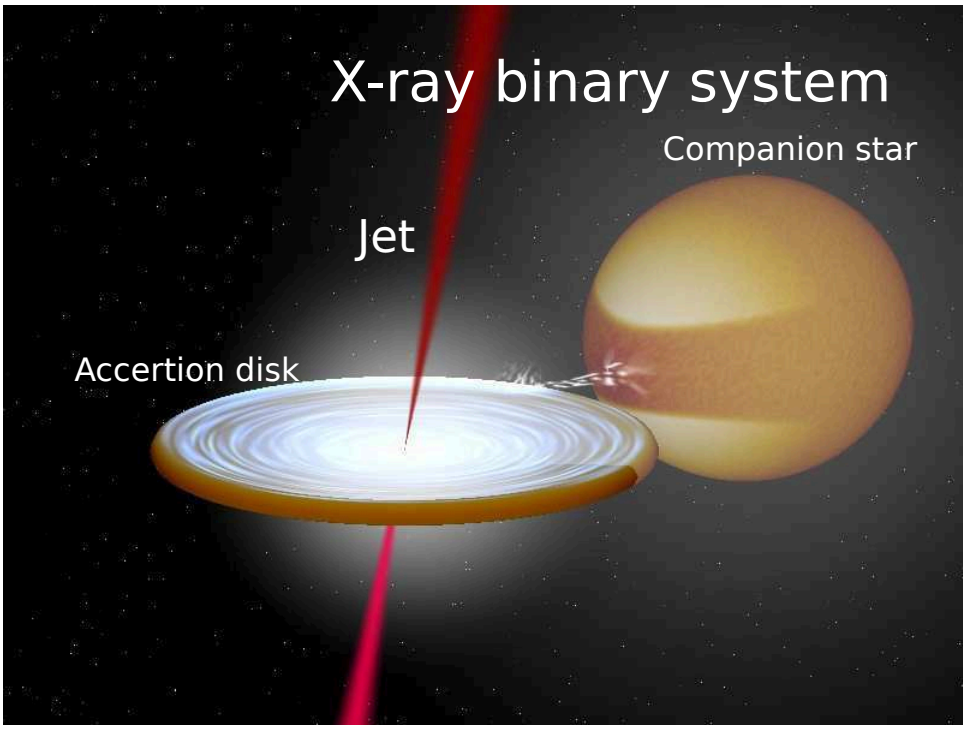

Figure 3: The structure of an X-ray binary system of an accreting black hole and a stellar component. The matter from the donor the star gets accreted onto the black hole producing X-ray radiation and relativistic jets. Image produced with BinSim code developed by Robert Hynes.

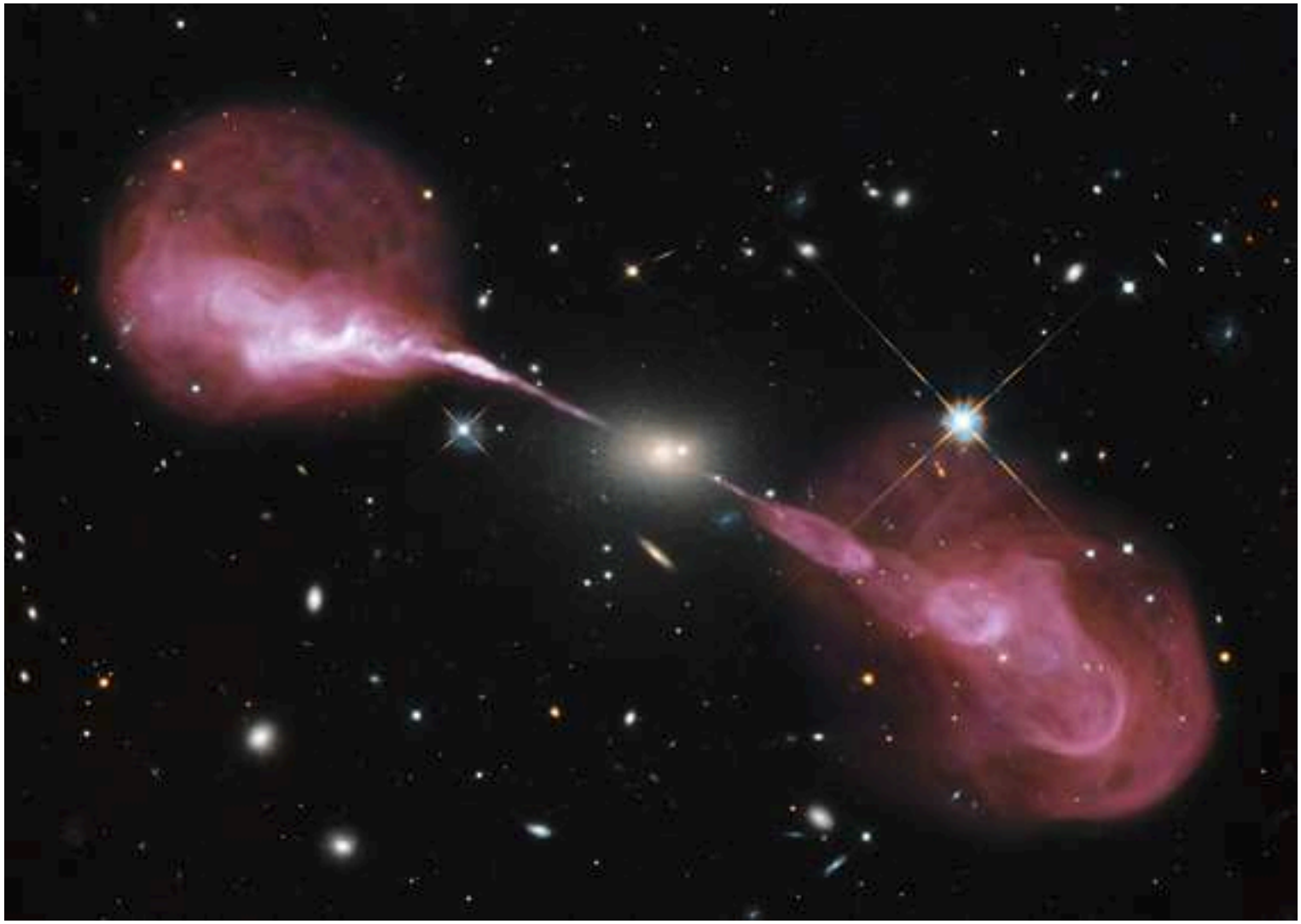

Figure 4: The image of relativistic jets flowing out of the AGN in the elliptical Hercules A galaxy. The image obtained by superimposing optical pictures obtained from Hubble telescope together with radio-band images from VLBI. Credit: NASA, ESA, S. Baum and C. O'Dea (RIT), R. Perley and W. Cotton (NRAO/AUI/NSF), and the Hubble Heritage Team (STScI/AURA)

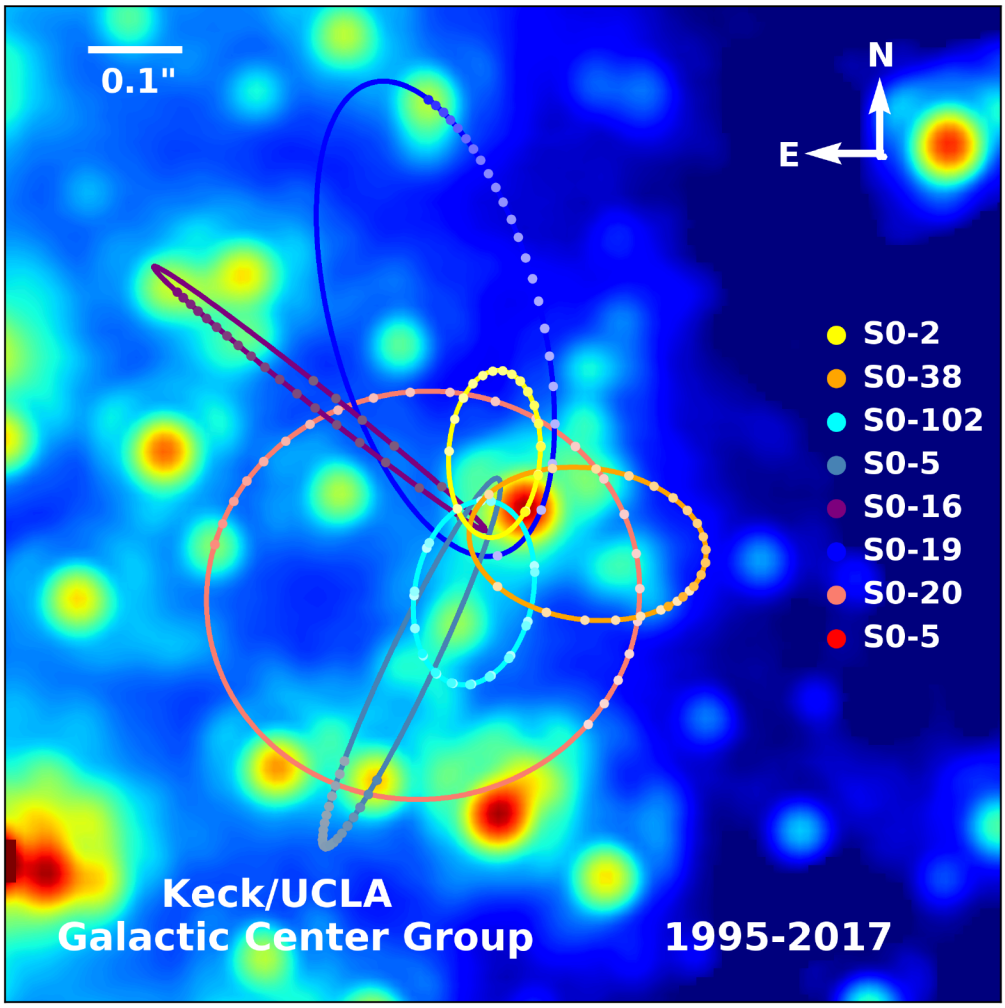

Figure 5: Trajectories of the stars orbiting the centre of our Galaxy using the observational data for 1995–2017. Image credits: UCLA Galactic Center Group - W.M. Keck Observatory Laser Team

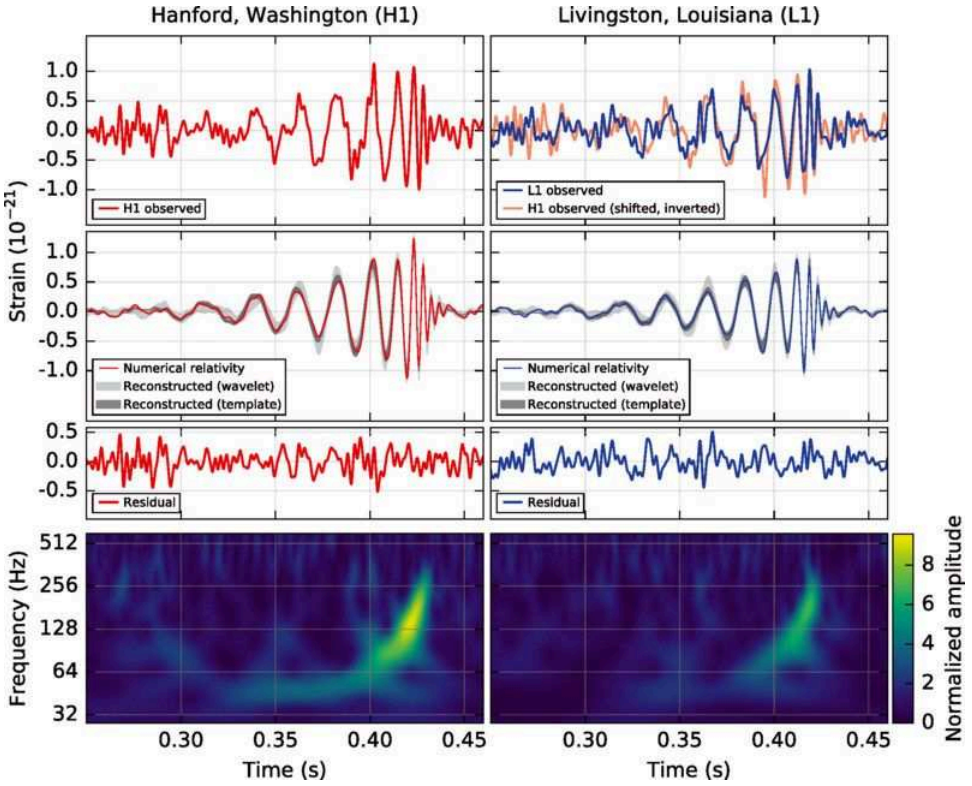

Figure 6: The first ever detected gravitational signal **GW150914** from two LIGO detectors in Hanford, Washington and Livingston, Louisiana. Credits: Abbott et al. (2016). Copyright: CC BY 3.0

tions of gravitational waves by LIGO collaboration announced on February, 11th, 2016. In the first detection (Abbott et al. 2016), signal **GW150914** (Figure 6), two colliding black holes of masses $35M_\odot$ and $30M_\odot$ were observed to produce a black hole of $62M_\odot$ with the rest of energy radiated away in the form of gravitational waves. Recent detection of a signal from two colliding neutron stars **GW170817** (Abbott et al. 2017) with the resulting black hole's mass of $2.74M_\odot$ confirmed the mechanism of stellar black hole production out of collapsing hypermassive neutron star. Even though currently the detectors cannot resolve the "ringdown signal" produced when the black hole forms, little doubts remain that the resulting objects are indeed black holes.

To finish this brief review of black-hole astronomy one should mention

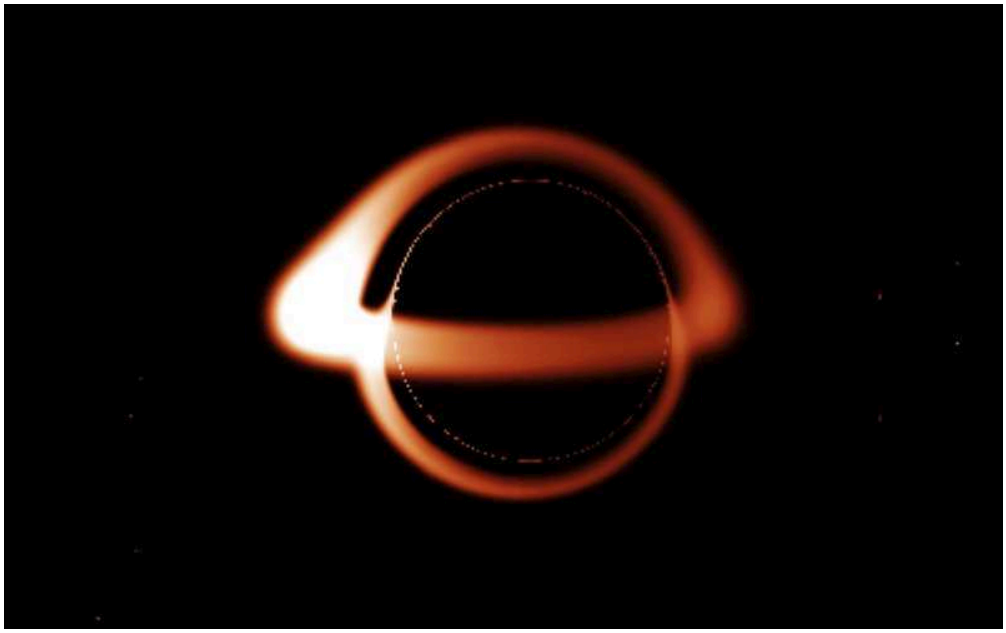

Figure 7: Simulated image of the light-aberration effects around an accreting black hole in Sgr A* (the centre of our Galaxy). The black region inside is the black-hole shadow. Source: Wikipedia, image in Public Domain, created by B.D.Carter.

the possibility of observation of *black-hole shadow*, a manifestation of gravitational lensing effect produced by black holes' photon region. With the publication of observational data of the centre of our Galaxy by *Event Horizon Telescope* (EHT) and *Black Hole Cam* collaborations expected in the near future one believes to be able to read out the signature of the shadow on the images of the central region. Figure 7 by taking into account gravitational-lensing effects gives an impression of how a black hole would actually look like for an observer in its vicinity.

2 Review of previous results

2.1 Accretion models

In this Chapter I shall give a review of results on *analytical* models of accretion leaving aside the major topics relevant to modern astrophysics in particular the discussion of viscosity and turbulence origins in the accretion disks, magneto-rotational instability and the bulk of numerical simulations. All those topics, important as they are, laid beyond the direction of my research and will be mentioned only briefly to present connections of the idealised models we worked upon to actual astrophysical problems.

The first accretion models were developed to explain interaction of ordinary stars with the interstellar medium being accreted in radial in-flows. In the pioneer work of Bondi & Hoyle (1944) authors considered a Newtonian model of accreting dust (pressureless perfect fluid) onto a star gradually increasing its mass. In the follow-up paper Bondi (1952) generalised the model for the case of perfect fluid with polytropic equation of state and set the foundation of the "Bondi-Hoyle flows" type accretion. The generally-relativistic treatment of the Bondi-Hoyle model already with the black holes in view was given by Michel (1972). It was suggested that the radial accretion may take place in isolated black holes (Shvartsman 1971) and in binary systems with strongly magnetised flows (Bisnovatyi-Kogan & Syunyaev 1972). In any case magnetic field was found to play the key role in the possibility to observe radiation from radial flows: in the absence of it they are very faint (Shvartsman 1971) and when it is present are believed to be able to radiate up to 10—30% of the accreted mass (Shvartsman 1971, Bisnovatyi-Kogan & Ruzmaikin 1974).

The idea that *disk accretion* onto a black hole can explain the nature of quasars can be traced back to the work of Salpeter (1964). He suggested that through action of viscous forces in the accreting gas it will gradually lose its gravitational energy released in the form of electromagnetic radiation (the process called *angular momentum transfer*) and through succession of circular orbits reach the last stable one, from which it plunges into the black hole, and presented the first estimates on luminosity produced in such a process. The foundations of the thin-disk accretion model, "standard model accretion" were laid down in the works of Shakura & Sunyaev (1973) in Newtonian formalism and by Novikov & Thorne (1973) and Page & Thorne (1974) in the generally-relativistic one. In their work Shakura & Sunyaev

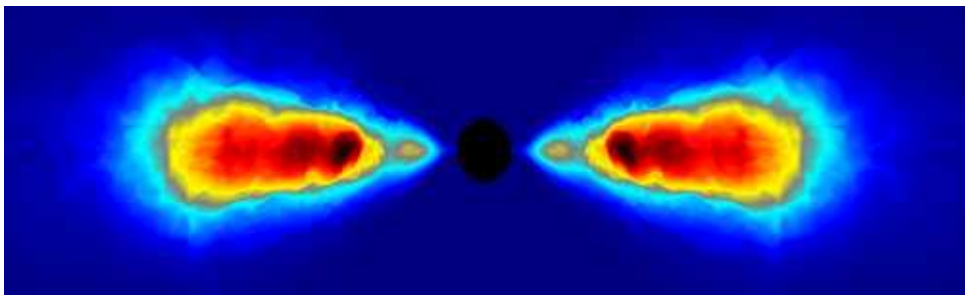

Figure 8: Accretion disk around a Kerr black hole. Darker zones denote higher matter density. Image obtained with HARM 2-D simulation code.

(1973) have realised that molecular viscosity cannot be sufficient to bring about the observed rate of angular momentum transfer and made a very fruitful ansatz for the viscosity in the disks, the so-called "α-prescription", which enabled them to unify the viscosity arising from chaotic magnetic fields and the turbulent viscosity by one *ad hoc* parameter α and compute various characteristics of accretion disks consistent with observations.

The model of geometrically thick accretion disks that will be the main subject of the present work was first proposed by Fishbone & Moncrief (1976) and a short time later in a series of papers by a working group from Poland: Abramowicz, Jaroszyński & Sikora (1978), Kozłowski, Jaroszyński & Abramowicz (1978), who developed analytical theory of toroidal configurations of perfect fluid around black holes by solving the relativistic Euler equation:

$$(e+p)u^\mu \nabla_\mu u^\nu + (g^{\mu\nu} + u^\mu u^\nu)\partial_\mu p = 0,$$

see Chapter 4 for the definition of the quantities in it. The first models developed assumed that some of the dynamical parameters remain constant within the disk: $\ell \equiv -u_\phi/u_t$ for (Abramowicz et al. 1978) and $\ell^* \equiv u_\phi u^t$ (Fishbone & Moncrief 1976). The country of origin of the most part of the authors inspired the name of these toroidal configurations: *Polish Doughnuts* widely adopted within the scientific community nowadays. In this work however I shall reserve this name only for the disks analytically obtained by this group i. e. for those with constant specific angular momentum otherwise denoting the toroidal solutions of Euler equation as *geometrically thick tori*.

In the following years the model of geometrically thick tori was developed for analytical description of super-critical accretion flows. Paczynsky & Wiita (1980) using a pseudo-Newtonian potential constructed their model of a

thick disk merged with a Keplerian thin disk, Jaroszyński, Abramowicz & Paczyński (1980) presented the generally-relativistic version of it. Abramowicz, Calvani & Nobili (1980) investigated the luminosity limits from such disks, Sikora (1981) performed simulations for them and considered reflection effects that can influence the flux at infinity. Abramowicz & Piran (1980) used the thick disks to model collimation of the relativistic jets from the quasars. Paczynski (1980) and Paczynski & Abramowicz (1982) presented some *ad hoc* models for the surface of actual accretion from a Polish Doughnut.

Other works were aiming at improving the limitations of the model and of the obtained solutions. The fact that Polish Doughnuts with constant angular momentum are only marginally stable with respect to the Rayleigh-Taylor instability motivated one to search for other more general angular momentum distributions. Chakrabarti (1985) obtained solutions with specific angular momentum distribution given as a power-law function of the von Zeipel radius, $\ell \propto \mathcal{R}^{\lambda}$ (see definition of this quantity in Section 3.2.3). Daigne & Mochkovitch (1997) proposed a power law with respect to the radial coordinate, $\ell \propto r^{\lambda}$. Qian et al. (2009) considered angular momentum distribution that was dependent on θ coordinate explicitly to obtain thinner tori and thereby approximate Keplerian disks.

Besides the above-mentioned Rayleigh-Taylor instability [see (Abramowicz & Prasanna 1990) for its relativistic formulation] Polish doughnuts were found to be unstable with respect to non-axisymmetrical perturbations by Papaloizou & Pringle (1984). Another type of instability the tori were believed to be subject to was the runaway instability: with black hole mass gradually growing configuration may become destabilised because of equipotential surfaces' shift. First analyses conducted by Abramowicz, Calvani & Nobili (1983) have shown that the disks with constant angular momentum are subject to it for a very wide range of parameters. Further studies were investigating assumptions of the theory that may give rise to the instability in particular: constant angular momentum distribution and the absence of self-gravity. Their results are well reviewed in the papers of Daigne and Font where they give a detailed analysis of the runaway instability in simulations of disks with constant (Font & Daigne 2002) and power-law (Font & Daigne 2004) specific angular momentum distributions. The result of their investigation was that while the constant angular momentum disks are unstable, for a certain range of power-law exponents they are heavily stabilised. The present-day state of art of the problem is that the runaway instability was

found to be an artefact of the assumption of the absence of self-gravity and disappears once it is fully taken into account (Montero et al. 2010, Rezzolla et al. 2010, Mewes et al. 2016).

With the advent of computational astrophysics in the late 1980's the geometrically thick tori became increasingly used in numerical simulations of accretion. Zurek & Benz (1986) used Polish Doughnuts as initial configuration for their numerical study of instabilities in accretion disks to show that in the late stages the circulating matter assumes the power-law rotation curve $\ell \propto r^{\lambda}$. Igumenshchev et al. (1996) constructed a code for 2-D simulations of perfect fluid motion in pseudo-Newtonian formalism using Polish Doughnuts as the initial configuration. 2-D magnetohydrodynamical codes such as HARM Gammie, McKinney & Tóth (2003), Noble, Gammie, McKinney & Del Zanna (2006) that was used in our study of generalised angular momentum distribution (Witzany & Jefremov 2018) as well as 3-D codes (De Villiers, Hawley & Krolik 2003, McKinney, Tchekhovskoy, Sadowski & Narayan 2014) continue to use either a Polish Doughnut of Fishbone-Moncrief ansatz for the initial data distribution. Besides being used for the initial configurations geometrically thick tori are also applied for integral tests of the codes (see e. g. Nagataki 2009).

Another direction for generalisation of perfect fluid tori solution was an addition of new fields to the matter model. Okada, Fukue & Matsumoto (1989) working in pseudo-Newtonian formalism obtained a solution for some particular form of toroidal magnetic field. For a general case of axially symmetric space-times Komissarov (2006) derived his "magnetised-tori" solutions by making similar assumptions about the magnetic field as one does about barotropicity of the perfect fluid equation of state [see also our redirivation of his result in Witzany & Jefremov (2018) and generalisation to the angle θ dependent ansatz by Gimeno-Soler & Font (2017)]. Off-equatorial perfect fluid configurations, "polar clouds", were obtained analytically under assumption of external dipole magnetic field and small charge for the disks in Schwarzschild for constant specific angular momentum by Kovář et al. (2016) and later for rigid rotation in Kerr with asymptotically uniform (Trova et al. 2018) and dipole (Schroven et al. 2018) magnetic fields.

Recently the geometrically thick tori found their application as the simplest finite perfect fluid configuration for studying properties of various metrics beyond the standardly used in astrophysics Kerr solution. Slanỳ & Stuchlík (2005) studied Polish Doughnuts on the Kerr-de Sitter background and later Stuchlík, Slanỳ & Kovář (2009) compared the tori in pseudo-

Newtonian and relativistic formalism in Schwarzschild spacetime. Kucáková, Slanỳ & Stuchlík (2011) performed a study of them in the Reissner-Nordström-(anti-)de Sitter metric. Meliani et al. (2015) constructed the tori on the background of a bosonic star using numerically obtained coefficients. In our work (Jefremov & Perlick 2016) we investigated circular motion in the NUT spacetime and Polish Doughnuts as its particular non-geodetic realisation.

2.2 (Taub-)NUT metric

NUT metric was obtained by Newman, Tamburino & Unti (1963) as a solution to Einstein's vacuum field equation and gained its name both due to initial letters of its authors' surnames and its unusual properties being as Charles Misner notably put it "a counter-example to almost anything". It describes a black hole of mass M (even though massless solutions are also allowed and are non-trivial) with the gravitomagnetic charge n shortly called NUT parameter that plays a role similar to that of magnetic monopole charge in electromagnetism and opposed to that of the "gravitoelectric charge" M (Lynden-Bell & Nouri-Zonoz 1998).

$$g_{\mu\nu}\mathrm{d}x^\mu\mathrm{d}x^\nu = \frac{r^2-2Mr-n^2}{r^2+n^2}\Big(\mathrm{d}t-2n(\cos\theta-1)\mathrm{d}\phi\Big)^2-\frac{r^2+n^2}{r^2-2Mr-n^2}\mathrm{d}r^2 - \left(r^2+n^2\right)\left(\mathrm{d}\theta^2+\sin^2\theta\mathrm{d}\phi^2\right)$$

Just as in the Schwarzschild or Kerr case, it may either be joined to the interior perfect fluid solution (see Bradley et al. 1999) or considered as a black-hole solution. In the latter case, the region beyond the horizon is isometric to the Taub's cosmological vacuum solution Taub (1951); therefore, the space-time that results from extending the NUT space-time over the horizon is known as the Taub-NUT solution.

Since the discovery of the NUT metric its physical relevance is a matter of debate due to the fact that it allows for existence of closed time-like curves in the domain of outer communication. The exact way how causality is violated depends on the global structure of the space-time which is given not only by the metric but also by the span of coordinates. The reason for that is the fact that solving Einstein's field equation only gives one a local expression for the metric; there are different ways of how to construct a global space-time from this local form of the metric and these different ways may lead to quite different physical interpretations. By assuming that time coordinate be periodical

with an appropriate period Misner (1963) demonstrated how to construct a global NUT space-time that is regular everywhere outside the horizon and SO(3) symmetric. Bonnor (1969) proposed another interpretation where the time cordinate is not periodical, however there is a singularity on the half-axis $\theta = \pi$ which he interpreted as a rotating massless rod. In this interpretation closed time-like curves exist only in a neighbourhood of this singularity. McGuire & Ruffini (1975) have shown the possibility of superimposing two NUT charges of opposite sign to get a metric that is regular everywhere except between the two sources on the axis. Lukács, Newman, Sparling & Winicour (1983) constructed a perfect fluid solution of the Einstein's field equation possesing some NUT properties and reducing to the NUT metric in vacuum limit. Manko & Ruiz (2005) generalised the NUT metric by introducing an additional parameter C into it that allows to distribute the singularity over both half-axes $\theta = 0$ and $\theta = \pi$ in a symmetric or asymmetric way. Recently, Clément, Gal'tsov & Guenouche (2015) showed that, in spite of the pathological behaviour near the axis, Bonnor's NUT spacetime may be viewed as a geodesically complete pseudo-Riemannian manifold. In their second paper (Clément et al. 2016) they have demonstrated that it is possible to utilise the NUT charge to construct traversable wormholes without violating null-energy condition for the matter.

The study of astrophysically relevant topics in NUT spacetime begins with the paper of Zimmerman & Shahir (1989) who investigated geodesic test-particle motion; the complete analytical solutions for geodesics in terms of Weierstraß elliptic functions were given by Kagramanova, Kunz, Hackmann & Lämmerzahl (2010). Charged particles' motion was studied in detail by Cebeci, Özdemir & Şentorun (2016). The lensing features of NUT objects have been comprehensively discussed by Nouri-Zonoz & Lynden-Bell (1997). The shadow of the NUT black hole, which is a particular lensing feature, was studied by Abdujabbarov et al. (2013) and the analytical formula for its shape, is contained as a special case in the work of Grenzebach, Perlick & Lämmerzahl (2014). Effects on magnetosphere of a neutron star having NUT parameter were investigated by Morozova, Ahmedov & Kagramanova (2008). Hackmann & Lämmerzahl (2012) calculated an upper bound for the NUT charge of the Sun by analysing the motion of Mercury. In our work (Jefremov & Perlick 2016) we studied influence of the NUT parameter on geodetic circular motion, von Zeipel cylinders and Polish Doughnuts with the aim of investigating its effects on accretion.

3 Spacetimes

In this section I present brief characteristics of the spacetimes we shall use as background field in further computations: these are Kerr and Taub-NUT. Each of them being member of the Plebański-Demiański class of solutions to the Einstein's field equation (see e. g. Griffiths & Podolský 2009) can be understood as special cases of one Kerr-NUT solution (Vaidya et al. 1976) when either NUT or Kerr parameter is set to zero. In spherical (t, r, θ, ϕ) coordinates this metric reads

$$g_{\mu\nu}\mathrm{d}x^\mu\mathrm{d}x^\nu = \frac{\Delta'}{\Sigma'}(\mathrm{d}t-\chi\mathrm{d}\phi)^2-\frac{\Sigma'}{\Delta'}\mathrm{d}r^2-\Sigma'\mathrm{d}\theta^2-\frac{\sin^2\theta}{\Sigma'}\Big(a\mathrm{d}t-(\Sigma'+a\chi)\mathrm{d}\phi\Big)^2 \quad (4)$$

where a is the BH spin (Kerr parameter), n is gravitomagnetic charge (NUT parameter), $\Delta' = r^2 - 2Mr + a^2 - n^2$, $\Sigma' = r^2 + (n + a\cos\theta)^2$, $\chi = a\sin^2\theta - 2n(\cos\theta+C)$ and M is BH mass. Here C is the Manko-Ruiz constant (Manko & Ruiz 2005). This metric with $M > 0$ describes a black hole provided that $M^2 + n^2 \geq a^2$ with the outer horizon at $r_{\mathrm{hor}} = M + \sqrt{M^2 + n^2 - a^2}$ and has a cone singularity on at least one of the half-axes in $z = r\cos\theta$ direction.

We shall now take a close look at the Kerr ($n = 0$) and NUT ($a = 0$) limits of this metric and recapitulate results on circular motion in them that will be needed for further sections of the present work.

3.1 Kerr spacetime

Kerr solution was obtained by Roy Kerr (1963) and describes a black hole characterised by mass M and proper angular momentum (spin) J_{Kerr} that enters into the metric as Kerr (or spin) parameter $a := J_{\mathrm{Kerr}}/M$. In spherical Boyer-Lindquist coordinates the Kerr metric is given by

$$\begin{aligned} g_{\mu\nu}\mathrm{d}x^\mu\mathrm{d}x^\nu =& \frac{\Sigma - 2Mr}{\Sigma}\mathrm{d}t^2 + 2\frac{2Mra\sin^2\theta}{\Sigma}\mathrm{d}t\mathrm{d}\phi - \frac{\Sigma}{\Delta}\mathrm{d}r^2 \\ & - \Sigma\mathrm{d}\theta^2 - \sin^2\theta\frac{\Sigma(r^2+a^2) + 2Mra^2\sin^2\theta}{\Sigma}\mathrm{d}\phi^2 \end{aligned} \quad (5)$$

with $\Delta = r^2 - 2Mr + a^2$ and $\Sigma = r^2 + a^2\cos^2\theta$. Since the properties of Kerr solution and of test-particle motion in it are already well-studied (see e. g. Chandrasekhar 1983), I will restrict myself in this section to only basic description of physical structure of the domain of outer communication and present formulae that will be relevant for the accretion models that we

develop later. In the case when $M \geq a$ Kerr metric describes an axially symmetrical and stationary black hole with its outer event horizon at

$$r_{\rm hor} = M + \sqrt{M^2 - a^2}\,. \tag{6}$$

The limiting case $a = M$ is called extreme Kerr black hole solution and is characterised by a number of very peculiar effects in the near horizon region (see e. g. Bardeen et al. 1972). Otherwise, if $M < a$ the expression (6) becomes complex and the metric describes a *naked singularity* not concealed by the event horizon. The *cosmic censorship conjecture* claims that for any physically relevant processes naked singularities cannot arise (see Wald 1984, pp. 302—304 for precise formulations). Indeed, it is possible to show in particular (see e. g. Hartle 2003) that astrophysical black holes can never be spun up by external matter including accretion flows to that values. However it is believed that for black holes surrounded by accretion disks their spin must be relatively close to M with its upper value being $\approx 0.998M$ (Thorne 1974).

The zeroes of g_{tt}-term from the metric (5) give one another important radius, the radius of the *ergoregion* or *ergosphere*, whose value outside of the horizon is given by

$$r_{\rm erg} = M + \sqrt{M^2 - a^2 \cos^2\theta}\,. \tag{7}$$

Within this radius t-coordinate ceases to be time-like, i. e. it is impossible to move only along its coordinate curves. In fact, it is impossible not to rotate in the direction of black hole's rotation there for any particle having positive energy (note, however, that Kerr solution admits states with negative energies). Besides that the surface $g_{tt} = 0$ denotes the surface of infinite redshift for radially in-falling observers, however since other (e. g. rotating) observers are possible inside it that do can send light signals to the outside this aspect of the ergosphere's properties is not that crucial for the observational appearance of Kerr black holes. The existence of the ergoregion is the most prominent manifestation of the *frame-dragging* effect in this space-time: any body in free fall from infinity will gain angular velocity (be "dragged") in direction of the black hole's rotation given by the frame-dragging velocity:

$$\Omega_{FD} = -\frac{g_{t\phi}}{g_{\phi\phi}} = \frac{2Mra}{\Sigma(r^2 + a^2) + 2Mra^2 \sin^2\theta}. \tag{8}$$

After crossing the ergosphere radius it becomes impossible for any such body to withstand this effect whatever force it may apply. The structure of a Kerr

black hole solution in the domain of outer communication is given in the Figure 9.

Geodetic circular motion for massive particles in the Kerr geometry is possible only in the equatorial plane with $\theta = \pi/2$. Energy and angular momentum per particle mass that a particle needs to have in order to stay on a geodesic circular orbit at a radius r are

$$\begin{aligned} E := -u_t &= \frac{r^{3/2} - 2Mr^{1/2} \pm aM^{1/2}}{r^{3/4}(r^{3/2} - 3Mr^{1/2} \pm 2aM^{1/2})^{1/2}}\,, \\ L := u_\phi &= \pm\frac{M^{1/2}(r^2 \mp 2aM^{1/2}r^{1/2} + a^2)}{r^{3/4}(r^{3/2} - 3Mr^{1/2} \pm 2aM^{1/2})^{1/2}}. \end{aligned} \tag{9}$$

Here the upper sign corresponds to the prograde, with the angular momentum of the particle being parallel to the BH spin, and the lower one – to the retrograde orbits i. e. those with these vectors being antiparallel. The (Keplerian) angular velocity that a particle has on such an orbit is:

$$\Omega_K := \frac{u^\phi}{u^t} = \frac{M^{1/2}}{aM^{1/2} \mp r^{3/2}}. \tag{10}$$

Later we shall make much use of yet another characteristic quantity of circular motion, the specific angular momentum

$$\ell := -\frac{u_\phi}{u_t}\,,$$

whose Keplerian value is given by

$$\ell_K = \pm\frac{M^{1/2}(r^2 \mp 2aM^{1/2}r^{1/2} + a^2)}{r^{3/2} - 2Mr^{1/2} \pm aM^{1/2}}\,. \tag{11}$$

The Keplerian values of specific angular momentum at characteristic radii of the spacetime are of especial interest for the perfect fluid configurations with its value being constant (most notably Polish Doughnuts). Radius of the marginally/innermost stable circular orbit (ISCO, denoted "ms") can be found analytically by solving the quartic equation:

$$r_{\rm ms}^2 - 6Mr_{\rm ms} \pm 8aM^{1/2}r_{\rm ms}^{1/2} - 3a^2 = 0\,. \tag{12}$$

The solution of this equation is quite lengthy and we shall not present it here, those interested can find it at e. g. Bardeen et al. (1972) or Chandrasekhar

Figure 9: The external structure of a Kerr black hole for the spin parameter values $a = 0.5M$ (top) and nearly extreme $a = 0.998M$ with a zoom of the near-horizon region (bottom). Black circle covers the area inside horizon, the blue line denotes the outer boundary of the ergosphere. The radii of $r_{\rm ph}$, $r_{\rm mb}$, $r_{\rm ms}$ (see definition in text) on the right to the BH are given for prograde and on the left for retrograde rotation.

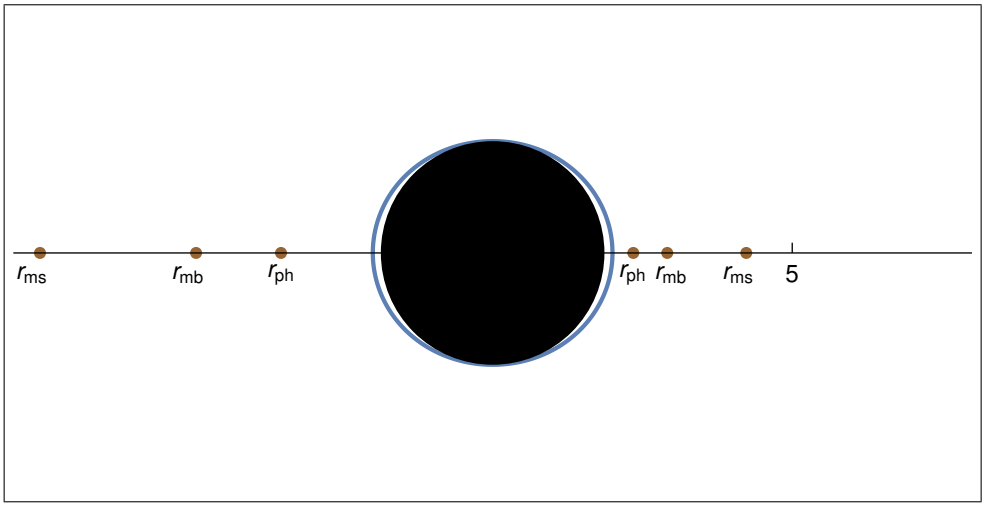

(a) $a = 0.5M$

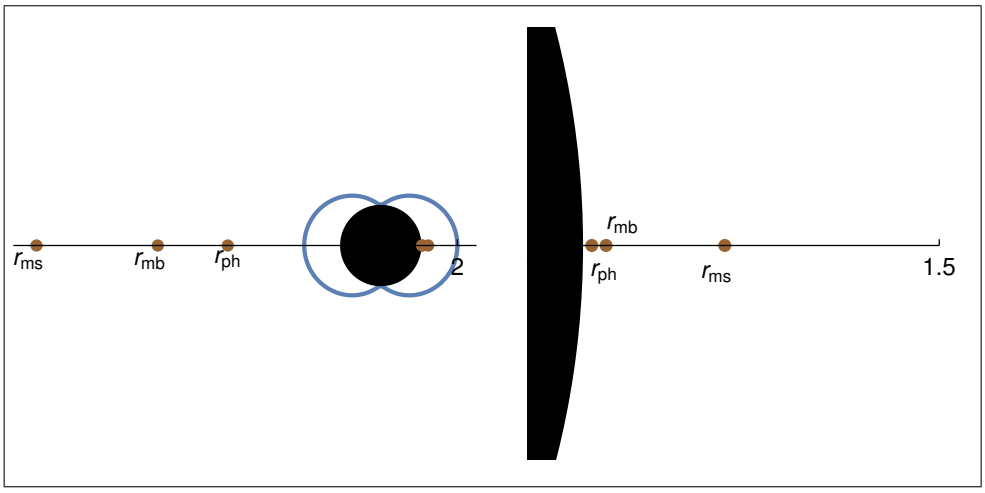

(b) $a = 0.998M$

(1983). The marginally bound orbit, i. e. that with a particle on it having energy enough to escape to infinity, has radius

$$r_{\rm mb} = 2M \mp a + 2M^{1/2}(M \mp a)^{1/2} \,. \tag{13}$$

The radius of the photon orbit in Kerr which is in the same time the limiting geodesic orbit for massive particles is

$$r_{\rm ph} = 2M \left\{ 1 + \cos\left[\frac{2}{3} \arccos\left(\mp \frac{a}{M} \right) \right] \right\} \,. \tag{14}$$

The positions of these radii for Kerr spacetimes with $a = 0.5M$ and the nearly extremal one with $a = 0.998M$ are given in the Figure 9.

3.2 NUT spacetime(s)

Unlike Kerr solution the NUT (Newman-Unti-Tamburino) metric needs a more detailed introduction. As it was mentioned in the reviewing chapter this metric demonstrates some quite unusual and to a certain extent pathological properties which like the physical identification of the Manko-Ruiz constant are not understood until the present day. In spherical coordinates the NUT metric is given by the expression (Griffiths & Podolský 2009):

$$g_{\mu\nu}\mathrm{d}x^\mu \mathrm{d}x^\nu = \frac{\Delta_n}{\Sigma_n}\Big(\mathrm{d}t - 2n(\cos\theta + C)\mathrm{d}\phi\Big)^2 - \frac{\Sigma_n}{\Delta_n}\mathrm{d}r^2 - \Sigma_n(\mathrm{d}\theta^2 + \sin^2\theta \mathrm{d}\phi^2) \tag{15}$$

where

$$\begin{aligned} \Delta_n &= r^2 - 2Mr - n^2 \,, \\ \Sigma_n &= r^2 + n^2 \,. \end{aligned} \tag{16}$$

This metric represents a black hole solution for *any* real values of $M \neq 0$ or $n \neq 0$ with the outer horizon radius given by

$$r_{\rm hor} = M + \sqrt{M^2 + n^2} \,. \tag{17}$$

We shall now discuss the physical relevance of the Manko-Ruiz parameter C following our work (Jefremov & Perlick 2016). From the way how it enters into the metric (15) we observe that at least some of its different values describe the same space-time if we perform certain coordinate transformations. First, we see that by transforming

$$\overline{t} = t \,, \quad \overline{\phi} = -\phi \,, \quad \overline{\theta} = \pi - \theta \,, \quad \overline{r} = r \tag{18}$$

C changes into $\overline{C} = -C$. This demonstrates that NUT metrics with C and $-C$ are globally isometric, where the isometry is given by a simultaneous inversion of the ϕ coordinate and reflection at the equatorial plane. The possibility of further isometries is closely related to the span of the time coordinate t, whether it is periodic or not. We observe that the coordinate transformation

$$t' = t - 2n(C - C')\phi\,, \quad \phi' = \phi\,, \quad \theta' = \theta\,, \quad r' = r \tag{19}$$

transforms a NUT metric with C to a NUT metric with C' for any pair of real numbers C and C'. However, (19) is not a globally well defined transformation unless we assume that t is periodic with period $4\big|n(C-C')\big|\pi$. The reason is that ϕ is assumed to be periodic with period 2π. We may summarise these observations in the following way: if we are not willing to assume the time coordinate to be periodic with the appropriate period, NUT space-times with Manko-Ruiz parameters C and C' are non-isometric and, thus, *physically distinct* providing that $|C| \neq |C'|$. However, they are *locally* isometric, as demonstrated by (19), on any neighbourhood that does not contain a complete ϕ-line. If the time coordinate has period T, NUT space-times with Manko-Ruiz parameters C and C' *are* globally isometric if $4|n(C - C')|\pi = \mathrm{T}$.

The Manko-Ruiz parameter is of particular relevance in view of the fact that the NUT metric features a singularity on the axis which is different from the trivial coordinate singularity of spherical polars familiar even from flat space. We can read this from the contravariant time-time component of the metric which can easily be calculated from (15),

$$g^{tt} = -\frac{4n^2(\cos\,\theta + C)^2}{\Sigma_n \sin^2\theta} + \frac{\Sigma_n}{\Delta}\,. \tag{20}$$

While the second term is finite everywhere outside of the horizon, the first one diverges for $\theta \to 0$ unless $C = -1$ and for $\theta \to \pi$ unless $C = 1$. Moreover, the $g_{\phi\phi}$ term of the metric (15) closely connected to g^{tt}

$$g_{\phi\phi} = \frac{4n^2\Delta(\cos\theta + C)^2 - \Sigma_n^2 \sin^2\theta}{\Sigma_n} \tag{21}$$

changes its sign at a certain distance from the singular half-axes and becomes timelike leading to existence of causality violating regions around them.

Having a $g_{t\phi}$-term the NUT metric exhibits the frame-dragging effect with angular velocity

$$\Omega_{FD} = \frac{4n\Delta_n(\cos\theta + C)}{4n^2\Delta_n(\cos\theta + C)^2 - \Sigma_n^2 \sin^2\theta}. \tag{22}$$

However, unlike in Kerr the g_{tt} term never vanishes outside of the horizon meaning that t coordinate lines stay everywhere time-like and there is no ergoregion.

There are two different ways of how to interpret the NUT singularity outside of the horizon, depending on whether or not one is willing to make the time coordinate periodic. The first interpretation was brought forward by Misner (1963). He considered the metric (15) with $C = -1$ which is regular except on the negative half-axis, $\theta = \pi$. By a coordinate transformation (19) with $C' - C = 2$ he got a NUT metric with $C' = 1$ which is regular except on the positive half-axis, $\theta = 0$. This transformation requires the time coordinate to be periodic with period $8|n|\pi$. One can now cut out the singular regions from these two copies of the space-time and glue them together to get a new one without any singularity. Of course, assuming that the time coordinate is periodic means that there is a closed time-like curve through *any* event in the domain of outer communication, i. e., that the space-time violates the causality conditions (Wald 1984) in an extreme way. However, one could argue that this is of no practical relevance if one assumes the period $\mathrm{T} = 8|n|\pi$ to be very large. Misner's construction can be generalised to gluing together a NUT metric with C and a NUT metric with $C' = -C$, for any $C \neq 0$, provided that the time coordinate is periodic with period $8|nC|\pi$. However, in the case $|C| \neq 1$ this is not very interesting because the resulting space-time still has a singularity on the axis.

The second interpretation, which goes back to Bonnor (1969), is based on the assumption that the t coordinate is not periodic. Then (19) is not a globally allowed transformation and, for any choice of C, we have a true singularity on at least one half-axis. Bonnor interpreted this singularity as a massless spinning rod. He considered only the case that $C = -1$ where the singularity is on the negative half-axis. For the isomorphic case $C = 1$ it is on the positive half-axis and for all other values of C it occurs on both of them. In the case $C = 0$ causality violating regions are distributed symmetrically and for any other value of C asymmetrically around the half-axes. In Bonnor's version the NUT metric is locally SO(3) symmetric, near any point off the axis, but not globally in contrast to Misner's version with

$|C| = 1$. As we read from (21) the ϕ lines are timelike near the singularity, meaning that also in Bonnor's interpretation the NUT metric contains closed time-like curves in the domain of outer communication. Figure 10 illustrates the influence of Manko-Ruiz constant on the geometry of NUT spacetime in the Bonnor's interpretation.

Contrary to the gravitomagnetic charge n the Manko-Ruiz constant C cannot be easily identified with any of black hole characteristics familiar from classical mechanics or electromagnetism. The fact that all NUT metrics with different values of C for a given n are locally isometric to each other makes its character even more cryptic and raises the question on possible observational effects it could cause. Kagramanova et al. (2010) have investigated geodetic motion in this space-time and found that the integrals of motion can all be rescaled to incorporate the Manko-Ruiz constant, so its influence undetectable. It was one of the main objectives of our work (Jefremov & Perlick 2016) to investigate its possible influence on various types of circular motion in this space-time and in particular on accretion models that I shall present later in this work. In the next subsections after giving the characteristic radii of the space-time I shall reproduce some results valid for geodetic motion as well as a specific type of non-geodetic motion relevant for the accretion flows that will be considered in the next Chapters based on (Kagramanova et al. 2010, Jefremov & Perlick 2016) to give the reader an impression of the current state of research in the field.

3.2.1 Structure of circular geodesics

The most distinctive feature of geodesic circular motion in the NUT space-time is that it no longer takes place in the equatorial plane but rather on a surface given by

$$\cos^2\theta = \frac{4n^2}{Q(r)}\,, \tag{23}$$

where

$$Q(r) := \frac{6n^6 r + 16M^2n^2r^3 - 4n^4r^3 + 6n^2r^5 + M(r^6 + 15n^4r^2 - 15n^2r^4 - n^6)}{r\Delta^2}\,. \tag{24}$$

Due to this fact not only energy E and angular momentum L at different radii have different values but Carter constant $\varkappa$ as well:

$$E = \frac{\sqrt{\Sigma_n \Delta}}{\sqrt{\Sigma_n^2 - 4n^2\Delta\tan^2\theta}}\,, \tag{25}$$

Figure 10: Influence of the Manko-Ruiz constant on the singularity distribution (red line) and the form of the causality violating region (marked by green colour) in the domain of outer communication of NUT spacetime with $n = 0.2M$. (a) features the spacetime with $C = 0$ and the causality violating region distributed symmetrically along the half-axes; (b) has $C = 1$ and singularity and causality violation along positive half-axis only; (c) and (d) with $C = 0.3$ and $C = 2$ respectively have singularity on both half-axes with causality violating regions distributed asymmetrically.

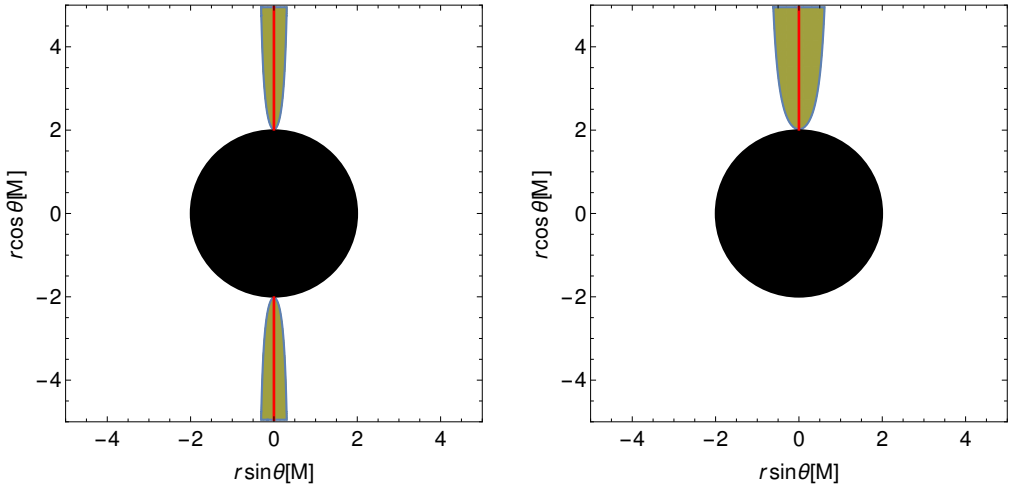

(a) $C = 0$

(b) $C = 1$

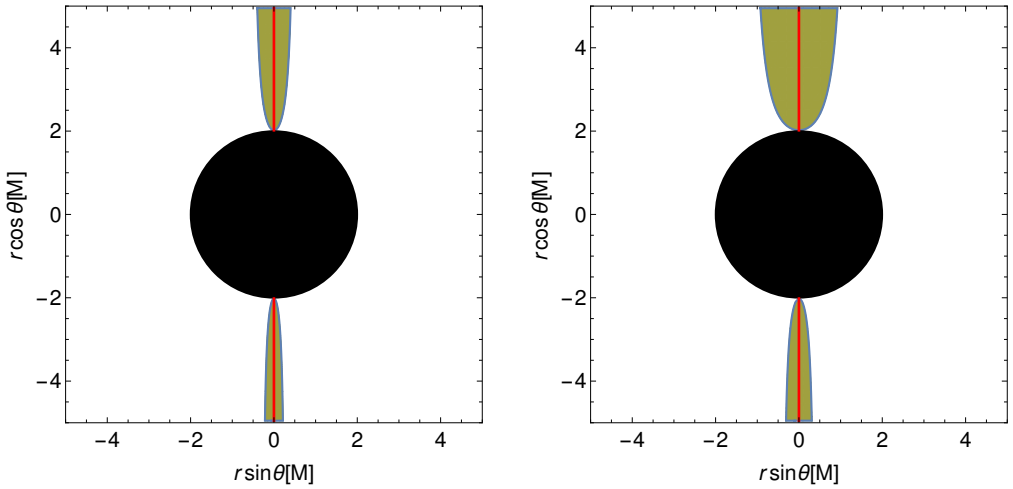

(c) $C = 0.3$

(d) $C = 2$

Figure 11: Characteristic structure of circular geodesic motion in NUT space-time with $n = 0.3M$. The thick blue line denotes the surface of circular geodesics given by (23), the locations of the last stable circular orbit $r_{\rm ms}$, marginally bound orbit $r_{\rm mb}$ and the photon orbit $r_{\rm ph}$ are given by intersections of the corresponding circles (dashed lines) with the circular-geodesics curve.

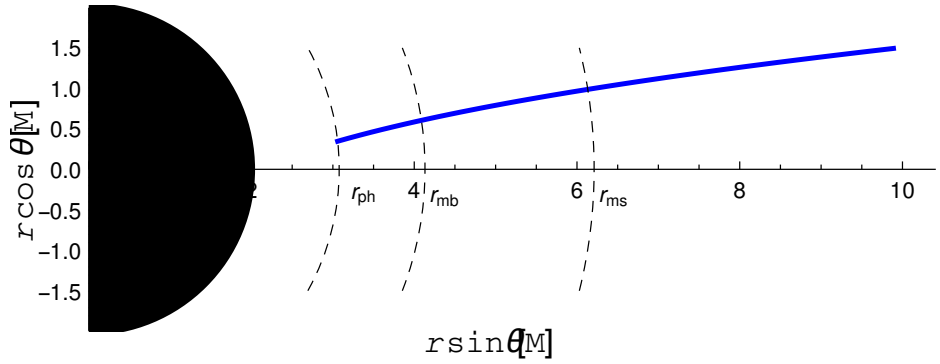

$$L = \frac{\sqrt{4\Sigma_n\Delta}n(1+C\cos\theta)}{\cos\theta\sqrt{\Sigma_n^2 - 4n^2\Delta\tan^2\theta}}\,, \tag{26}$$

$$\varkappa = n^2 - \frac{4\Sigma_n\Delta n\Big((1+C\cos\theta)^2 - \sin^2\theta\Big)}{\cos^2\theta\Big(\Sigma_n^2 - 4n^2\Delta\tan^2\theta\Big)}\,. \tag{27}$$

The Keplerian specific angular momentum is then given as

$$\ell_K = \frac{2n(1+C\cos\theta)}{\cos\theta}\,, \tag{28}$$

with $\cos\theta$ from (23).

The radius of the last stable orbit is found by solving the equation

$$\begin{aligned} Mr_{\rm ms}^6 - 6M^2r_{\rm ms}^5 - 15Mn^2r_{\rm ms}^4 + (4M^2n^2 - 16n^4)r_{\rm ms}^3 + 15Mn^4r_{\rm ms}^2 \\ -6M^2n^4r_{\rm ms} - Mn^6 = 0\,, \end{aligned} \tag{29}$$

which obviously cannot be done analytically. However, it can be verified that this equation has a unique solution for $r > r_{\rm hor}$ and in the limit $n \to 0$ it reduces to the well-known equation for the ISCO in Schwarzschild space-time.

The radius of the marginally bound orbit is given by

$$r_{\rm mb} = M + \sqrt{M^2 + n^2 + \left(\frac{n^2(M^2+n^2)}{2M}\right)^{2/3}} + \sqrt{2M^2 + 2n^2 - \left(\frac{n^2(M^2+n^2)}{2M}\right)^{2/3} + \frac{2M^4 + 3M^2n^2 + n^4}{M\sqrt{M^2 + n^2 + \left(\frac{n^2(M^2+n^2)}{2M}\right)^{2/3}}}} \tag{30}$$

and the photon orbit radius

$$r_{\rm ph} = M + 2(M^2+n^2)^{1/3}\,{\rm Re}\Big((M + i\,n)^{1/3}\Big)\,. \tag{31}$$

As for any geodesics the corresponding θ coordinate of the orbit should be found by substituting these values into the expression (23). Figure 11 illustrates the principal structure of geodetic circular motion in NUT spacetime.

3.2.2 The influence of Manko-Ruiz constant on geodetic flows

We shall now discuss the imprints (or rather their absence) of the Manko-Ruiz constant on geodesic motion investigated in detail by Kagramanova et al. (2010). The coordinate geodesic equations in the NUT metric are:

$$\begin{aligned}
\dot{r}^2 &= R := \frac{1}{4M^2}\left(\Sigma_n^2 E^2 - \Delta(r^2 + L^2 + K)\right), \\
\dot{\theta}^2 &= \Theta := \frac{1}{4M^2}\left(K + L^2 - n^2 - \frac{\Big(L - 2nE(\cos\theta + C)\Big)^2}{\sin^2\theta}\right), \\
\dot{\phi} &= \frac{1}{2M}\left(\frac{L - 2nE(\cos\theta + C)}{\sin^2\theta}\right), \\
\dot{t} &= \frac{1}{2M}\left(E\frac{\Sigma_n^2}{\Delta}2n\Big(\cos\theta + C\Big)\frac{\Big(L - 2nE(\cos\theta + C)\Big)}{\sin^2\theta}\right).
\end{aligned} \tag{32}$$

A dot denotes a derivative with respect to the Mino time $\mathfrak{t}$ related to the proper time τ via $\Sigma_n {\rm d}\mathfrak{t} = 2M{\rm d}\tau$. By the coordinate transformation (19)

with $C' = 0$, which in any case is well-defined locally near any point off the axis, one can get rid of the Manko-Ruiz parameter C in (15). This transforms the equations for time-like geodesics to

$$\begin{aligned}
\dot{r}^2 =& \frac{1}{4M^2}\left(\Sigma^2 E'^2 - \Delta(r^2 + L'^2 + K')\right) \\
\dot{\theta}^2 =& \frac{1}{4M^2}\left(K' + L'^2 - n^2 - \frac{\Big(L' - 2nE'\cos\theta\Big)^2}{\sin^2\theta}\right), \\
\dot{\phi} =& \frac{1}{2M}\left(\frac{L' - 2nE'\cos\theta}{\sin^2\theta}\right), \\
\dot{t}' =& \frac{1}{2M}\left(E'\frac{\Sigma^2}{\Delta} + 2n\cos\theta\frac{\Big(L' - 2nE'\cos\theta\Big)}{\sin^2\theta}\right).
\end{aligned} \tag{33}$$

where the new integrals of motion are related to the old ones from (32) by

$$E' = E\,, \quad L' = L - 2n(C - C')E\,, \quad \varkappa' = \varkappa + 4n(C - C')EL - 4n^2(C - C')^2E^2\,. \tag{34}$$

Here and in the following formulae C' should be set $= 0$. The transformed values of angular velocity Ω' and specific angular momentum ℓ' are then related to the old ones through:

$$\Omega' = \frac{\Omega}{1 - 2n(C - C')\Omega} \tag{35}$$

and

$$\ell' = \frac{L - 2n(C - C')E}{E} = \ell - 2n(C - C'). \tag{36}$$

These facts mean that whereas the equations of geodetic motion (32) do depend on the value of the Manko-Ruiz constant, the family of trajectory curves obtained from them is independent of it in the sense that the values of $E, L, \varkappa$ defining each of such curves can be rescaled incorporating C by the corresponding transformation (34). The geometric location of the trajectory curves stays the same for any value of C, the only thing that changes are the values of the integrals of motion characterising a given curve, which themselves can be computed only once the metric (and thus C) is specified.

3.2.3 Von Zeipel flows and Manko-Ruiz constant

In the following Chapters on accretion we shall consider circular and polytropic flows obeying the Euler equation (see Section 4). Abramowicz (1971) has shown that they will obey the relativistic version of the von Zeipel theorem stated below and we shall hence call them the *von Zeipel flows*. An important characteristic of them is the von Zeipel radius defined as

$$\mathcal{R}^2 = \frac{\ell}{\Omega}\,. \tag{37}$$

In the case of the axially symmetric and stationary spacetimes given by

$$g = g_{tt}\mathrm{d}t^2 + 2g_{t\phi}\mathrm{d}td\phi + g_{\phi\phi}\mathrm{d}\phi^2 + g_{rr}\mathrm{d}r^2 + g_{\theta\theta}\mathrm{d}\theta^2. \tag{38}$$

this quantity can be expressed as

$$\mathcal{R}^2 = \frac{\ell}{\Omega} = \frac{-\Omega^{-1}g_{t\phi} - g_{\phi\phi}}{g_{tt} + \Omega g_{t\phi}} = \frac{-\ell g_{t\phi} - g_{\phi\phi}}{\ell^{-1}g_{t\phi} + g_{tt}}\,. \tag{39}$$

The surfaces defined by this quantity being constant are called *von Zeipel cylinders* because in the Newtonian limit for asymptotically flat spacetimes they are indeed topological cylinders. In the case when the von Zeipel theorem is valid, i. e. when $\mathrm{d}\Omega$ (and consequently $\mathrm{d}\mathcal{R}$) is a multiple of $\mathrm{d}\ell$ the surfaces of constant $\mathcal{R}$ from (39) give one specific angular momentum level surfaces in the whole domain of outer communication providing that its distribution on *one particular surface* crossed by all surfaces $\mathcal{R}$ = const. is prescribed. Figure 12 represents the case of rotating perfect fluid configurations in Kerr with the angular momentum distribution obtained in the Section 4.

In the case when the von Zeipel theorem is not valid, in particular for the Polish Doughnuts with $\ell(r,\theta)$ = const. that we will consider in the NUT spacetime later, one has to prescribe the angular momentum distribution *globally* and the surfaces $\mathcal{R}$ = const. will be surfaces of constant angular velocity.

Specifying the expression (39) for the NUT spacetime we obtain:

$$\mathcal{R}^2 = \frac{2\ell n(\cos\theta + C) - 4n^2(\cos\theta + C)^2 + \Sigma_n^2\Delta_n^{-1}\sin^2\theta}{1 - 2\ell^{-1}n(\cos\theta + C)}\,. \tag{40}$$

Performing the simultaneous transformation of the left- [defined as in (37)] and right-hand parts of this expression with using (35) and (36) we obtain

Figure 12: Von Zeipel cylinders in Kerr space-time with $a = 0.9375M$. Specific angular momentum distribution fulfills the von Zeipel theorem and is given by (60) with $\kappa = -0.37$ (a) and $\kappa = 0.89$ (b) and corresponding values for ℓ_0 from the Table 2. The radii of the von Zeipel cylinders are given in the boxes. The red dashed line denotes the inner boundary of time-like motion giving the surface where the fluid 4-velocity becomes light-like.

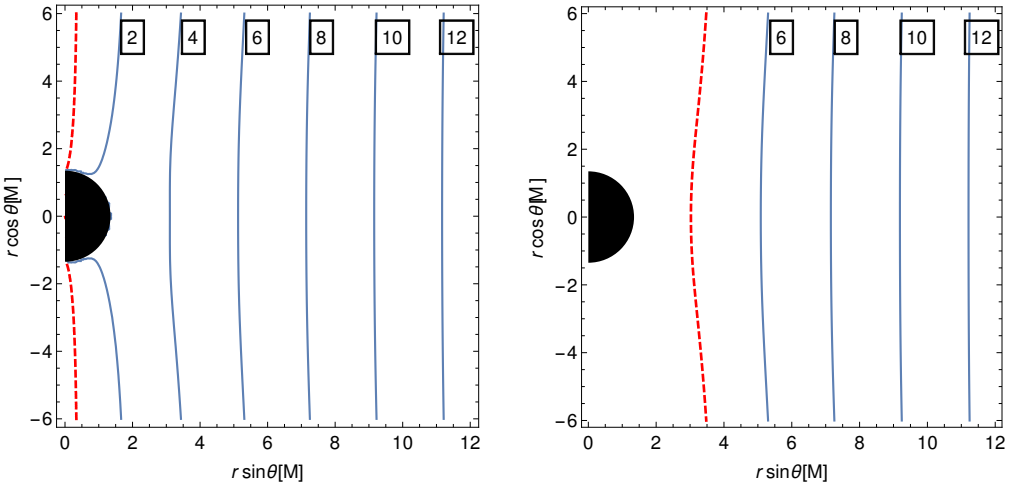

(a) $\kappa = -0.37$ (b) $\kappa = 0.89$

the result that the geometrical locations of von Zeipel cylinders of the NUT metrics with equal values of M and n but with different C are all invariant under the transformation (19) even though the numerical values of $\mathcal{R}$ defining these surfaces are different. In particular they are all equivalent to the metric with the same M and n and $C = 0$, so for all our computations we can set C to this value and obtain the corresponding values of ℓ and Ω by performing transformations (35) and (36). The von Zeipel radii $\mathcal{R}'$ for the metric with $C' = 0$ are expressed through those with $C \neq 0$ as

$$\mathcal{R}'^2 = \mathcal{R}^2 - 2nC\ell^{-1}\mathcal{R}^2 - 2nC\ell + 4n^2C^2. \tag{41}$$

Figure 13 illustrates the invariance of von Zeipel surfaces for different values of C. This result like the case of geodetic motion shows that it is not possible to distinguish between NUT space-times with equal M and n but different C by considering the geometrical location of barotropic fluid's circular trajectories.

Figure 13: The influence of Manko-Ruiz constant on the von Zeipel cylinders in the NUT spacetime. Two spacetimes with $n = 0.6M$ and different C are considered: $C = 1$ (left) and $C = 0$ (right). The geometrical location of the von Zeipel surfaces for constant $\ell = 5.42M$ (for $C = 1$) and $\ell' = \ell - 2nC = 4.22M$ (for $C' = 0$) remains unchanged, however they correspond now to different values of von Zeipel radii (in the boxes on the plot) with the relation between them given by (41). The red dashed line has the same meaning as in the Figure 12.

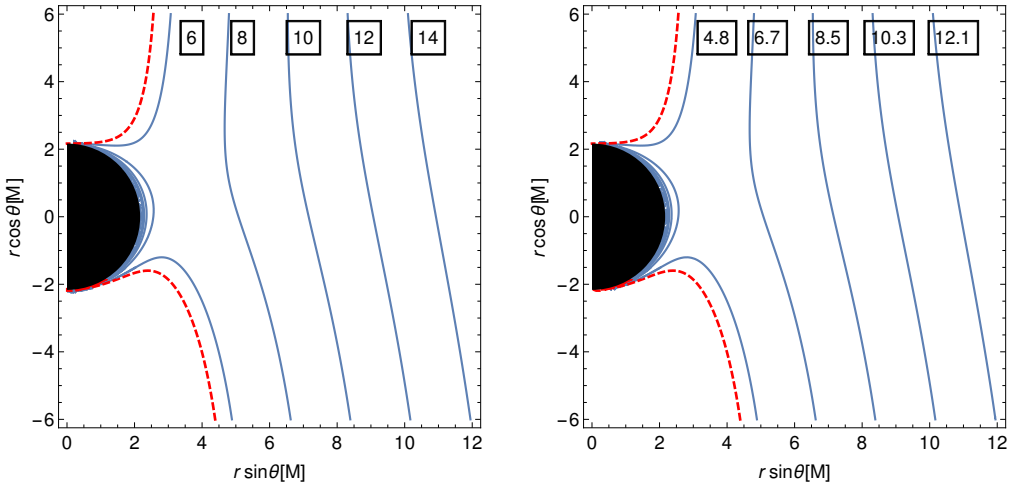

(a) $C = 1$ (b) $C = 0$

4 New ansatz for the perfect fluid tori

We will now recapitulate some basic theory on perfect fluid's circular motion in general-relativistic approach and present our new results published in (Witzany & Jefremov 2018). In the general theory of relativity perfect fluid is described by energy-momentum tensor in the form:

$$T^{\mu\nu} = (e + p)u^\mu u^\nu + pg^{\mu\nu}, \tag{42}$$

where e is the total energy of the fluid, p – its pressure and u^μ is fluid's 4-velocity. Since we shall not take into account external forces influencing the fluid this tensor must satisfy the equation

$$\nabla_\nu T^{\mu\nu} = 0. \tag{43}$$

Here and in the definition of $T^{\mu\nu}$ we shall use metric coefficients given only by the black hole thus neglecting fluid's self-gravity. By projecting this equation on the directions parallel and orthogonal to the fluid 4-velocity we obtain the energy-conservation equation:

$$u^\mu \partial_\mu e + \rho h \nabla_\mu u^\mu = 0 \tag{44}$$

and the general-relativistic version of the Euler equation:

$$\rho h u^\mu \nabla_\mu u^\nu + (g^{\mu\nu} + u^\mu u^\nu)\partial_\mu p = 0; \tag{45}$$

here $h := (e + p)/\rho$ is fluid's specific *enthalpy*.

In what follows we assume that the spacetime is stationary and axially symmetric:

$$g = g_{tt}\mathrm{d}t^2 + 2g_{t\phi}\mathrm{d}t d\phi + g_{\phi\phi}\mathrm{d}\phi^2 + g_{rr}\mathrm{d}r^2 + g_{\theta\theta}\mathrm{d}\theta^2.$$

For the fluid motion we assume that its motion be circular: $u^r = u^\theta = 0$ and that all characteristic quantities of the flow share the symmetries of the spacetime, i. e. are independent of t and ϕ. Under these assumptions the energy-conservation equation (44) is trivially fulfilled and the equation of motion of the fluid (45) can be written as (see e. g. Rezzolla & Zanotti 2013)

$$\frac{\partial_\mu p}{\rho h} = \partial_\mu \ln(u^t) - \frac{\ell}{1 - \Omega\ell}\partial_\mu \Omega, \tag{46}$$

where we have combined the non-zero 4-velocity components in 2 new variables: angular velocity $\Omega := u^\phi/u^t$ and specific angular momentum $\ell := -u_\phi/u_t$.

If we demand that the fluid equation of state be barotropic, i. e. $p = p(e)$, then the left-hand side of the equation (46) becomes a full differential, which means that such must be also the right-hand side. Since the first term in it is already a full differential, this puts restrictions on the second one: It must either vanish yielding perfect fluid configurations with constant ℓ or Ω or become a full differential as well, then $\ell = \ell(\Omega)$ must be fulfilled. This fact is known as the relativistic von Zeipel theorem (Abramowicz 1971). Assuming the latter case now we can integrate (46) to obtain the integral form of the Euler equation

$$\int \frac{p'(e)}{\rho h}\mathrm{d}e := W(e) - W_s = \ln(u^t) - L(\Omega) - W_s\,. \tag{47}$$

The function $L(\Omega)$ is set equal to one particular arbitrarily chosen primitive function of the second term on the right-hand side of (46):

$$L(\Omega) := \int \frac{\ell}{1-\Omega\ell}\mathrm{d}\Omega\,. \tag{48}$$

This choice in turn fixes the effective potential $W(e)$ defined as that particular primitive function of the left-hand side of (46) for which the corresponding velocity field is given as

$$W(e(r,\theta)) = \ln(u^t) - L(\Omega)\,. \tag{49}$$

The actual density distribution is then adjusted by the "surface value" of the effective potential W_s which defines the surface where the specific total internal energy e is equal to zero and thus gives the boundary of the configuration.

From the definition of the angular velocity it follows that ℓ and Ω are connected through the expression:

$$\Omega = \frac{u^\phi}{u^t} = \frac{\ell g^{\phi\phi} - g^{t\phi}}{\ell g^{t\phi} - g^{tt}}\,, \tag{50}$$

so the right-hand side of (46) is in general a function of coordinates and of either of these variables. Having assumed validity of the von Zeipel theorem,

we obtain the coordinate dependence $\Omega = \Omega(r, \theta)$ from (50) which we rewrite for the matter of convenience in the form:

$$(\ell g^{t\phi} - g^{tt})\Omega - \ell g^{\phi\phi} + g^{t\phi} = 0\,. \tag{51}$$

The function $\ell(\Omega)$ can be selected fairly arbitrarily here, the only restriction that we shall put on it will come from our aim to obtain the angular velocity field *in the closed form*. We observe that if Ω should be a root of the polynomial equation of order n, then this function must be of the form:

$$\ell(\Omega) = \frac{\mathcal{P}^{n-1}(\Omega)}{\tilde{\mathcal{P}}^{n-1}(\Omega)}, \tag{52}$$

where $\mathcal{P}^j(\Omega)$ and $\tilde{\mathcal{P}}^j(\Omega)$ are polynomials of the order $\leq j$ in Ω (see Appendix for details to this result). We will further concentrate on the simplest nontrivial case where $n = 2$, which however is already sufficient to reproduce some well-known toroidal configurations and choose the form of $\ell(\Omega)$ as

$$\ell = \frac{\ell_0 + \lambda\Omega}{1 + \kappa\ell_0\Omega}\,, \tag{53}$$

where ℓ_0, κ, λ are some constants.

The angular velocity field is obtained after substituting (53) into the equation (51):

$$\begin{aligned} \Omega &= \frac{\mathcal{A} - \sqrt{\mathcal{A}^2 + 4(\ell_0 g^{\varphi\varphi} - g^{t\varphi})(\lambda g^{t\varphi} - \kappa\ell_0 g^{tt})}}{2(\lambda g^{t\varphi} - \kappa\ell_0 g^{tt})}\,, \\ \mathcal{A} &= g^{tt} + \lambda g^{\varphi\varphi} - \ell_0 g^{t\varphi}(1 + \kappa)\,. \end{aligned} \tag{54}$$

The case of the Polish Doughnuts with $\ell = \ell_0 = \text{const.}$ is recovered from this expression by taking the limit $\kappa, \lambda \to 0$ or by substituting $\ell = \ell_0$ directly into (50):

$$\Omega = \frac{\ell_0 g^{\phi\phi} - g^{t\phi}}{\ell_0 g^{t\phi} - g^{tt}}\,. \tag{55}$$

The function $L(\Omega)$ can then be computed by substituting expressions (53, 54) into (48):

$$\begin{aligned} L =& -\frac{1}{2}\ln\left[1 + (\kappa - 1)\ell_0\Omega - \lambda\Omega^2\right] \\ & - \frac{\ell_0(1 + \kappa)}{2\mathcal{C}}\ln\left[\frac{\mathcal{C} - \ell_0(1 - \kappa) - 2\lambda\Omega}{\mathcal{C} + \ell_0(1 - \kappa) + 2\lambda\Omega}\right]\,, \\ \mathcal{C} =& \sqrt{\ell_0^2(\kappa - 1)^2 + 4\lambda}\,. \end{aligned} \tag{56}$$

4.1 Degeneracy in parameters

Some combinations of parameters of the ansatz (53) correspond to the same function $\ell = \ell(\Omega)$, which means that (53) is degenerate in them. To find under which parameters this degeneracy occurs we equate two different expressions for the angular momenta to obtain the equation:

$$\frac{\ell_0 + \lambda\Omega}{1 + \kappa\ell_0\Omega} = \frac{\bar{\ell_0} + \bar{\lambda}\Omega}{1 + \bar{\kappa}\bar{\ell_0}\Omega}\,. \tag{57}$$

Equating coefficients before different powers of Ω we come to a conclusion that the degeneracy conditions are:

$$\begin{cases} \ell_0 = \bar{\ell_0}\,, \\ \lambda = \dfrac{\bar{\lambda}\kappa}{\bar{\kappa}}\,, \\ (\kappa - \bar{\kappa})(\bar{\lambda} - \bar{\kappa}\ell_0^2) = 0\,. \end{cases} \tag{58}$$

From this system we find that the non-trivial condition here is given by the second bracket in the third equation of (58):

$$\bar{\lambda} = \bar{\kappa}\ell_0^2\,. \tag{59}$$

Substituting this result into (57) we see that the combination of parameters given by the system (58) actually corresponds to angular momentum being constant: $\ell = \ell_0$. Furthermore, we observe that under additional restriction that $\bar{\lambda} = 0$ the system has only trivial solution, i. e. the degeneracy vanishes. This fact motivated us for this first investigation of this class of solutions to set $\lambda = 0$ and look closely at fluid configurations with functions $\ell(\Omega)$ depending on only two parameters:

$$\ell = \frac{\ell_0}{1 + \kappa\ell_0\Omega}\,. \tag{60}$$

This expression has two well-known special cases:

- $\kappa = 0$ corresponds to the Polish Doughnuts with $\ell = \text{const.} = \ell_0$ (Kozłowski et al. 1978), (Abramowicz et al. 1978).
- $\kappa = 1$ corresponds to the Fishbone-Moncrief tori, with $\ell^* := u_\phi u^t = \text{const.} = \ell_0$ (Fishbone & Moncrief 1976).

4.2 Constructing the tori

Once the explicit form of the function $p = p(e)$ is postulated, one can proceed with finding matter distribution by integrating the left-hand side of (46). A particular form of this function is the polytrope:

$$p = K\rho^{\Gamma} \tag{61}$$

which in spite of its simplicity already encompasses many of the physically relevant fluid models. Here constants K and Γ are respectively polytropic constant and polytropic exponent (Rezzolla & Zanotti 2013, pp.118—123). With (61) the specific internal energy is

$$\epsilon = \frac{K\rho^{\Gamma-1}}{\Gamma-1}\,. \tag{62}$$

Using the first law of thermodynamics which for the isentropic fluids can be written as

$$\mathrm{d}p = \rho \mathrm{d}h\,, \tag{63}$$

we get the expression for the effective potential as

$$W - W_s = \ln h\,; \tag{64}$$

solving it for ρ we obtain:

$$\rho = \left[\frac{\Gamma-1}{K\Gamma}\Big(\exp(W-W_s)-1\Big)\right]^{1/(\Gamma-1)}\,. \tag{65}$$

Substituting in it now the expression for W from (49) we obtain the desired solutions in the closed form.

The resulting tori have all in all 4 parameters $\kappa, \lambda, \ell_0, W_s$ defining their dynamics and 2 parameters, K and Γ, defining their thermodynamics. As it was mentioned above some of the dynamical parameters' combinations cause degeneracies and to avoid them we shall set in the following $\lambda = 0$. With this choice the velocity field function $L(\Omega)$ from (56) becomes:

$$L = \frac{1}{\kappa-1}\ln\left[1+(\kappa-1)\ell_0\Omega\right]\,, \tag{66}$$

where for Ω the corresponding value obtained from (54) should be substituted.

Moreover, since we are interested in the toroidal configuration we can, for the reason of comparison that we will perform in the next sections, fix two other dynamical parameters by demanding that the tori have their boundary equipotential surface passing through some two points in the (r, θ) subspace. This condition for 2 radii $r_{\rm in}$ and $r_{\rm out}$ ($r_{\rm in} < r_{\rm out}$) in the equatorial plane is mathematically formulated as the system:

$$W(r = r_{\rm in}, \theta = \pi/2; \kappa, \ell_0) = W(r = r_{\rm out}, \theta = \pi/2; \kappa, \ell_0) = W_s \,, \qquad (67)$$

where by $W(r = r_{\rm in}, \theta = \pi/2; \kappa, \ell_0)$ etc. one should mean the right-hand side of (49) with the variables set to the corresponding values. Condition (67) is however not sufficient to identify these radii as inner and outer radii of a toroidal configuration, since in general there can be several disjoint equipotential surface (Fig. 17a) and one has to make sure that $r_{\rm in}$ and $r_{\rm out}$ indeed belong to the same closed surface among them. This issue will be discussed below for the specific type of solutions that we consider here.

Through these restrictions only one parameter remains free and can be used for comparison and estimating of the difference of the obtained solutions. We choose this parameter to be κ thus fixing ℓ_0 and W_s through the equations (67).

4.3 Properties of the solutions

In our work (Witzany & Jefremov 2018) we have considered 24 perfect fluid tori in Kerr spacetime with $a = 0.9375M$ for the parameters $\lambda = 0$ and κ ranging in the interval $[-1.11, 1.31]$. We have chosen the values of the inner and outer radii of the tori from the equation (67) to be $r_{\rm in} = 5M$ and $r_{\rm out} = 12M$. The corresponding values of the parameters ℓ_0 and W_s are given in the Table 2. With all this being set the effective potential W is defined completely and we can already investigate the geometrical form as well as dynamical characteristics of the perfect fluid configuration even without specifying the precise form of the equation of state (61), since the equipotential surfaces of W are invariant under its choice.

4.3.1 Dynamical properties

We observe on the Figure 14 that the specific angular momentum distribution in the equatorial plane within the tori is influenced qualitatively by our choice of the parameter κ: some of the distributions exhibit monotonous

Table 2: Parameters of the perfect fluid tori with $\lambda = 0$ and the equipotential surface $W = W_s$ passing through $r_{\rm in} = 5M$ and $r_{\rm out} = 12M$ in Kerr spacetime with $a = 0.9375M$.

κ	$\ell_0\,[M]$	$W_s, 10^{-2}$	κ	$\ell_0\,[M]$	$W_s, 10^{-2}$
-1.11	2.5889	-6.74212	0.15	3.2606	-5.61255
-1.	2.6418	-6.65603	0.26	3.32871	-5.49531
-0.9	2.69052	-6.57617	0.36	3.39239	-5.38553
-0.79	2.74492	-6.48637	0.47	3.46449	-5.26112
-0.69	2.79522	-6.40281	0.57	3.53203	-5.14454
-0.58	2.85157	-6.30863	0.68	3.60865	-5.01232
-0.48	2.90383	-6.22083	0.78	3.68053	-4.88834
-0.37	2.96253	-6.12169	0.89	3.76223	-4.74762
-0.27	3.0171	-6.02914	0.99	3.83902	-4.61558
-0.16	3.07854	-5.92452	1.1	3.92644	-4.46560
-0.06	3.13577	-5.82673	1.2	4.00877	-4.32478
0.05	3.20034	-5.71607	1.31	4.10268	-4.16471

Figure 14: Specific angular momentum distribution in the tori for different values of κ in Kerr spacetime with $a = 0.9375M$. Other parameters of the distribution are given by their respective values from Table 2. For comparison we also plot the Keplerian distribution of the quantity.

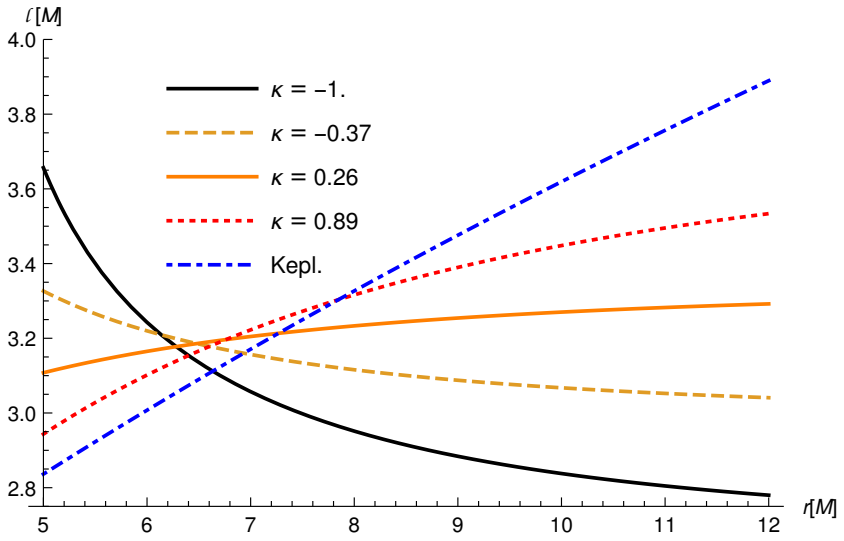

Figure 15: Angular velocity distribution in the tori for different values of the parameter κ in Kerr spacetime with $a = 0.9375M$. Other parameters of the distribution are given in Table 2. Again the blue dash-dotted line represents the Keplerian distribution of the quantity.

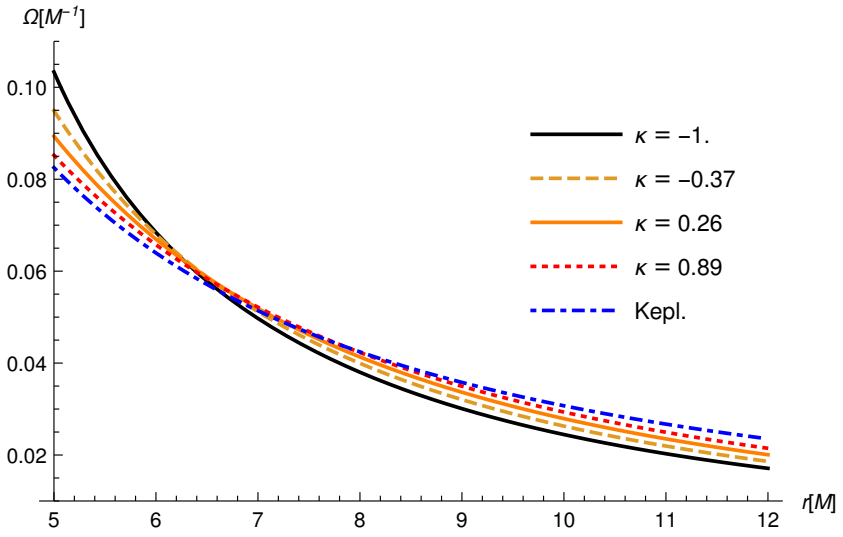

increase whereas others decrease of the quantity. This behaviour can also be seen analytically: with $\lambda = 0$ and Ω decreasing with the radius as it does in our case (see Figure 15) and given that no singularities occur due to the denominator the formula (53) makes the character of the angular momentum distribution dependent on the sign of the parameter κ.

Furthermore, mutual orientation of the Keplerian specific angular momentum distribution (11) and that obtained by the formula (60) is crucial for understanding the structure of the effective potential for the given values of ℓ_0 and κ. The distributions that we consider here can be analysed by the scheme developed by Font & Daigne (2004) for non-constant specific angular momentum distribution in the equatorial plane. At the points where the Keplerian specific angular momentum distribution is crossed by the actual one the fluid moves on geodesics and $\mathrm{d}W(r,\theta) = 0$. Figure 16 presents characteristic structure of the effective potential in the equatorial plane in terms of r and ℓ. Out of different possible specific angular momentum distributions with respect to the Keplerian one as discussed by Font & Daigne (2004) interesting from the point of view of constructing toroidal configurations are those crossing the Keplerian distribution (11) at least once. If this is the

Figure 16: Characteristic variable surfaces (ℓ, r) for the radial derivative of the effective potential in the equatorial plane $\partial_r W(r, \pi/2)$ in Kerr spacetime with $a = 0.9375M$. The orange line denotes the surface where $\partial_r W(r, \pi/2) = 0$ and coincides with the Keplerian distribution of the specific angular momentum, the blue line denotes the critical values of the parameters at which $\partial_r W(r, \pi/2) = \infty$ and the bluish area in between represents parameter family where $\partial_r W(r, \pi/2) > 0$. Dashed green and dotted red lines denote the angular momentum distribution with $\kappa = -0.37$ and $\kappa = 0.89$ and represent effective potentials having respectively one or two extrema outside of the horizon. See (Font & Daigne 2004) for full discussion.

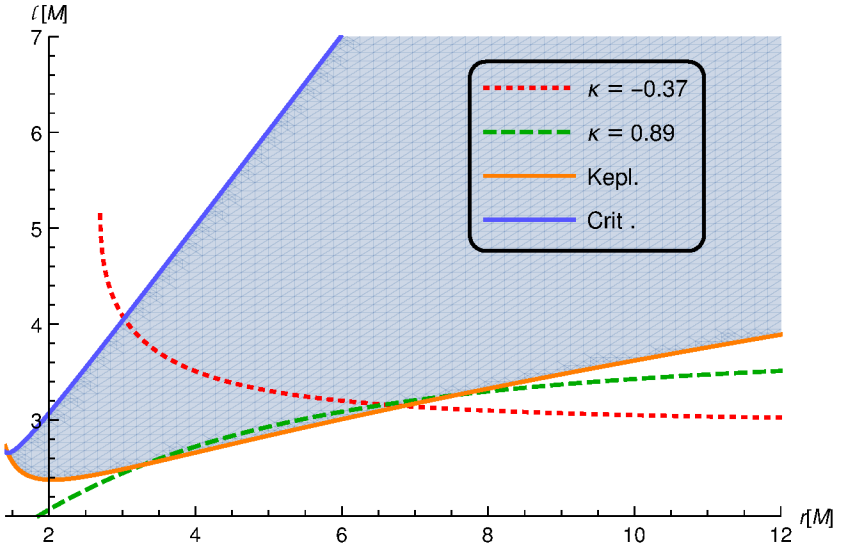

case, then at one of these points the effective potential defined as (49) must have a local maximum. If there are two intersections as in the case of the distribution with $\kappa = 0.89$ on Figure 16, then the effective potential has in addition a *cusp* $r_{\rm c}$, a saddle point which corresponds to the local minimum in the equatorial plane. The equipotential surface corresponding to that saddle-point value of the effective potential is self-crossing. Figure 17 presents two different types of equipotential surfaces – with and without a cusp – allowing for toroidal configurations which one can obtain with the specific angular momentum distribution (60).

We can now return to the question on the sufficient condition for $r_{\rm in}$ and $r_{\rm out}$ to be marginal radii of the *same* closed equipotential surface. As the

Figure 17: Equipotential surfaces for the effective potential W in Kerr spacetime with $a = 0.9375M$ for $\kappa = -0.37$ (a) and $\kappa = 0.89$ (b) and respective values of ℓ_0 from the Table 2. Centre $r_{\rm cen}$ and cusp $r_{\rm c}$, if present, are denoted with a black dot, the red thick line on the picture (a) denotes the self-crossing equipotential surface passing through $r_{\rm c}$.

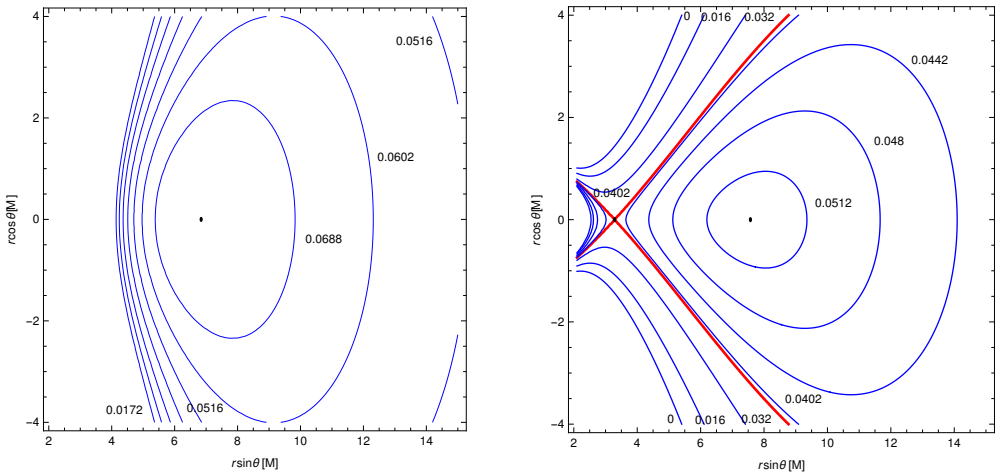

(a) $\kappa = -0.37$ (b) $\kappa = 0.89$

Figure 18: The shape of the perfect fluid tori confined between $r_{\rm in} = 5M$ and $r_{\rm out} = 12M$ with the parameters from the Table 2. The values of the effective potential (and hence density) increase towards the centre of the torus.

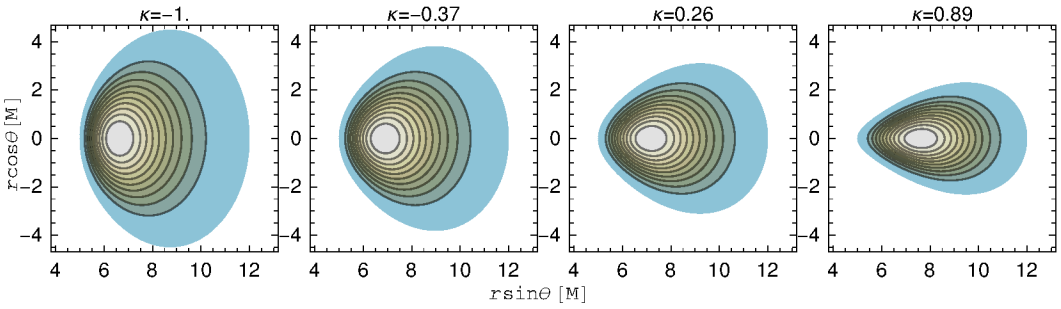

effective potential structures allowing for tori in our case [i. e. with ℓ from 60] have precisely one *closed* surface the additional condition to (67) can be formulated as:

$$r_{\rm in} > r_{\rm c}(\kappa, \ell_0). \tag{68}$$

This condition of course makes sense only for the tori that do have a cusp. Those that do not as e. g. on the Figure 17b also do not possess disjoint equipotential surfaces and thus need not this additional condition.

The special and the most widely-used case of constant angular momentum distribution within the perfect fluid configuration is analysed by Font and Daigne in their first paper on the subject (Font & Daigne 2002). In this case the condition to get toroidal configurations easily translates into a condition on the lower value of ℓ: $\ell > \ell_K(r_{\rm ms})$ where ℓ is now a constant equal to ℓ_0 from the expression (60). If we further demand that the resulting tori also have a cusp, then we should restrict our choice of the value of ℓ on the interval $\ell_K(r_{\rm mb}) < \ell < \ell_K(r_{\rm ms})$. The value of ℓ at the marginally bound orbit $r_{\rm mb}$ brings about the effective-potential structure with the equipotential surface of the cusp being closed at infinity [see (Font & Daigne 2002) for details]. We shall have a closer look at the equipotential surfaces for constant angular momentum distribution later on when comparing the well-studied Kerr case with our new results for the NUT metric.

The geometrical shape of the resulting tori is given in the Figure 18. We observe on it that the most evident characteristic feature that changes in dependence on the parameter κ is their thickness. On the Figure 19 we see that for the considered range of κ half-width along the z-axis is monotonously

Figure 19: Maximal relative half-thickness of the tori $z_{\max}/(r_{\text{out}} - r_{\text{in}})$ as a function of the parameter κ with $z_{\max}$ being maximal absolute value of the tori half-thickness. The parameters of the tori are taken from the Table 2.

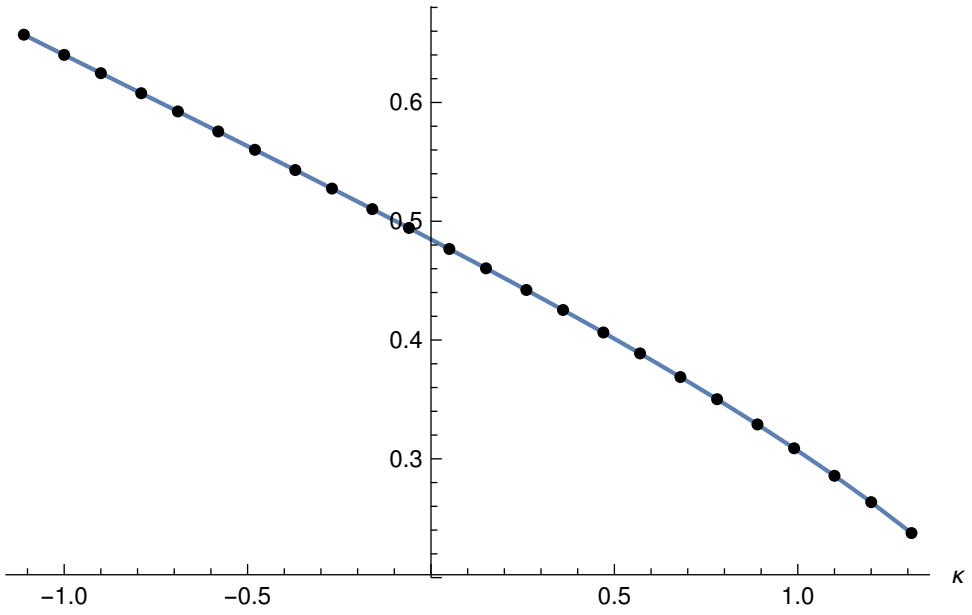

decreasing. This fact along with the observation that with increasing values of κ the specific angular momentum distribution approaches the Keplerian one (cf. Figure 14) seems to suggest that for such angular momentum profiles the fluid concentrates in the region close to the equatorial plane where it would move, if the profile were completely Keplerian.

I finish this brief overview of the dynamical properties of our result for non-constant specific angular momentum distribution by noting that its form as it was mentioned in Chapter 2 plays the key role in development of various instabilities the tori are subject to. As an illustration one can mention the instability with respect to the radial perturbation, *the Rayleigh-Taylor instability*. In the Newtonian case for perfect fluids orbiting a gravitating centre the stability condition reads as

$$\frac{\mathrm{d}\ell^2}{\mathrm{d}r} > 0 \tag{69}$$

otherwise the configurations are unstable and the case $\ell = \text{const.}$ (the "Polish Doughnuts") constitutes the border between the two and is believed to be marginally stable (Rezzolla & Zanotti 2013). In the generally relativistic case this criterion is modified (Seguin 1975), however also here the direction of angular momentum increase plays the key role in the question of the Rayleigh-Taylor stability (Abramowicz & Prasanna 1990). Our tori allowing for both types of angular momentum behaviour can thus model both stable and unstable perfect fluid configurations.

4.3.2 Thermodynamics of the tori

The thermodynamics of the tori is further fixed by specifying the polytropic exponent Γ and the polytropic constant K. In our work (Witzany & Jefremov 2018) we adjusted tori parameters, where it did not contradict our model, to the values given in the code HARM code. In the version of the code that we used for our simulation the value of polytropic exponent was fixed to $\Gamma = 13/9$ to account for highly relativistic electrons in the fluid and mostly non-relativistic ions. In the present work we shall leave this value unchanged and check the resulted tori for consistency after having fixed the value of the polytropic constant K.[3] Restrictions on this parameter are com-

[3]Note that the values we obtain here for K are different from those used in the HARM simulation discussed later: there for each simulation K is computed separately via density value at the tori centre as given in Table 5 (see Witzany & Jefremov 2018, for details).

ing from the requirement that the resulting tori have mass which does not perturb the space-time metric, so that we can keep considering our problem on the background determined only by the black hole. The mass of the tori is given by:

$$\mathcal{M} := \int_V \rho u^t \sqrt{-g} \mathrm{d}^3 x \,, \tag{70}$$

From the requirement that $\mathcal{M} \ll M$ we obtain the restriction on K that

$$K \gg \frac{\Gamma - 1}{\Gamma} \left[\int_V u^t \left[\exp(W - W_s) - 1 \right]^{1/(\Gamma-1)} \sqrt{-g} \mathrm{d}V \right]^{\Gamma-1} =: K_m \,. \tag{71}$$

Besides the bulk mass being small in comparison to the mass of the gravitational field source we also need to demand that the gravitational forces associated with the matter inside the tori (the region we denote by V) are nowhere bigger than the gravitational tidal forces of the central source. Mathematically the necessary condition for that can be expressed by demanding that some characteristic scalar representing matter is much smaller than a characteristic curvature scalar. We have chosen this condition to be $\max_V [\rho^2/\mathrm{Kr}] \ll 1$, where Kr is the Kretschmann scalar of the metric, that in the Kerr case is equal to:

$$\mathrm{Kr} = R_{\alpha\beta\gamma\delta} R^{\alpha\beta\gamma\delta} = -96M^2 \frac{10a^6 - 180a^4 r^2 + 240a^2 r^4 - 32r^6}{+15a^2(a^4 - 16a^2 r^2 + 16r^4)\cos 2\theta + 6a^4(a^2 - 10r^2)\cos 4\theta + a^6 \cos 6\theta} \,. \tag{72}$$

Here $R^{\alpha}{}_{\beta\gamma\delta}$ is the Riemann tensor of the space-time. Hence the condition on K will be

$$K \gg \frac{\Gamma - 1}{\Gamma} \max_V \left[\frac{(\exp[W - W_s] - 1)}{\mathrm{Kr}^{(\Gamma-1)/2}} \right] =: K_{\mathrm{Kr}} \,. \tag{73}$$

We can then combine both of these conditions in one:

$$K \gg \max\{K_m, K_{\mathrm{Kr}}\} \,. \tag{74}$$

The values of the resulting restricting parameters K_m and K_{Kr} are given in the Table 3. It is seen from it that if we want to assume a certain value for K which will be the same for all the tori, then, in order to satisfy the inequality (74) it must be of the order of unity or greater. Setting for simplicity $K = 1$

Table 3: Restricting values for the parameter K (see explanation in the text) arising from the mass condition, K_m and from the tidal-forces condition, $K_{\rm Kr}$, for the tori between $r_{\rm in} = 5M$ and $r_{\rm out} = 12M$ in Kerr (Table 2) and with $\Gamma = 13/9$.

κ	$K_m, 10^{-2}\left[M^{\frac{8}{9}}\right]$	$K_{\rm Kr}, 10^{-2}\left[M^{\frac{8}{9}}\right]$
-1.11	13.27	4.26
-1.	12.40	4.04
-0.9	11.64	3.85
-0.79	10.85	3.64
-0.69	10.16	3.46
-0.58	9.43	3.26
-0.48	8.80	3.09
-0.37	8.13	2.90
-0.27	7.54	2.73
-0.16	6.92	2.55
-0.06	6.38	2.39
0.05	5.80	2.22
0.15	5.30	2.07
0.26	4.77	1.90
0.36	4.31	1.76
0.47	3.82	1.60
0.57	3.40	1.46
0.68	2.95	1.30
0.78	2.56	1.17
0.89	2.16	1.02
0.99	1.81	0.89
1.1	1.45	0.75
1.2	1.14	0.63
1.31	0.84	0.50

Table 4: Bulk mass $\mathcal{M}$ and the coolness parameter T/μ for the tori with $K = 1$ and $\Gamma = 13/9$.

κ	$\mathcal{M}, 10^{-3}[M]$	$T/\mu, 10^{-3}$	κ	$\mathcal{M}, 10^{-3}[M]$	$T/\mu, 10^{-3}$
-1.11	10.628	7.646	0.15	1.349	3.320
-1.	9.122	7.173	0.26	1.064	3.024
-0.9	7.921	6.765	0.36	0.846	2.763
-0.79	6.759	6.337	0.47	0.645	2.485
-0.69	5.830	5.965	0.57	0.495	2.240
-0.58	4.933	5.573	0.68	0.360	1.978
-0.48	4.217	5.230	0.78	0.262	1.748
-0.37	3.527	4.867	0.89	0.178	1.504
-0.27	2.980	4.549	0.99	0.120	1.289
-0.16	2.456	4.211	1.1	0.073	1.063
-0.06	2.044	3.914	1.2	0.043	0.867
0.05	1.653	3.599	1.31	0.021	0.665

we can now compute tori masses using the formula (70). Assuming further the equation of state of ideal monoatomic gas:

$$p = \frac{\rho}{\mu} T \,, \tag{75}$$

where μ is mass of the particles in the gas, we can compute temperature T which is then given by

$$T = K \rho^{\Gamma - 1} \mu \,. \tag{76}$$

For the self-consistency test of the assumptions we made about the polytropic index Γ we should now rather look not at the absolute values of the temperature but at the coolness parameter of the gas given as T/μ. Table 4 gives both values for the tori mass and for the coolness parameter and Figure 20 presents tori mass as a function of parameter κ. We observe from them that both the test character of our tori is satisfied by the choice of K we made and the T/μ relation in its maximum justifies our considerations about the value of Γ we made in this Chapter.

Figure 20: Tori mass computed with $\Gamma = 13/9$ and $K = 1$ for the fluid configurations with the parameter values from Table 2 as a function of parameter κ.

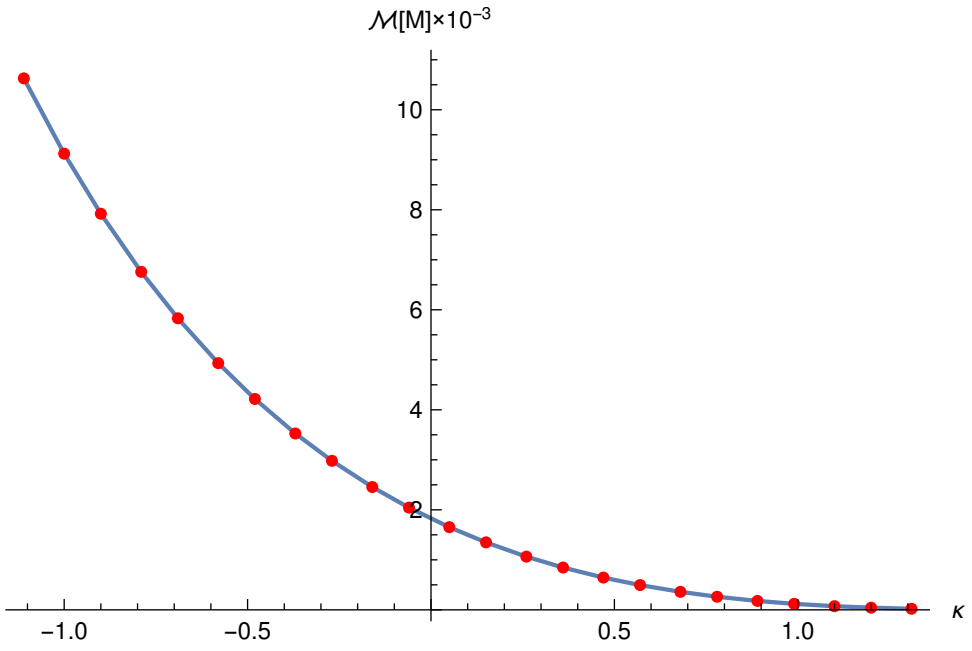

Table 5: Simulation parameters.

Variable	Value
Black hole spin a	$0.9375M$
Resolution	512×512
Inner radius of torus	$5M$
Outer radius of torus	$12M$
Inner boundary of simulation	$0.98r_{\rm hor}$
Outer boundary of simulation	$40M$
Polytropic exponent Γ	$13/9$
Polytrope constant K	$\rho_{\rm cen}^{1-\Gamma}$

5 Perfect fluid tori as initial data for accretion simulations

In this Chapter I shall summarise the results of the part of our work (Witzany & Jefremov 2018) where the new solutions were applied in accretion simulations. It is clear on the first glance that the perfect fluid tori represent essentially overidealised flows of matter around a gravitating source which on their own cannot model accretion simply because as it was assumed in the Chapter 4 the velocity of the fluid does not have the r-component. Suggesting some small values for it Kozłowski, Jaroszyński & Abramowicz (1978) estimated the accretion rate for the Polish Doughnuts considering only configurations that have a cusp and the W_s-surface passing through it (i. e. the fluid reaching the cusp point). The main interest of these solutions for *modern* astrophysics is that they can be used as easy-to-construct initial configurations for more sophisticated and therefore only numerically computable models. Generally, as initial configurations for simulations, should they be given analytically, one applies either Polish Doughnuts with constant specific angular momentum or Fishbone-Moncrief tori. Our tori by allowing one to cover a much wider spectrum of initial conditions including both nearly Keplerian as well as highly non-Keplerian specific angular momentum distributions may serve to model very different physical set-ups and stages of accretion-disk evolution.

In our work we have implemented the constructed 24 tori as initial perfect fluid configurations and evolved them within the HARM code (Gammie et al.

Figure 21: Development in time of mass accretion rate for the tori with selected values of the parameter κ and the corresponding parameters from Table 2.

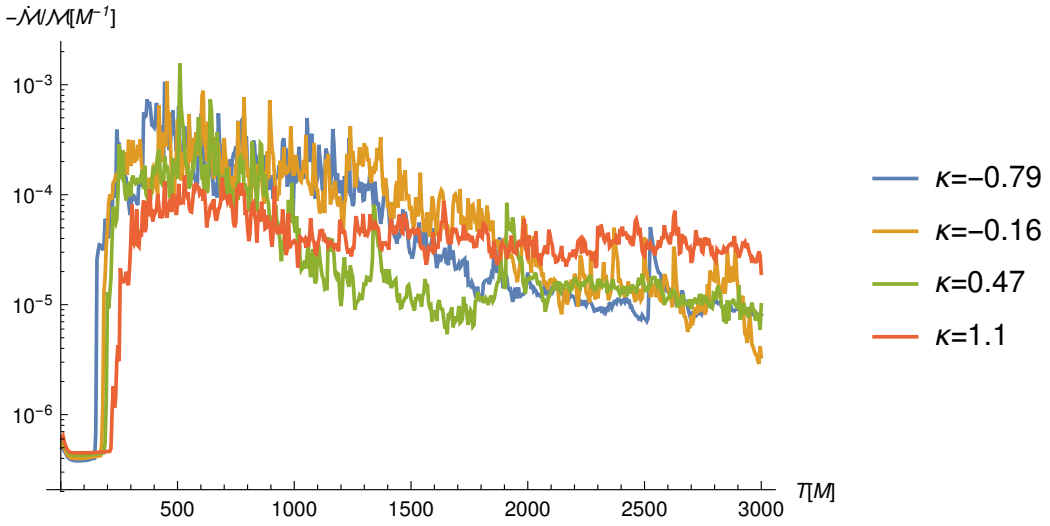

2003, McKinney & Gammie 2004, Noble et al. 2006) for two-dimensional accretion simulations. The working principle of HARM is such that it takes an initial perfect fluid configuration, perturbs it by adding some small randomly distributed density and magnetic field irregularities and lets the perturbed configuration evolve according to the equations of ideal GRMHD (Gammie et al. 2003). Table 5 summarises general parameters of our simulation.

On Figure 21 we observe development in time of the mass accretion rate for some values of κ. Figures 22 and 23 illustrate the mass-density distribution development inside the tori for a particular chosen value of $\kappa = 0.47$. Figure 24 represents the overall decrease of integral characteristics $\mathcal{M}, \mathcal{E}, \mathcal{L}$ of the tori due to accretion. The role of the parameter κ can be detected already from the Figure 21: whereas in the late stages of evolution its influence does not seem to be noticeable, the initial ones clearly differ depending on its value. Accretion rates of energy, angular momentum and mass averaged over the time $0 - 500M$ (Figure 25) and $2000M - 3000M$ (Figure 26) confirm this observation. Correlation between the parameter κ and the accretion rates observed in the first $500M$ of time in the simulation can be explained by the fact that, as seen from the Figure 27, this parameter is closely related to the frequency of the fastest-growing mode of *magnetorotational instability* MRI

Figure 22: Development of mass density ($\rho/\rho_{\max}$) inside the torus initially situated between $r_{\text{in}} = 5M$ and $r_{\text{out}} = 12M$ with $\kappa = 0.47$ at early orbital times t. Blue colour corresponds to the lower densities, the red colour to the bigger ones. $\rho_{\max}$ is defined for each step of simulation separately. The left picture shows initial toroidal configuration before turbulence develops. The right one pictures the early stage of accretion where the disk is destabilised and big portions of matter are accreted by the BH [cf. Figure 21].

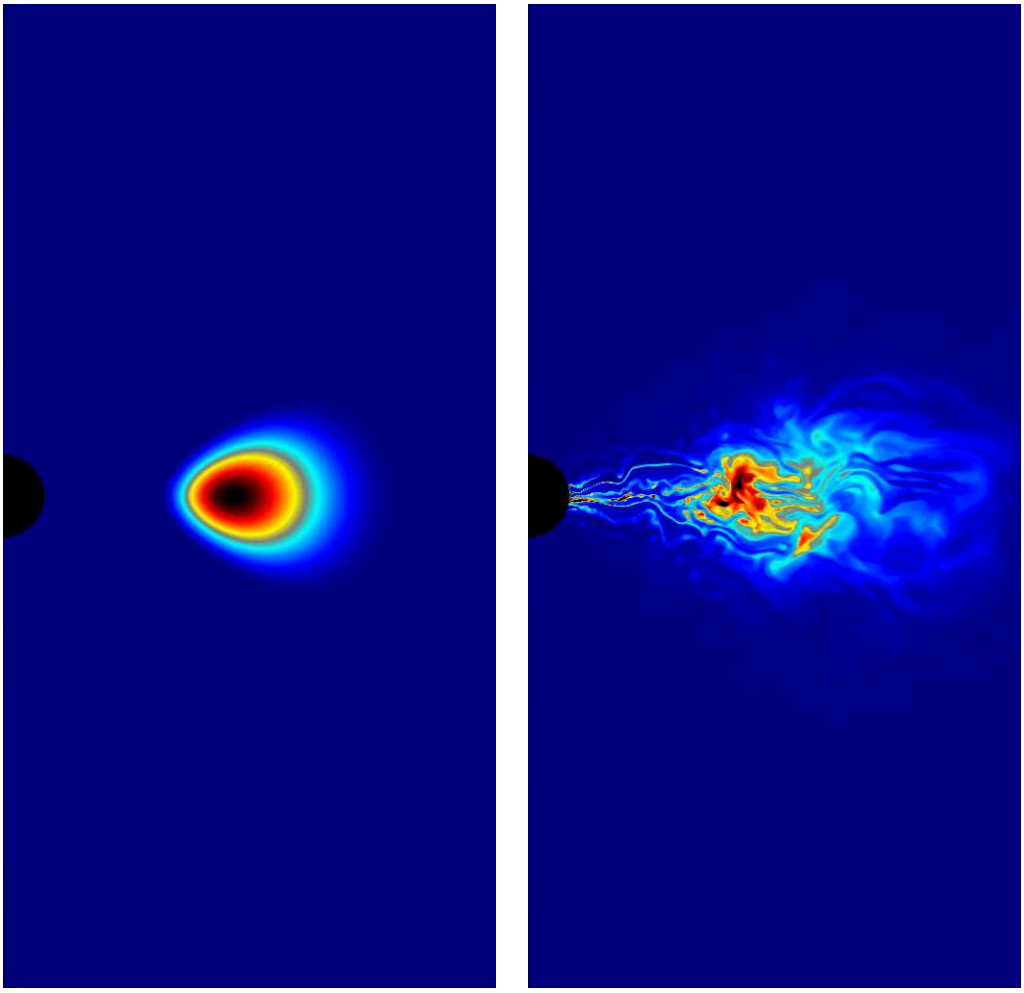

(a) $t = 10M$ (b) $t = 510M$

Figure 23: Late stages of development of mass density ($\rho/\rho_{\max}$) for the torus from Fig. 22. The left snapshot depicts the torus at mass accretion peak at $t = 1910M$. The right snapshots corresponds to the asymptotic state of the disc with nearly constant mass accretion rate.

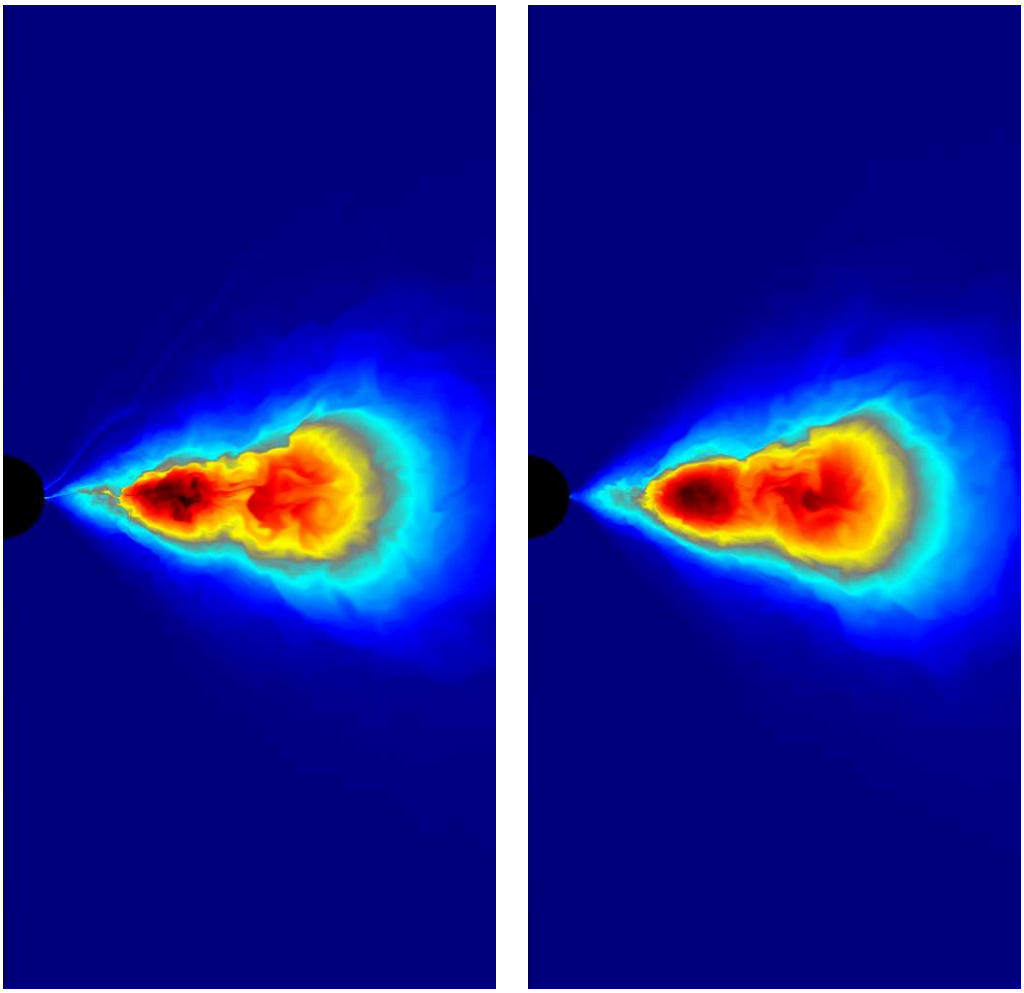

(a) $t = 1910M$ (b) $t = 2160M$

Figure 24: The decrease of integral characterstics $\Delta\mathcal{M}, \Delta\mathcal{E}, \Delta\mathcal{L}$ of the tori after the simulation time ($t = 3000M$) with respect to their initial value $\mathcal{M}_\mathrm{i}, \mathcal{E}_\mathrm{i}, \mathcal{L}_\mathrm{i}$ as a function of parameter κ.

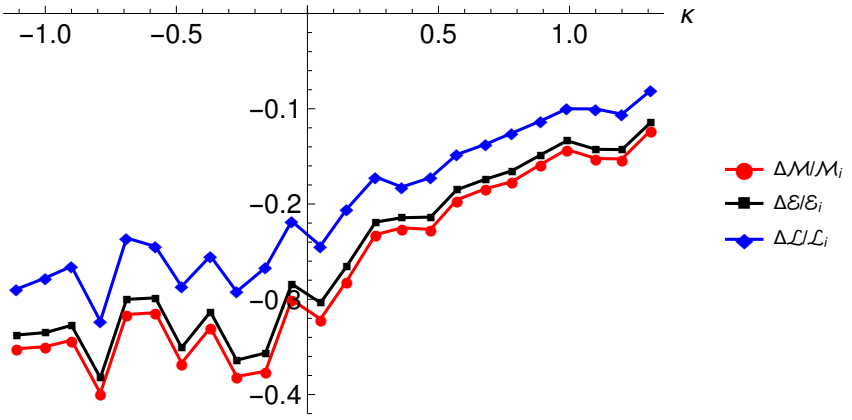

Figure 25: Accretion rates of mass, energy and angular momentum averaged over first $500M$ of the simulation in dependence on the parameter κ

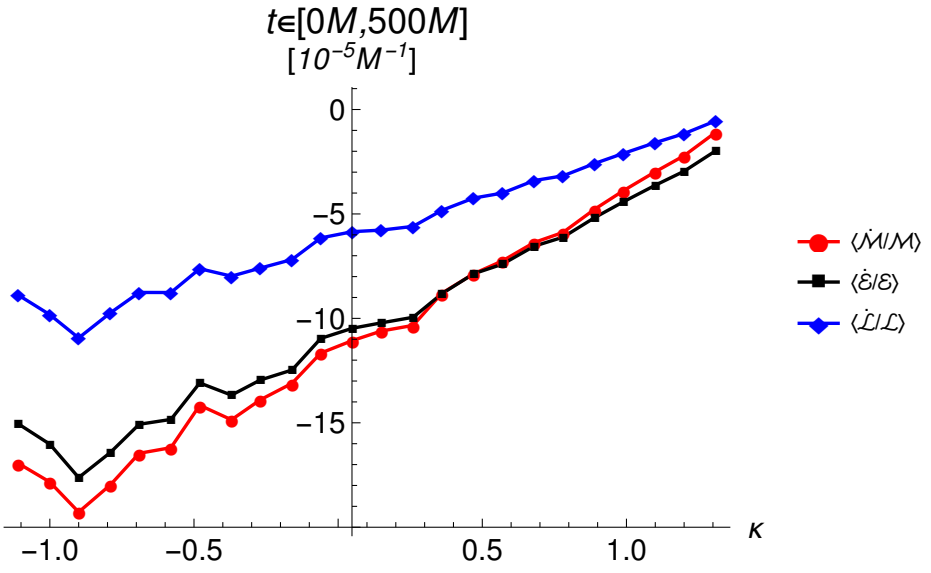

Figure 26: Accretion rates of mass, energy and angular momentum averaged over the last $1000M$ of the simulation in dependence on the parameter κ

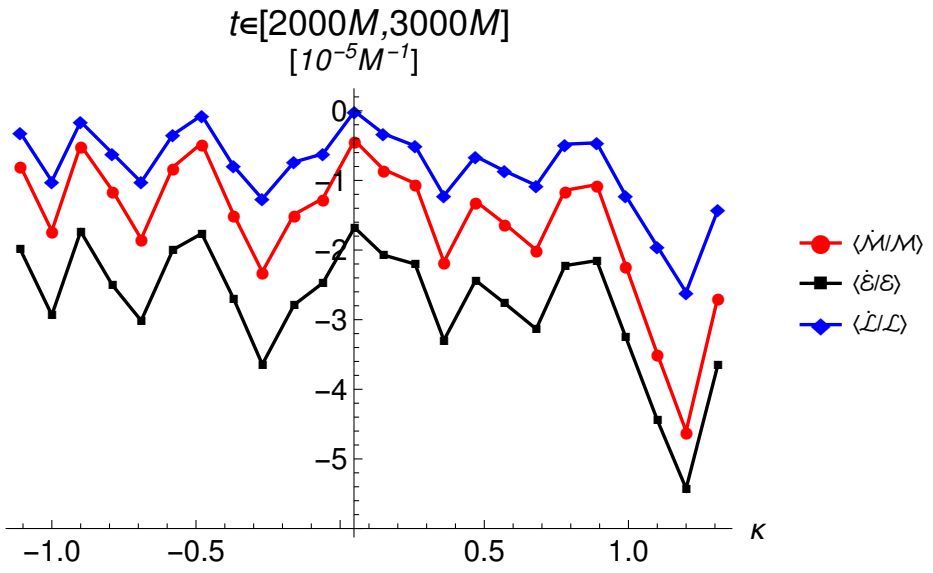

$\omega_{\max}$ in the disk as given by the formula (Gammie 2004):

$$-\omega_{\max}^2 = \frac{1}{2}\sigma_{\mu\nu}\sigma^{\mu\nu} \tag{77}$$

with the right-hand side being the shear scalar (Semerák 1998):

$$\frac{1}{2}\sigma_{\mu\nu}\sigma^{\mu\nu} = \frac{1}{4}\frac{\sqrt{g_{t\phi}^2 - g_{tt}g_{\phi\phi}}}{(g_{tt} + g_{t\phi}\Omega + g_{\phi\phi}\Omega^2)^2}\left[(\Omega_{,r})^2 g^{rr} + (\Omega_{,\theta})^2 g^{\theta\theta}\right] . \tag{78}$$

Thus, we can offer an explanation that the tori with stronger MRI growth, i. e. those corresponding to the lower values of parameter κ, are developing turbulence faster than those with the weaker one. Turbulence in turn destabilises the configuration and brings about an increase in accretion rate of matter. Indeed, the results from Figure 24 can be explained by this assumption if we compare *turbulently-quiescent* tori with higher values of κ with those with lower ones where the turbulence plays a big and not (at least easily) quantifiable role. In the late stages of the evolution in all the disks turbulence enters into non-linear regime and any visible dependence on the

Figure 27: The growth rate of the fastest-growing mode of MRI evaluated at the pressure maximum of the tori [at the point $(r = r_{\rm cen}, \theta = \pi/2)$] as a function of the parameter κ.

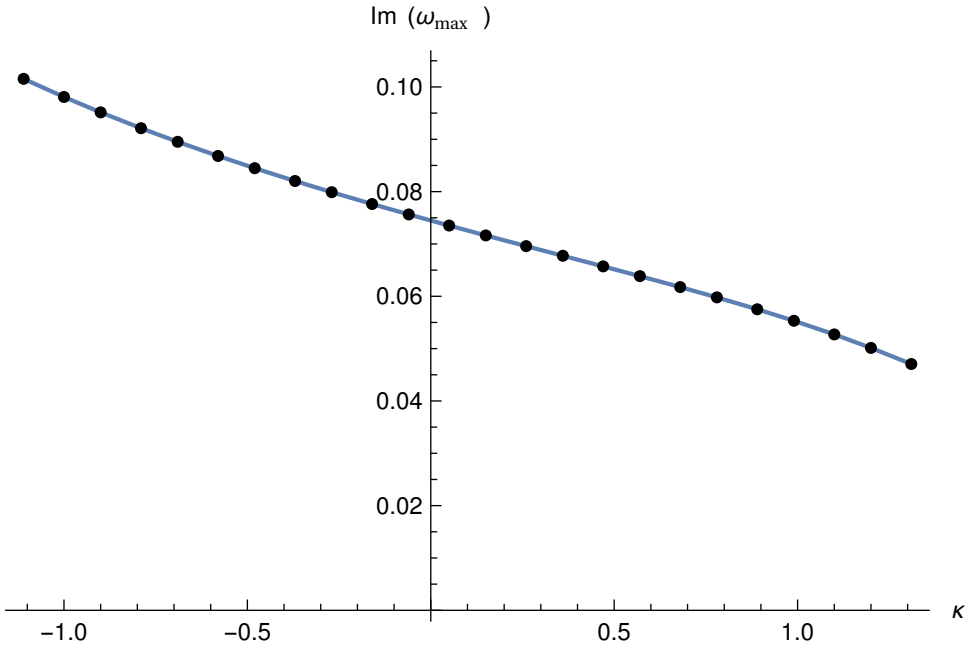

initial MRI growth rate estimates gets erased (Figure 26). The latter argument can also explain why we see deviation from this dependence already for the first $500M$ of simulation time for the lowest values of κ: the very thick tori corresponding to them enter the non-linear mode of turbulence very quickly and thus cease to be described by the linear approximation characterised by $\omega_{\max}$.

6 Polish Doughnuts in NUT space-time.

The construction of perfect fluid tori in NUT space-time is quite straightforward and follows the procedure given in the Chapters above. Our purpose in this Chapter will be not to investigate the changes in their form caused by different parametrisations of the tori themselves as it was for the tori in Kerr but rather to study the principal influence that *parameters of the space-time* may have on those configurations. We shall, therefore, in what follows restrict ourselves to the most widely-used and well-known case of Polish Doughnuts with constant specific angular momentum $\ell = \ell_0 = \text{const}$.

As it was mentioned this case corresponds to the parameters of the tori having values $\kappa = 0$ and $\lambda = 0$ and we need to use the expression (66) for L with Ω from (55). The effective potential is then written as:

$$W = -\frac{1}{2}\ln\left(\frac{\Delta\Sigma_n \sin^2\theta}{\Sigma_n^2 \sin^2\theta - \Delta(\ell - 2nC - 2n\cos\theta)^2}\right). \tag{79}$$

We observe that the way how the Manko-Ruiz constant enters the effective potential allows one to absorb it into ℓ by redefining its values $\ell' = \ell + 2nC$ as it was discussed in the introduction of the NUT metric. We can, therefore, without restricting generality set it as $C = 0$. For any different value of C the equipotential surfaces will remain where they stay in this case only they will correspond to respectively different values of specific angular momentum.

As before we shall construct and compare our tori by giving their inner- and outermost radii r_{in} and r_{out}. However, since the symmetry of the tori with respect to the equatorial plane is broken we cannot assume $\theta = \pi/2$ for the azimuthal coordinate of the edges as we did in the equation (67) for Kerr. In order to fix the parameters W_s and ℓ we need then to leave the θ coordinate undefined in (67) and add a corresponding condition to restrict it. The resulting system is

$$\begin{cases} W(r = r_{\text{in}}, \theta; \ell) = W(r = r_{\text{out}}, \theta; \ell)\,, \\ W(r = r_{\text{out}}, \theta; \ell) = W_s\,, \\ \partial_\theta W = 0 \end{cases} \tag{80}$$

and as usual the condition (68) must be satisfied. The last equation of the system (80) has a solution

$$\cos\theta = \frac{2n}{\ell}$$

Table 6: Parameters of the Polish Doughnuts in NUT and Kerr space-times with the equipotential surface $W = W_s$ passing through $r_{\rm in} = 7M$ and $r_{\rm out} = 12M$.

$n[M]$	$a[M]$	$\ell[M]$	$W_s, 10^{-2}$
0	0	3.85	4.62
0.2	0	3.89	4.60
0.4	0	4.02	4.55
0.6	0	4.22	4.45
0	0.2	3.76	5.44
0	0.6	3.58	7.65

which is equivalent to the expression (28) meaning that for a fixed value of the parameter ℓ found by solving the first 2 equations of the system the outer and the inner edge of the torus lie on the same cone as where the torus' centre, that moves on a geodesics, does. Substituting this result into the first two equations of (80) we obtain the parameters of the tori. For different values of the NUT parameter we list them in the Table 6, where for comparison we also give some results for the Kerr space-time. Otherwise, if instead of fixing $r_{\rm in}$ and $r_{\rm out}$ we fix ℓ and W_s, then $r_{\rm in}$ and $r_{\rm out}$ are found by the intersections of the cone with the surface $W = W_s$ and the centre of the torus $r_{\rm cen}$ by cone's intersection with the surface of the geodetic circular orbits given by (23). Figure 28 illustrates the differences in structure of W in the NUT metric in comparison to Schwarzschild. On the basis of the Table 6 we construct Polish Doughnuts lying between $r_{\rm in} = 7M$ and $r_{\rm out} = 12M$ in the NUT and Kerr metrics (Figure 29).

Obtaining the density distribution in NUT metric follows in all detail the derivation we presented for the Kerr case. Once again having tentatively assumed some value for the polytropic exponent ($\Gamma = 13/9$ as previously) we fix the polytropic constant K by the condition (74) and for the Kretschmann scalar in NUT we have the expression:

$$\mathrm{Kr} = \frac{48\left((M^2-n^2)(r^6-15n^2r^4+15n^4r^2-n^6)+4Mn^2r(3r^4-10n^2r^2+3n^4)\right)}{(r^2+n^2)^6}\,. \tag{81}$$

The resulting restricting values for K are listed in the Table 7. On them we observe that as before the condition $K \gg \max\{K_m, K_{\rm Kr}\}$ is well satisfied with the choice we did in the Chapter 4, i. e. $K = 1$. With the thermo-

Figure 28: Equipotential surfaces for the effective potential W from (79) with $\ell = 3.9M$ in the NUT space-time with $n = 0.3M$ and in Schwarzschild, $(n = 0)$. In the NUT case the inner-, $r_{\rm in}$, and outermost, $r_{\rm out}$, radii of any closed equipotential surface $W = W_s$ are given by its intersections with the cone $\cos\theta = 2n/\ell$ (orange line); the local maximum $(r_{\rm cen}, \theta(r_{\rm cen}))$ and the saddle point $(r_{\rm cusp}, \theta(r_{\rm cusp}))$ of W are found by the cone's intersections with the surface of geodetic circular orbits (dashed blue line) and denoted by thick black dots on the both pictures. (In Schwarzschild the above considerations are trivial.)

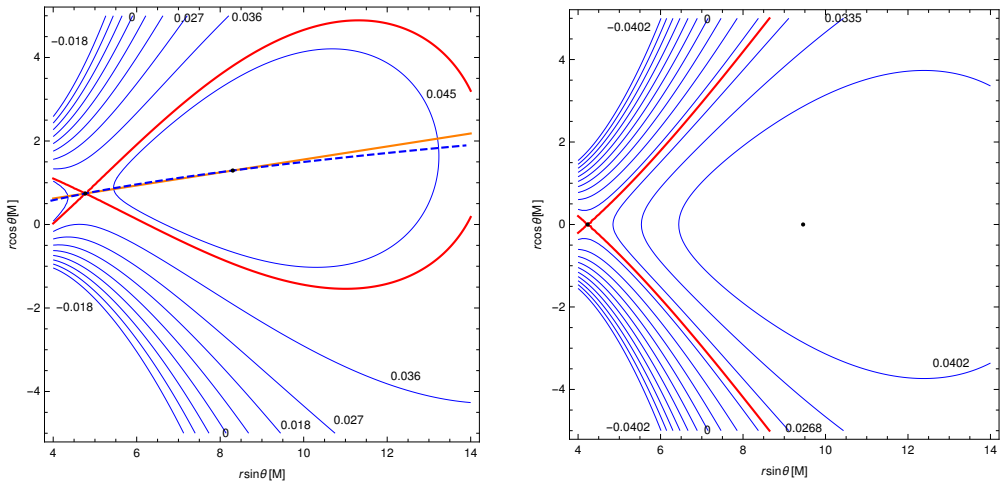

(a) NUT, $n = 0.3M$

(b) Schwarzschild, $n = 0$

Table 7: Restrictions on parameter K for the Polish Doughnuts in Kerr and NUT space-times with configuration parameters from Table 6.

$n[M]$	$a[M]$	$K_m, 10^{-3}\left[M^{\frac{8}{9}}\right]$	$K_{\mathrm{Kr}}, 10^{-3}\left[M^{\frac{8}{9}}\right]$
0	0	9.21	6.25
0.2	0	8.93	6.12
0.4	0	8.13	5.74
0.6	0	6.82	5.08
0	0.2	10.98	7.14
0	0.6	14.14	8.63

Table 8: Total mass $\mathcal{M}$ and maximal temperature pro molecule mass T/μ for the Polish Doughnuts in Kerr and NUT space-times with parameters from Table 6.

$n[M]$	$a[M]$	$\mathcal{M}, 10^{-5}[M]$	$T/\mu, 10^{-4}$
0	0	2.625	7.679
0.2	0	2.453	7.520
0.4	0	1.983	7.032
0.6	0	1.337	6.183
0	0.2	3.905	8.848
0	0.6	6.900	10.798

dynamics being thus fixed we compute the mass of the tori $\mathcal{M}$ and their temperature per molecule mass, see Table 8.

6.1 A note on accretion simulations in NUT

As with the newly obtained perfect fluid solution, so also with the Polish Doughnuts in the NUT spacetime we wanted to perform a simulation of the accretion process to get results that would be more relevant for the observational expectations from these black holes. We came, however, to the conclusion that the HARM code as it is given cannot be used for such simulations. The reason for this is the fact that the so-called "primitive variables" which are updated at each time step during the simulation, in particular those characterising magnetic field and velocity of the fluid, are computed with respect to the *normal-observer* covector field $n_\mu = (1/\sqrt{g^{tt}}, 0, 0, 0)$ (see Noble

Figure 29: Polish Doughnuts in NUT and Kerr space-times with their edges at $r_{\text{in}} = 7M$ and $r_{\text{out}} = 12M$ and parameters from the Table 6.

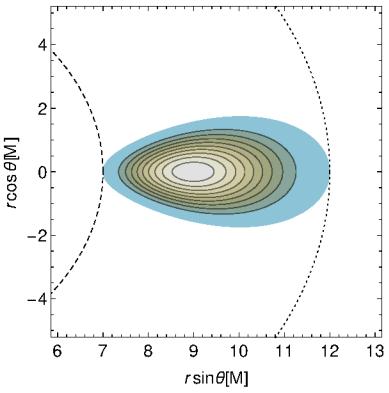

(a) Schwarzschild

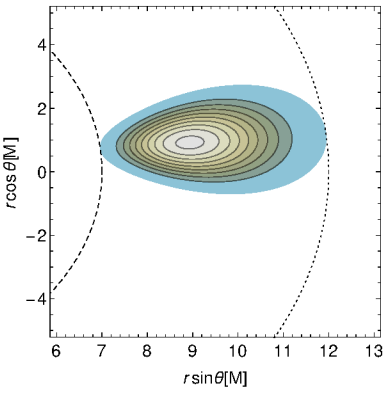

(b) NUT, $n = 0.2M$

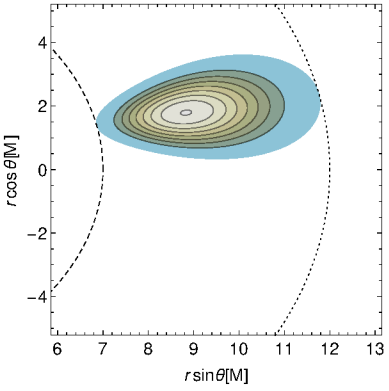

(c) NUT, $n = 0.4M$

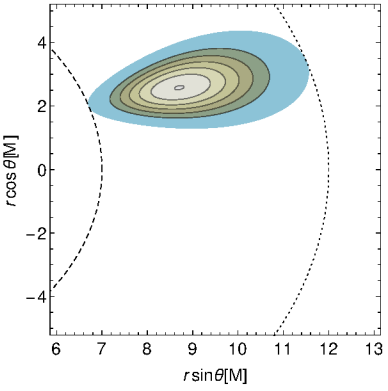

(d) NUT, $n = 0.6M$

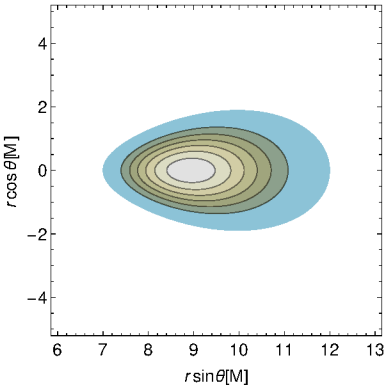

(e) Kerr, $a = 0.2M$

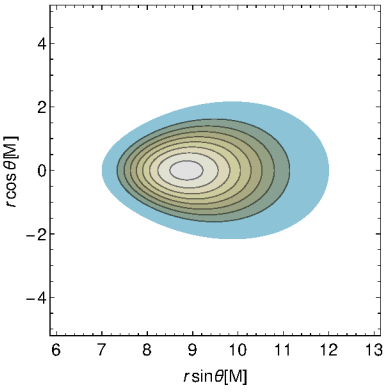

(f) Kerr, $a = 0.6M$

et al. 2006, with the corresponding metric signature). The NUT spacetime, as it was discussed, contains causality violating region(s) around at least one of its axes where g^{tt} changes its sign, becomes negative in our notation, and the covector field n_μ complex. This is a manifestation of the fact that the space-time is not globally hyperbolic: hypersurfaces $t = \text{const.}$ are no longer spacelike in the causality violating region and the initial-value problem as implemented in the HARM code cannot be well-posed.

Another issue that arises in connection with accretion simulations in NUT is the boundary condition at the conical singularity. The one applied in the HARM code (see McKinney & Gammie 2004, Noble et al. 2006) was given inside the black hole in the Kerr-Schild coordinates which are smooth on its event horizon. However, since the conical singularity is a *physical* singularity, not a coordinate one as that at the event horizon in Boyer-Lindquist coordinates, there are no coordinate systems that would be smooth on it. To solve this issue one would probably need to understand the physical nature of this singularity.

With all this I believe that HARM code cannot be used for accretion simulations in the NUT spacetime. The afore-mentioned problems raise doubts of whether it is possible to perform any meaningful accretion simulation in NUT at all.

7 Spin-induced advance in circular orbits in Kerr

In this section I will summarise results of my parallel research that may be relevant as a preliminary study for the problem of accretion of particles having classical spin. As it was shown in the previous sections, the positions $r_{\rm ph}, r_{\rm mb}$ and $r_{\rm ms}$ play a very important role in structure of the geometrically thick tori especially for the case with $\ell = \text{const}$. For the Keplerian thin accretion disks such as considered by Novikov & Thorne (1973) the role of $r_{\rm ms}$ is even more significant since it defines the inner edge of the accretion disk and consequently the energetic output of it. In our works (Jefremov et al. 2015, Tsupko et al. 2016) we have considered the influence of the proper angular momentum (classical spin) of a classical test particle on its circular orbits and especially on the last stable one.

Motion of a classical test particle with spin is governed by the Matthisson-Papapetrou-Dixon equations (Mathisson 1937, Papapetrou 1951, Dixon 1970)

$$\begin{aligned} \frac{Dp^\mu}{D\tau} &= -\frac{1}{2} R^\mu{}_{\nu\rho\sigma} v^\nu S^{\rho\sigma}, \\ \frac{DS^{\mu\nu}}{D\tau} &= p^\mu v^\nu - p^\nu v^\mu. \end{aligned} \tag{82}$$

Here $D/D\tau$ denotes the covariant derivative along particle's trajectory, τ is an affine parameter of the orbit, $R^\mu{}_{\nu\rho\sigma}$ is the Riemannian tensor, p^μ and v^μ are 4-momentum and 4-velocity of the test particle, $S^{\rho\sigma}$ is its spin-tensor.

Already in the first works (see e. g. Corinaldesi & Papapetrou 1951) deriving these equations it has been noticed that an additional spin supplementary condition (SSC) need be imposed to close the system. The arbitrarity in choice of it is connected with the arbitrarity in choosing the referential worldline whereabout one measures spin [see (Kyrian & Semerák 2007, Steinhoff 2011) for more recent discussion]. In our consideration we use the Tulczyjew spin condition (Tulczyjew 1959, Dixon 1970) given by

$$p_\mu S^{\mu\nu} = 0. \tag{83}$$

The system of equations (82) with (83) in a general spacetime admits of two conserved quantities: particle's mass $m^2 = p^\mu p_\mu$ and the magnitude of its specific spin $s^2 = S^{\mu\nu} S_{\mu\nu}/(2m^2)$ (Saijo et al. 1998). We fix the affine parameter τ by demanding that:

$$v^\mu p_\mu / m = 1. \tag{84}$$

Figure 30: Possible orientations of the vectors of the total angular momentum of the particle **J**, its spin **s** and the spin of the black hole **a** for the particle moving in the equatorial plane of the black hole.

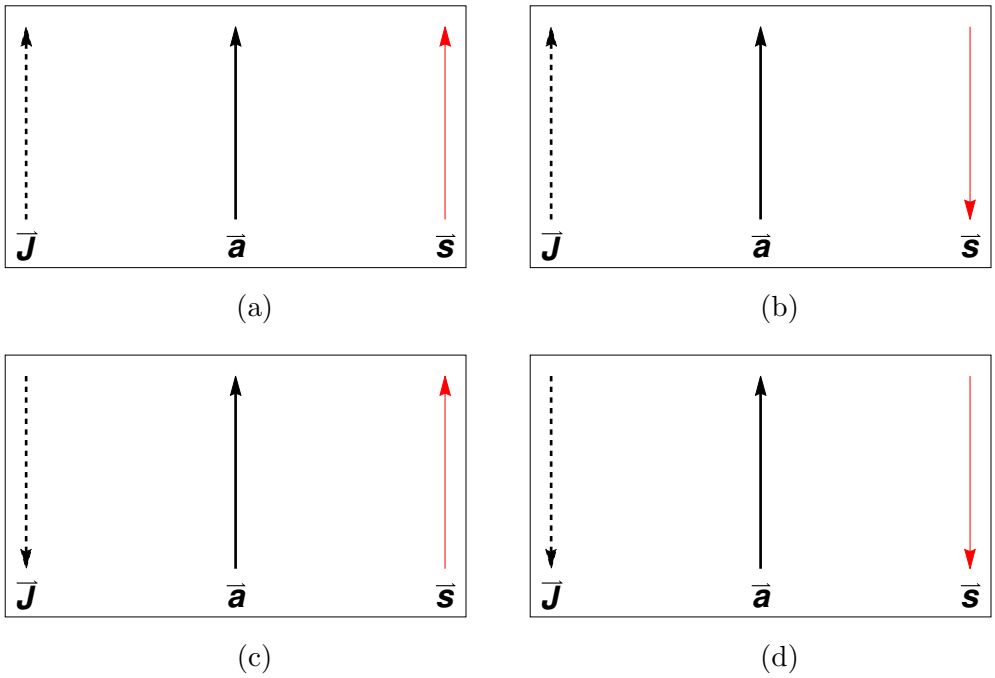

In Kerr geometry owing to its symmetries also for the case of particles having spin energy E and total angular momentum (i. e. including both orbital and spin part) along z-axis ($z \equiv r\cos\theta$) J_z are conserved. We shall further restrict our consideration of the problem to the motion in the equatorial plane ($\theta = \pi/2$), which means that the total angular momentum has its components only along z. Another important point is that for the motion in this plane all components of the spin tensor are described by its magnitude s with spin vector being parallel to the z-axis when s is positive and antiprallel when it is negative, i. e. spin of the particle, spin of the BH and the total angular momentum are collinear (see Figure 30).

The corresponding equations of motion are written as (Saijo et al. 1998):

$$
\begin{aligned}
&(\Sigma_s \Lambda_s \dot{r})^2 = R_s, \\
&\Sigma_s \Lambda_s \dot{t} = a\left(1 + \frac{3Ms^2}{r\Sigma_s}\right)[J - (a+s)E] + \frac{r^2+a^2}{\Delta} P_s, \\
&\Sigma_s \Lambda_s \dot{\varphi} = \left(1 + \frac{3Ms^2}{r\Sigma_s}\right)[J - (a+s)E] + \frac{a}{\Delta} P_s,
\end{aligned}
\tag{85}
$$

where

$$
\begin{aligned}
&\Sigma_s = r^2\left(1 - \frac{Ms^2}{r^3}\right), \\
&\Lambda_s = 1 - \frac{3Ms^2 r[-(a+s)E + J]^2}{\Sigma_s^3}, \\
&R_s = P_s^2 - \Delta\left\{\frac{\Sigma_s^2}{r^2} + [-(a+s)E + J]^2\right\}, \\
&P_s = \left[r^2 + a^2 + \frac{as(r+M)}{r}\right]E - \left(a + \frac{Ms}{r}\right)J.
\end{aligned}
\tag{86}
$$

Here $\dot{x} \equiv \mathrm{d}x/\mathrm{d}\tau$, E is the conserved energy per unit particle mass, and $J = J_z/m$ is the conserved total angular momentum per unit particle mass.

7.1 Small-spin corrections to the geodetic circular orbits

Using the standard procedure for finding last stable circular orbits we define the effective potential for the radial motion

$$
V_{\mathrm{sp}}(r; J, E) = \mathfrak{a}E^2 + \mathfrak{b}J^2 - 2\mathfrak{c}EJ - \mathfrak{d}, \tag{87}
$$

where

$$\begin{aligned}
\mathfrak{a} &= \left\{ \left[r^2 + a^2 + \frac{as(r+M)}{r} \right]^2 - \Delta(a+s)^2 \right\} / r^4, \\
\mathfrak{b} &= \left[\left(a + \frac{Ms}{r} \right)^2 - \Delta \right] / r^4, \\
\mathfrak{c} &= \left[\left(a + \frac{Ms}{r} \right) \left(r^2 + a^2 + \frac{as(r+M)}{r} \right) - \Delta(a+s) \right] / r^4, \\
\mathfrak{d} &= \Delta \left(1 - \frac{Ms^2}{r^3} \right)^2 / r^2
\end{aligned} \tag{88}$$

such that

$$\dot{r}^2 = V_{\rm sp}(r; J, E). \tag{89}$$

Then we require that both it and its two derivatives vanish

$$\begin{cases}
V_{\rm sp} = 0\,, \\
\dfrac{{\rm d}V_{\rm sp}}{{\rm d}r} = 0\,, \\
\dfrac{{\rm d}^2 V_{\rm sp}}{{\rm d}r^2} = 0
\end{cases} \tag{90}$$

and obtain the system of equations on three unknown characteristics of ISCO, E, J and r. [See system (50) in (Jefremov et al. 2015) given there in the variables $x := J - aE$ and $u := 1/r$]. This system cannot be solved analytically for the ISCO and in our work we used perturbative approach, assuming the value of spin to be small, which is indeed the case in the domain of applicability of the MPD equations. Having assumed for the variables in question the following ansatz:

$$\begin{aligned}
J &= J_0 + sJ_1, \\
E &= E_0 + sE_1 \\
r &= r_0 + sr_1,
\end{aligned} \tag{91}$$

we substituted it into the system (90) and developed the result in a series in s, retaining only linear terms in it. Thus we have obtained expressions for

Figure 31: Radii of the innermost stable circular orbit $r_{\rm ms}$ (left) and the value of linear spin correction to them r_1 (right) in Kerr space-time for different values of BH spin a. The negative values of parameter a correspond to the Kerr spacetime where for the positive direction of the z-axis the direction of the total angular momentum of the particle is chosen which is equivalent to switching from the orientation (a) to the orientation (d) in Figure 30 when entering the domain of negative a.

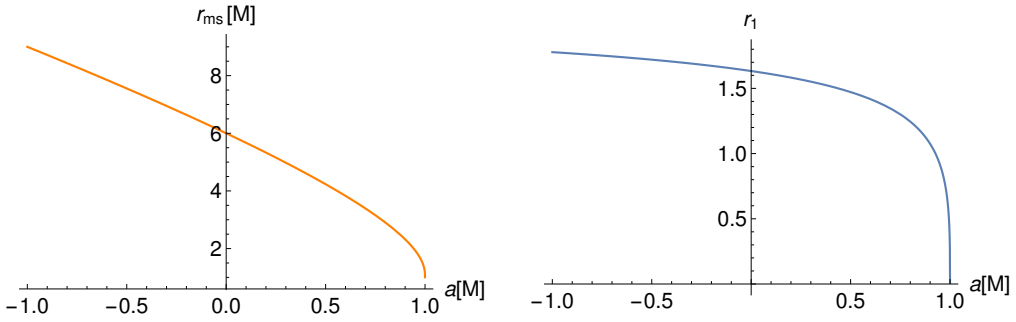

the spin corrections to these quantities:

$$
\begin{aligned}
E_0 &= \sqrt{1-\frac{2}{3}\frac{M}{r_0}},\\
J_0 &= \pm\frac{r_0}{\sqrt{3}} + a\sqrt{1-\frac{2}{3}\frac{M}{r_0}};\\
E_1 &= \mp\frac{1}{\sqrt{3}}\frac{M}{r_0^2},\\
J_1 &= \frac{2M^{1/2}r_0^{3/2} \mp a(3r_0+M)}{\sqrt{3}r_0^2},\\
r_1 &= -4\frac{a \mp \sqrt{Mr_0}}{r_0}.
\end{aligned}
\tag{92}
$$

Here components with the subscript 0 correspond to the geodetic values: r_0 is the solution of (12) and E_0, J_0 can be explicitly given by (9). Figure 31 illustrates the behaviour of the spin correction to the ISCO radii. We shall now specify this result to two extremal cases of the Kerr parameter a: $a \to 1$, the extreme Kerr BH, and $a \to 0$, the slowly rotating Kerr BH.

7.1.1 Extreme Kerr black hole

In the case of the extreme Kerr spacetime ($a \to M$) the last stable orbits of pro- and retrograde rotating particles are maximally separated from each other: in the first example $r_{\rm ms} = M$ in the second it is $r_{\rm ms} = 9M$. The retrograde case can straightforwardly be computed by using (92):

$$\begin{aligned} J_{\rm ms} &= -\frac{22\sqrt{3}}{9}M + \frac{82\sqrt{3}}{243}s, \\ E_{\rm ms} &= \frac{5\sqrt{3}}{9} + \frac{\sqrt{3}}{243}\frac{s}{M}, \\ r_{\rm ms} &= 9M + \frac{16}{9}s. \end{aligned} \tag{93}$$

In order to obtain the linearised expressions for the ISCO parameters in the prograde case, as is usually performed due to divergences that arise in calculations, we consider a BH slightly different from the extreme one, i. e. that with $a = (1-\delta)M$, where δ is some small parameter. Using (92), we get:

$$\begin{aligned} J_{\rm ms} &= \left(\frac{2}{\sqrt{3}} + \frac{2\times 2^{2/3}\delta^{1/3}}{\sqrt{3}}\right)M + \left(-\frac{2}{\sqrt{3}} + \frac{4\times 2^{2/3}\delta^{1/3}}{\sqrt{3}}\right)s, \\ E_{\rm ms} &= \left(\frac{1}{\sqrt{3}} + \frac{2^{2/3}\delta^{1/3}}{\sqrt{3}}\right) + \left(-\frac{1}{\sqrt{3}} + \frac{2\times 2^{2/3}\delta^{1/3}}{\sqrt{3}}\right)\frac{s}{M}, \\ r_{\rm ms} &= \left(1 + 2^{2/3}\delta^{1/3}\right)M - 2\times 2^{2/3}\delta^{1/3}s. \end{aligned} \tag{94}$$

Note that the relevance of retaining δ or spin terms in this result depends on the respective order of smallness of these parameters.

7.1.2 Slowly rotating Kerr black hole

The case of a slowly rotating Kerr BH, i. e. with $a \ll M$ requires to make some assumptions about the relation between a and s. Assuming that both of these parameters are of the same order of magnitude we need to take into account also the second order corrections. The method is analogous to that applied above to get (92) [see (Jefremov et al. 2015) for more detailed

description] and we obtain:

$$
\begin{aligned}
J_{\rm ms} &= \pm 2\sqrt{3}M - \frac{2\sqrt{2}}{3}a + \frac{\sqrt{2}}{3}s \mp \frac{11}{36\sqrt{3}}\frac{a}{M}s \mp \frac{4\sqrt{3}M}{27}\left(\frac{a}{M}\right)^2 \mp \frac{1}{4M\sqrt{3}}s^2,\\
E_{\rm ms} &= \frac{2\sqrt{2}}{3} \mp \frac{1}{18\sqrt{3}}\frac{a}{M} \mp \frac{1}{36\sqrt{3}}\frac{s}{M} - \frac{\sqrt{2}}{81}\frac{a}{M}\frac{s}{M} - \frac{5}{162\sqrt{2}}\left(\frac{a}{M}\right)^2 - \frac{5}{432\sqrt{2}M^2}s^2,\\
r_{\rm ms} &= 6M \mp 4\sqrt{\frac{2}{3}}a \mp 2\sqrt{\frac{2}{3}}s + \frac{2}{9}\frac{as}{M} - \frac{7M}{18}\left(\frac{a}{M}\right)^2 - \frac{29}{72M}s^2.
\end{aligned}
\tag{95}
$$

Again to estimate which terms here are relevant one needs to estimate the relation between a and s. The third term in the expression for $r_{\rm ms}$ gives us the idea of the character of spin-orbital interaction: it is attractive when they are aligned and repulsive when antiparallel. In the limit $a \to 0$ (95) reduces to the result of Favata (2011) for the Schwarzschild case.

7.1.3 Exact solutions for particles on circular orbits

In our paper (Jefremov et al. 2015) we have obtained corrections to the circular orbits characteristics E and J. However it is also possible to obtain exact solutions for them if we consider the first two equations of the system (90):

$$
\begin{cases}
\mathfrak{a}E^2 + \mathfrak{b}J^2 - 2\mathfrak{c}EJ - \mathfrak{d} = 0\\
\mathfrak{a}'E^2 + \mathfrak{b}'J^2 - 2\mathfrak{c}'EJ - \mathfrak{d}' = 0\,.
\end{cases}
\tag{96}
$$

Here prime denotes a derivative with respect to the r-component. Clearly this system is solvable analytically for E and J as unknowns for any form of the equation coefficients. The resulting solution is rather clumsy and non-instructive, so I shall not give it here. The development of it in a series on s gives the formulas (85) from (Jefremov et al. 2015).

7.1.4 Exact solutions for the ISCO in the extreme Kerr spacetime

Analysing numerical simulations of the problem Tanaka et al. (1996) suggested that in the extremal Kerr case the radius of the ISCO is not dependent on particle's spin for the prograde orbit. Using these considerations we have made an ansatz $r = M$ into the system (90) which enabled us to solve it

obtaining corresponding expressions for J and E. The exact solution is then

$$\begin{aligned} J_{\rm ms} &= 2\frac{M^2 - s^2}{M\sqrt{3 + 6s/M}}, \\ E_{\rm ms} &= \frac{M^2 - s^2}{M^2\sqrt{3 + 6s/M}}, \\ r_{\rm ms} &= M. \end{aligned} \tag{97}$$

Developing (97) in series in s, we get the linear in spin terms which are in agreement with (94) with $\delta = 0$.

7.2 Advance in efficiency due to spin

Mathematically speaking the models of Keplerian disks do not have an outer boundary and thus extend from infinity up to the ISCO or any other radius chosen to be their inner boundary. An important characteristic of these accretion models is their (energetic) efficiency ε: it gives the part of energy that a particle loses while gradually being accreted from infinity, where it rests and has its total energy equal to its mass, through a series of circular orbits all the way to the last one. This energy is lost through some dissipative processes and is of great importance for observations of accretion disks because it then is used to produce heat and radiation, i. e. the main observational characteristics of the disks (Novikov & Thorne 1973). Assuming now that this last orbit coincides with the ISCO the efficiency is given:

$$\varepsilon = 1 - E_{\rm ms}. \tag{98}$$

Figure 32a gives energetic efficiency as a function of Kerr parameter a. Maximal efficiency for the Kerr black hole is achieved when $a = 1$, i. e. for the extreme black hole. In our second work on the topic (Tsupko et al. 2016) we have computed advance in this quantity for the Schwarzschild and extreme Kerr case. The result is that the particles with spin being parallel to the BH spin on prograde orbits show increase in efficiency compared with the spinless case up to the linear order given by

$$\Delta\varepsilon = \frac{1}{\sqrt{3}} - \frac{M^2 - s^2}{M^2\sqrt{3 + 6s/M}} \approx \frac{1}{\sqrt{3}}\frac{s}{M}. \tag{99}$$

Figure 32b illustrates this advance for a particle having $\mathbf{s} \parallel \mathbf{a}$.

Figure 32: Efficiency of Keplerian accretion disks with their inner boundary located at $r_{\rm ms}$ (left) and the linear correction to it due to particle's spin in the Kerr space-time as a function of the Kerr parameter (right). For the correction to efficiency the particle's spin magnitude was chosen as $|s| = 0.01$ and spin direction as parallel to the BH spin: $\mathbf{s} \parallel \mathbf{a}$. The negative values of a have the same meaning as in Fig. 31.

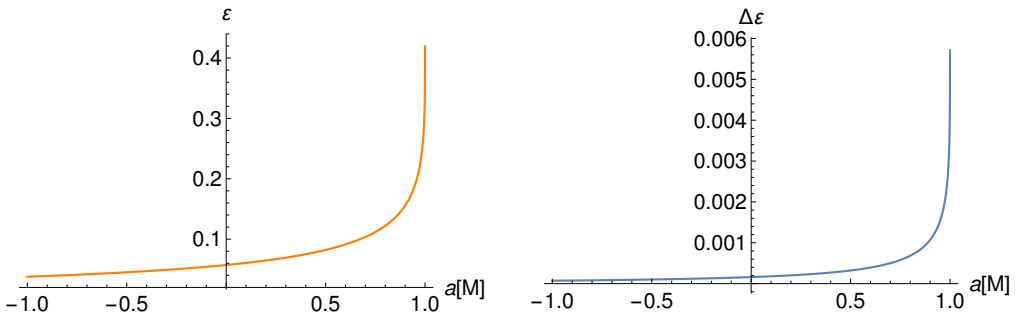

(a) (b)

7.3 Open questions

The results that we presented in this Chapter could be of much importance for accretion flows of spinning particles especially since we know that most elementary particles relevant for accretion models do have spin albeit quantum one. The questions that arise in this connection are in the first place whether such quantum systems with aligned spins are at least in principle possible to obtain on the astrophysically significant scales. And if yes, whether the results on classical spin description with MPD equations that we used here can shed some light on their motion. Speaking of practical realisation of such a system one can think of ionised gas whose atoms have non-compensated spin. Whether it is possible to obtain any significant effect from it that would not be washed out by thermalisation and would be non-negligible in comparison with all other effects (e. g. Coulomb interaction) present in such a system is yet another open question here.

The closest accretion set-up that could be described by the MPD equations directly is that of classical spinning particles. The easiest case one can think of here would be accretion of uniformly spinning dust with no interaction between particles to prevent collisions and chaotisation of their spins. It is to be investigated whether this accretion set-up can have any relevance to

the astrophysical processes. Speaking of fluid accretion the obtained results may be relevant for studies of motion of vortices and solitons in accreting flows which can probably be modelled as spinning particles.

The relevance and interpretation of the exact solution for the extreme Kerr black hole (97) should be done with great care in view of arbitrarity of possible choice of the SSC. In our work we have used the Tulczyjew's spin supplementary condition $S^{\mu\nu}p_\mu = 0$, which is up to linear order in spin equivalent to the Pirani's SSC $S^{\mu\nu}u_\mu = 0$ (Bini & Damour 2014). This fact gives some weight to the results on linear corrections to the orbital characteristics obtained in this Chapter. However the precise physical and observational role of the spin supplementary condition especially for the case of fluid accretion is not clear to the author and could be a subject of further investigation. Another issue that arises with respect to the obtained results is the meaning of the formula (97), which is exact in spin. This result on its own cannot tell us what really happens with the orbital characteristics in the orders higher than linear: that would demand computation of further multipole-momenta tensors (Dixon 1974, Steinhoff & Puetzfeld 2010) whose influence will be of the same order as that of the higher powers of s.

Concluding this Chapter it remains to mention that the best setup where the MPD equations and the obtained solutions can be relatively straightforwardly applied is motion of a spinning spherically symmetrical object around a considerably more massive one. In astrophysical context this seems to correspond perfectly to the problem of motion of a pulsar or any rapidly rotating star in vicinity of a supermassive black hole. Indeed, in this case the main assumptions concerning masses and spin magnitudes are fulfilled and as tidal forces exhibited by such a black hole on the neutron star are relatively mild one should not expect its major deformations. The obtained results then can give more precise parameters of the orbit of the rotating object.

Concluding remarks

The new ansatz for the function $\ell = \ell(\Omega)$ which allows one to get analytical expressions for the angular velocity field for barotropic fluids in circular motion around Kerr black holes was presented in the present work following our paper (Witzany & Jefremov 2018). With this ansatz we obtained new toroidal configurations of the perfect fluid. These models now enable one to model essentially different accretion patterns with the disks being nearly Keplerian and relatively thin and stabilised with respect to the Rayleigh-Taylor instability and MRI as well as highly non-Keplerian, thick tori, unstable with respect to both of these instabilities. To investigate the behaviour of the obtained toroidal solutions within some more realistic accretion model we chose 24 of them with their edges situated at $r_{\rm in} = 5M$ and $r_{\rm out} = 12M$ and ran a simulation within 2-D HARM code in the Kerr spacetime with $a = 0.9375M$. We observed that whereas in the early stage of the simulation the processes in the disks demonstrate clear dependence on the initial parameters this dependence becomes practically undetectable for the later stages in our simulations. In our paper (Witzany & Jefremov 2018) we conjectured that the reason for this result might be the non-linear mode of the MRI in which the disks enter at these late times. Having chosen the polytropic equation of state for the perfect fluid in the tori we obtained restrictions on their parameters and computed mass and temperature which were consistent with the assumptions made about the polytropic parameters and the test character of the perfect fluid configurations.

In our work we have investigated one of the simplest forms of the functional dependence $\ell = \ell(\Omega)$ and obtained the known Polish Doughnuts and Fishbone-Moncrief tori as its special cases. As a future work one can undertake an investigation of other physically relevant setups with the help of our ansatz and use all the 8 degrees of freedom that its most general form allows to model them.

The study of circular motion in the NUT spacetime based on our work (Jefremov & Perlick 2016) was centered on finding the characteristic imprints of the Manko-Ruiz constant C and gravitomagnetic charge n on it. It was shown that just like for the geodetic motion the Manko-Ruiz constant does not give any observable predictions for perfect fluid tori and allows one to conjecture that it cannot be determined by any local experiment at all. The possibility to prove this rigorously should be investigated. The influence of the gravitomagnetic charge on the circular motion is however very remark-

able. The geodetic circular orbits no longer lie in the equatorial instead being elevated by an angle θ given by (23). The same is true for the Polish Doughnuts that we considered in this space-time. Following the scheme developed for the tori with general ansatz for $\ell = \ell(\Omega)$ we obtained mass and temperature of the Polish Doughnuts here.

An attempt to run a HARM accretion simulation in the NUT spacetime faced with obstacles that possibly will not be resolved until the – physical – nature of the NUT conical singularity is understood.

The last Chapter of the present work reproduced our results (Jefremov et al. 2015, Tsupko et al. 2016) on the motion of spinning particles in the Kerr spacetime focusing on its possible applications to accretion. We obtained analytical expressions for linear in spin corrections to the circular orbits and the last stable ones. For the case of the ISCO in the extreme Kerr black hole I presented our exact in spin solution according to which its radius does not change remaining at $r_{\rm ms} = M$. For a simple thin-disk accretion model we obtained the advance in energetic efficiency suggesting that such disks might produce luminosities different from the non-spinning ones. It is however unclear to which extent one can trust pole-dipole approximation and which of its predictions are physical. Further study should address these issues as well as answer the question on relevance of spin parameter in any accretion model.

Appendix

General form of the function $\ell(\Omega)$

The expression (53) is the simplest non-trivial form for the functional dependence $\ell = \ell(\Omega)$ that allows one to find new solutions for the perfect fluid tori apart from the known ones. If instead we demand only the possibility to get the velocity field in a closed form, i. e. only that the equation (51) be solvable analytically, then we should choose the order of the equation to be $n \leq 4$, so the most general form for the dependence $\ell(\Omega)$ will be

$$\ell(\Omega) = \frac{\mathcal{P}^{(3)}(\Omega)}{\tilde{\mathcal{P}}^{(3)}(\Omega)}. \tag{100}$$

Another thing that needs to be justified is our choice of ℓ and Ω with which we describe the flows. This question arises because it is possible via different combinations of u^ϕ, u^t, u_ϕ, u_t to construct different pairs of variables that might be more suitable, i. e. allow to have more degrees of freedom. In particular we can write the Euler equation in terms of ℓ^* and Ω as:

$$\frac{\partial_\mu p}{\rho h} = \partial_\mu(\ln u^t) - \ell^* \partial_\mu \Omega. \tag{101}$$

In this Appendix we shall derive the result (100) more strictly as well as justify the usage of (ℓ, Ω) variables for description of all the solutions that are potentially obtainable with the considerations developed in the Chapter 4. Mathematically equation (51) describes a surface in (ℓ, Ω) space possessing 4 parameters composed out of metric coefficients. Performing a transformation $(\ell, \Omega) \rightarrow (\mathcal{F}(\ell, \Omega), \mathcal{G}(\ell, \Omega))$ we want to find the lowest-order form of the equation for this surface in order to obtain the maximal possible number of analytical solutions. The most general form of a 4-parameter surface is given as

$$\sum_{i=1}^{n=4} c_i \mathcal{F}^{p_i} \mathcal{G}^{q_i} = 0, \tag{102}$$

with $p_i, q_i \in \mathbb{N} \cup \{0\}$, $\max\{p_i + q_i\} \leq 4$ and $(p_i, q_i) \neq (p_j, q_j)$. In order to minimise the order of the equation the values of p_i and q_i should be chosen as small as possible. Having assumed a von Zeipel flow and postulated the rational-function connection between $\mathcal{F}$ and $\mathcal{G}$

$$\mathcal{G}(\mathcal{F}) = \frac{\mathcal{P}^{(k)}(\mathcal{F})}{\tilde{\mathcal{P}}^{(l)}(\mathcal{F})} \tag{103}$$

we want to find the pairs (p_i, q_i) that allow for maximal values of polynomial powers k and l.

Without restriction of generality we can assume that

$$q_1 = \max q_i \neq 0. \tag{104}$$

Then, after substituting (103) into (102) we can write conditions on powers of the resulting terms:

$$\begin{cases} p_1 + kq_1 \leq 4, \\ p_2 + kq_2 + l(q_1 - q_2) \leq 4, \\ p_3 + kq_3 + l(q_1 - q_3) \leq 4, \\ p_4 + kq_4 + l(q_1 - q_4) \leq 4. \end{cases} \tag{105}$$

The first inequality gives us

$$k \leq \frac{4 - p_1}{q_1}; \tag{106}$$

to maximise k we assume $p_1 = 0, q_1 = 1$. The following 3 inequalities of the system along with (104) will give us further restrictions on k and l and the values of the rest of the p_i and q_i. The resulting pairs (p_i, q_i) are $(0, 1)$, $(1, 0)$, $(1, 1)$, $(0, 0)$ with

$$k \leq 3 \quad \text{and} \quad l \leq 3. \tag{107}$$

With this the form of (102) becomes

$$c_1\mathcal{G} + c_2\mathcal{F} + c_3\mathcal{F}\mathcal{G} + c_4 = 0, \tag{108}$$

and its most general solution

$$\mathcal{G}(\mathcal{F}) = \frac{\mathcal{P}^{(3)}(\mathcal{F})}{\tilde{\mathcal{P}}^{(3)}(\mathcal{F})}. \tag{109}$$

which are precisely those of the equation (51) and (100). This means that all transformations that preserve the lowest-order form of (102) are those that transform (51) to (108). Assuming that these transformations are rational functions of Ω and ℓ it is possible to show that they should all be of the form

$$\begin{aligned} \mathcal{F} &= \frac{k_1 + k_2\ell}{k_3 + k_4\ell}, \\ \mathcal{G} &= \frac{k_5 + k_6\Omega}{k_7 + k_8\Omega}, \end{aligned} \tag{110}$$

where k_i are some real numbers, i. e. there is one-to-one correspondence $\mathcal{F} \leftrightarrow \ell$ and $\mathcal{G} \leftrightarrow \Omega$ and we can apply the above developed considerations concerning relations between ℓ and Ω to (51) without losing any solutions that would arise for $\mathcal{F}$ and $\mathcal{G}$ from (110).

If we do not restrict ourselves to the lowest-order equation and perform transformations of variables of general type: $(\ell, \Omega) \to (\mathcal{F}(\ell, \Omega), \mathcal{G}(\ell, \Omega))$, we can also get analytical solutions for the angular velocity field in closed form for some of them, however, the number of free parameters in the expression $\mathcal{G} = \mathcal{G}(\mathcal{F})$ will decrease. So, for instance, for the transformation:

$$\mathcal{F} = \Omega, \qquad \mathcal{G} = \frac{\ell}{1 - \ell\Omega} = \ell^*, \tag{111}$$

that corresponds to the choice of variables leading to the form (101) of the Euler equation, we obtain the equation

$$(\Omega^2 \ell^* + \Omega) g^{tt} + \ell^* g^{\phi\phi} - (2\Omega\ell^* + 1) g^{t\phi} = 0, \tag{112}$$

that will have an analytical solution if

$$\ell^* = \frac{\mathcal{P}^{(2)}(\Omega)}{\tilde{\mathcal{P}}^{(3)}(\Omega)}. \tag{113}$$

The question that needs to be answered in this respect is whether there are some additional solutions in these new variables that are not included in the ansatz (100) within some combination of its parameters. Out of all possible coordinate transformations only rational ones are those that lead to equations with natural powers of the form

$$\sum_{i=1}^{n_i=4} \sum_{j=1}^{n_j=4} c_{ij} \mathcal{F}^{p_i} \mathcal{G}^{q_j} = 0. \tag{114}$$

To that one should of course also add the restrictions on the powers of the variables in order that (114) be solvable: for any pair of numbers (i, j) in it the condition must hold that

$$p_i + q_j \leq 4. \tag{115}$$

It is possible to show that under these conditions all the functions $\mathcal{G} = \mathcal{G}(\mathcal{F})$ for which (114) is solvable are isomorphic to some functions of the form

(52). This result could have been anticipated because otherwise, if we did gain some new solutions that would be out of scope of (51) with (114), it would be possible through some transformation $(\ell, \Omega) \to (\mathcal{F}(\ell, \Omega), \mathcal{G}(\ell, \Omega))$ to obtain general solutions for equations with powers $n > 4$ in Ω that we would get after we would transform the equation (114) with $\mathcal{G} = \mathcal{G}(\mathcal{F})$ dependence substituted in it back to the old variables $(\ell(\Omega), \Omega)$.

The morale of this Appendix: for all practical reasons one should abide by the equation (51) with its maximal-parameter solution in the form (100).

References

Abbott, B., Abbott, R., Adhikari, R., Ananyeva, A., Anderson, S., Appert, S., Arai, K., Araya, M., Barayoga, J., Barish, B. et al. (2017), 'Multi-messenger observations of a binary neutron star merger', *Astrophysical Journal Letters* **848**(2), L12.

Abbott, B. P., Abbott, R., Abbott, T., Abernathy, M., Acernese, F., Ackley, K., Adams, C., Adams, T., Addesso, P., Adhikari, R. et al. (2016), 'Observation of gravitational waves from a binary black hole merger', *Physical review letters* **116**(6), 061102.

Abdujabbarov, A., Atamurotov, F., Kucukakca, Y., Ahmedov, B. & Camci, U. (2013), 'Shadow of Kerr-Taub-NUT black hole', *Astrophysics and Space Science* **344**(2), 429–435.

Abramowicz, M. A. (1971), 'The relativistic von Zeipel's theorem', *Acta Astron.* **21**, 81–85.

Abramowicz, M. A., Calvani, M. & Nobili, L. (1980), 'Thick accretion disks with super-Eddington luminosities', *The Astrophysical Journal* **242**, 772–788.

Abramowicz, M. A., Calvani, M. & Nobili, L. (1983), 'Runaway instability in accretion disks orbiting black holes', *Nature* **302**(5909), 597.

Abramowicz, M. A. & Prasanna, A. (1990), 'Centrifugal force reversal near a Schwarzschild black-hole', *Monthly Notices of the Royal Astronomical Society* **245**, 720.

Abramowicz, M., Jaroszyński, M. & Sikora, M. (1978), 'Relativistic, accreting disks', *Astronomy & Astrophysics* **63**, 221–224.

Abramowicz, M. & Piran, T. (1980), 'On collimation of relativistic jets from quasars', *The Astrophysical Journal* **241**, L7–L11.

Bañados, E., Venemans, B. P., Mazzucchelli, C., Farina, E. P., Walter, F., Wang, F., Decarli, R., Stern, D., Fan, X., Davies, F. B. et al. (2018), 'An 800-million-solar-mass black hole in a significantly neutral Universe at a redshift of 7.5', *Nature* **553**(7689), 473.

Bardeen, J. M., Press, W. H. & Teukolsky, S. A. (1972), 'Rotating black holes: locally nonrotating frames, energy extraction, and scalar synchrotron radiation', *The Astrophysical Journal* **178**, 347–370.

Bini, D. & Damour, T. (2014), 'Two-body gravitational spin-orbit interaction at linear order in the mass ratio', *Physical Review D* **90**(2), 024039.

Bisnovatyi-Kogan, G. & Ruzmaikin, A. (1974), 'The accretion of matter by a collapsing star in the presence of a magnetic field', *Astrophysics and Space Science* **28**(1), 45–59.

Bisnovatyi-Kogan, G. S. (2010), 'Relativistskaya astrofizika i fizicheskaya kosmologiya. (Rus.: Relativistic astrophysics and physical cosmology)'.

Bisnovatyi-Kogan, G. & Syunyaev, R. (1972), 'Galaxy Nuclei and Quasars as Infrared Emission Sources', *Soviet Astronomy* **15**, 697.

Bondi, H. (1952), 'On spherically symmetrical accretion', *Monthly Notices of the Royal Astronomical Society* **112**(2), 195–204.

Bondi, H. & Hoyle, F. (1944), 'On the mechanism of accretion by stars', *Monthly Notices of the Royal Astronomical Society* **104**(5), 273–282.

Bonnor, W. B. (1969), 'A new interpretation of the NUT metric in general relativity', *Math. Proc. Cambr. Philos. Soc.* **66**, 145–151.

Bradley, M., Fodor, G., Gergely, L., Marklund, M. & Perjés, Z. (1999), 'Rotating perfect fluid sources of the NUT metric', *Class. Quantum Grav.* **16**, 1667–1675.

Cebeci, H., Özdemir, N. & Şentorun, S. (2016), 'Motion of the charged test particles in Kerr-Newman-Taub-NUT spacetime and analytical solutions', *Physical Review D* **93**(10), 104031.

Chakrabarti, S. K. (1985), 'The natural angular momentum distribution in the study of thick disks around black holes', *The Astrophysical Journal* **288**, 1–6.

Chandrasekhar, S. (1983), *The mathematical theory of black holes*, The International series of monographs on physics 69, 1st edn, Clarendon Press; Oxford University Press.

Clément, G., Gal'tsov, D. & Guenouche, M. (2015), 'Rehabilitating space-times with NUTs', *Physics Letters B* **750**, 591–594.

Clément, G., Gal'tsov, D. & Guenouche, M. (2016), 'NUT wormholes', *Physical Review D* **93**(2), 024048.

Corinaldesi, E. & Papapetrou, A. (1951), 'Spinning test-particles in general relativity. II', *Proc. R. Soc. Lond. A* **209**(1097), 259–268.

Daigne, F. & Mochkovitch, R. (1997), 'Gamma-ray bursts and the runaway instability of thick discs around black holes', *Monthly Notices of the Royal Astronomical Society* **285**(3), L15–L19.

De Villiers, J.-P., Hawley, J. F. & Krolik, J. H. (2003), 'Magnetically driven accretion flows in the Kerr metric. I. Models and overall structure', *The Astrophysical Journal* **599**(2), 1238.

Dixon, W. G. (1970), 'Dynamics of extended bodies in general relativity. I. Momentum and angular momentum', *Proc. R. Soc. Lond. A* **314**(1519), 499–527.

Dixon, W. G. (1974), 'Dynamics of extended bodies in general relativity III. Equations of motion', *Phil. Trans. R. Soc. Lond. A* **277**(1264), 59–119.

Favata, M. (2011), 'Conservative self-force correction to the innermost stable circular orbit: Comparison with multiple post-Newtonian-based methods', *Physical Review D* **83**(2), 024027.

Finkelstein, D. (1958), 'Past-future asymmetry of the gravitational field of a point particle', *Physical Review* **110**(4), 965.

Fishbone, L. G. & Moncrief, V. (1976), 'Relativistic fluid disks in orbit around Kerr black holes', *ApJ* **207**, 962–976.

Font, J. A. & Daigne, F. (2002), 'The runaway instability of thick discs around black holes – I. The constant angular momentum case', *Mon. Not. R. Astron. Soc.* **334**, 383–400.

Font, J. A. & Daigne, F. (2004), 'The runaway instability of thick discs around black holes – II. Non-constant angular momentum discs', *Mon. Not. R. Astron. Soc.* **349**, 841.

Gammie, C. F. (2004), 'The magnetorotational instability in the Kerr metric', *ApJ* **614**(1), 309.

Gammie, C. F., McKinney, J. C. & Tóth, G. (2003), 'HARM: a numerical scheme for general relativistic magnetohydrodynamics', *ApJ* **589**(1), 444.

Gimeno-Soler, S. & Font, J. A. (2017), 'Magnetised Polish doughnuts revisited', *Astronomy & Astrophysics* **607**, A68.

Grenzebach, A., Perlick, V. & Lämmerzahl, C. (2014), 'Photon regions and shadows of Kerr–Newman–NUT black holes with a cosmological constant', *Phys. Rev. D* **89**, 124004.

Griffiths, J. B. & Podolský, J. (2009), *Exact Space-Times in Einstein's General Relativity*, Cambridge UP.

Hackmann, E. & Lämmerzahl, C. (2012), 'Observables for bound orbital motion in axially symmetric space-times', *Phys. Rev. D* **85**, 044049.

Hartle, J. B. (2003), *Gravity: an introduction to Einstein's General Relativity*, illustrated edition edn, Benjamin Cummings.

Hawking, S. W. (1974), 'Black hole explosions?', *Nature* **248**(5443), 30.

Igumenshchev, I. V., Chen, X. & Abramowicz, M. A. (1996), 'Accretion discs around black holes: two-dimensional, advection-cooled flows', *Monthly Notices of the Royal Astronomical Society* **278**(1), 236–250.
URL: *http://dx.doi.org/10.1093/mnras/278.1.236*

Jaroszyński, M., Abramowicz, M. A. & Paczyński, B. (1980), 'Supercritical accretion disks around black holes', *Acta Astron.* **30**, 1–34.

Jefremov, P. I. (2016), 'Circular motion and Polish Doughnuts in NUT spacetime', *Proceedings of the International Astronomical Union* **12**(S324), 353–354.

Jefremov, P. I., Bisnovatyi-Kogan, G. S. & Tsupko, O. Y. (2017), Spin-induced changes in the parameters of ISCO in Kerr spacetime, *in* 'Proceedings of the 14th Marcel Grossman (MG14) Meeting on General Relativity, University of Rome "La Sapienza", Italy, 12 – 18 July 2015', pp. 3715–3721.

Jefremov, P. I. & Perlick, V. (2016), 'Circular motion in NUT space-time', *Classical and Quantum Gravity* **33**(24), 245014.

Jefremov, P. I. & Perlick, V. (2018), 'Corrigendum: Circular motion in NUT space-time (2016 Class. Quantum Grav. 33 245014)', *Classical and Quantum Gravity* .
URL: *http://iopscience.iop.org/article/10.1088/1361-6382/aad1f9/meta*

Jefremov, P. I., Tsupko, O. Y. & Bisnovatyi-Kogan, G. S. (2015), 'Innermost stable circular orbits of spinning test particles in Schwarzschild and Kerr space-times', *Physical Review D* **91**(12), 124030.

Kagramanova, V., Kunz, J., Hackmann, E. & Lämmerzahl, C. (2010), 'Analytic treatment of complete and incomplete geodesics in Taub-NUT space-times', *Phys. Rev. D* **81**, 124044.

Kerr, R. P. (1963), 'Gravitational field of a spinning mass as an example of algebraically special metrics', *Physical review letters* **11**(5), 237.

Komissarov, S. (2006), 'Magnetized tori around Kerr black holes: analytic solutions with a toroidal magnetic field', *Monthly Notices of the Royal Astronomical Society* **368**(3), 993–1000.

Kovář, J., Slanỳ, P., Cremaschini, C., Stuchlík, Z., Karas, V. & Trova, A. (2016), 'Charged perfect fluid tori in strong central gravitational and dipolar magnetic fields', *Physical Review D* **93**(12), 124055.

Kozłowski, M., Jaroszyński, M. & Abramowicz, M. A. (1978), 'The analytic theory of fluid disks orbiting the Kerr black hole', *Astron. Astrophys.* **63**, 209–220.

Kucáková, H., Slanỳ, P. & Stuchlík, Z. (2011), 'Toroidal configurations of perfect fluid in the Reissner-Nordström-(anti-) de Sitter spacetimes', *Journal of Cosmology and Astroparticle Physics* **2011**(01), 033.

Kyrian, K. & Semerák, O. (2007), 'Spinning test particles in a Kerr field–II', *Monthly Notices of the Royal Astronomical Society* **382**(4), 1922–1932.

Lukács, B., Newman, E., Sparling, G. & Winicour, J. (1983), 'A NUT-like solution with fluid matter', *General Relativity and Gravitation* **15**(6), 567–579.

Lynden-Bell, D. & Nouri-Zonoz, M. (1998), 'Classical monopoles: Newton, NUT space, gravomagnetic lensing, and atomic spectra', *Reviews of Modern Physics* **70**(2), 427.

Manko, V. S. & Ruiz, E. (2005), 'Physical interpretation of the NUT family of solutions', *Class. Quantum Grav.* **22**, 3555–3560.

Mathisson, M. (1937), 'Neue Mechanik materieller Systeme', *Acta Phys. Polon.* **6**, 163–2900.

McGuire, P. & Ruffini, R. (1975), 'Metric of two spinning charged sources endowed with the Newman-Tamburino-Unti parameter', *Phys. Rev. D* **12**, 3026–3029.

McKinney, J. C. & Gammie, C. F. (2004), 'A measurement of the electromagnetic luminosity of a Kerr black hole', *ApJ* **611**(2), 977.

McKinney, J. C., Tchekhovskoy, A., Sadowski, A. & Narayan, R. (2014), 'Three-dimensional general relativistic radiation magnetohydrodynamical simulation of super-Eddington accretion, using a new code harmrad with M1 closure', *Monthly Notices of the Royal Astronomical Society* **441**(4), 3177–3208.

Meliani, Z., Vincent, F., Grandclément, P., Gourgoulhon, E., Monceau-Baroux, R. & Straub, O. (2015), 'Circular geodesics and thick tori around rotating boson stars', *Classical and Quantum Gravity* **32**(23), 235022.

Mewes, V., Font, J. A., Galeazzi, F., Montero, P. J. & Stergioulas, N. (2016), 'Numerical relativity simulations of thick accretion disks around tilted Kerr black holes', *Phys. Rev. D* **93**(6), 064055.

Michel, F. C. (1972), 'Accretion of matter by condensed objects', *Astrophysics and Space Science* **15**(1), 153–160.

Misner, C. (1963), 'The flatter regions of Newman, Unti, and Tamburino's generalized Schwarzschild space', *J. Math. Phys* **4**, 924–937.

Misner, C., Thorne, K. & Wheeler, J. (1973), *Gravitation*, WH Freeman and Company, San Francisco.

Montero, P. J., Font, J. A. & Shibata, M. (2010), 'Influence of self-gravity on the runaway instability of black-hole–torus systems', *Phys. Rev. Lett.* **104**(19), 191101.

Morozova, V. S., Ahmedov, B. & Kagramanova, V. (2008), 'General relativistic effects of gravitomagnetic charge on pulsar magnetospheres and particle acceleration in the polar cap', *The Astrophysical Journal* **684**(2), 1359.

Nagataki, S. (2009), 'Development of a general relativistic magnetohydrodynamic code and its application to the central engine of long gamma-ray bursts', *The Astrophysical Journal* **704**(2), 937.

Newman, E. T., Tamburino, L. & Unti, T. W. J. (1963), 'Empty-space generalization of the Schwarzschild metric', *J. Math. Phys* **4**, 915–923.

Noble, S. C., Gammie, C. F., McKinney, J. C. & Del Zanna, L. (2006), 'Primitive variable solvers for conservative general relativistic magnetohydrodynamics', *ApJ* **641**(1), 626.

Nouri-Zonoz, M. & Lynden-Bell, D. (1997), 'Gravomagnetic lensing by NUT space', *Mon. Not. Roy. Soc* **292**, 714–722.

Novikov, I. D. & Thorne, K. S. (1973), 'Astrophysics of black holes', *Black holes* pp. 343–450.

Okada, R., Fukue, J. & Matsumoto, R. (1989), 'A model of astrophysical tori with magnetic fields', *Publications of the Astronomical Society of Japan* **41**, 133–140.

Paczynski, B. (1980), 'A model of a thick disk with a surface accretion layer', *Acta Astronomica* **30**, 347–363.

Paczynski, B. & Abramowicz, M. (1982), 'A model of a thick disk with equatorial accretion', *The Astrophysical Journal* **253**, 897–907.

Paczynsky, B. & Wiita, P. J. (1980), 'Thick accretion disks and supercritical luminosities', *Astronomy and Astrophysics* **88**, 23–31.

Page, D. N. & Thorne, K. S. (1974), 'Disk-accretion onto a black hole. I. Time-averaged structure of accretion disk', *The Astrophysical Journal* **191**, 499–506.

Papaloizou, J. & Pringle, J. (1984), 'The dynamical stability of differentially rotating discs with constant specific angular momentum', *Monthly Notices of the Royal Astronomical Society* **208**(4), 721–750.

Papapetrou, A. (1951), 'Spinning test-particles in general relativity. I', *Proc. R. Soc. Lond. A* **209**(1097), 248–258.

Qian, L., Abramowicz, M. A., Fragile, P. C., Horák, J., Machida, M. & Straub, O. (2009), 'The Polish doughnuts revisited-I. The angular momentum distribution and equipressure surfaces', *Astronomy & Astrophysics* **498**(2), 471–477.

Rezzolla, L., Baiotti, L., Giacomazzo, B., Link, D. & Font, J. A. (2010), 'Accurate evolutions of unequal-mass neutron-star binaries: properties of the torus and short GRB engines', *Classical and Quantum Gravity* **27**(11), 114105.

Rezzolla, L. & Zanotti, O. (2013), *Relativistic Hydrodynamics*, Oxford University Press.

Saijo, M., Maeda, K.-i., Shibata, M. & Mino, Y. (1998), 'Gravitational waves from a spinning particle plunging into a Kerr black hole', *Physical Review D* **58**(6), 064005.

Salpeter, E. (1964), 'Accretion of interstellar matter by massive objects.', *The Astrophysical Journal* **140**, 796–800.

Schroven, K., Trova, A., Hackmann, E. & Lämmerzahl, C. (2018), 'Charged fluid structures around a rotating compact object with a magnetic dipole field', *arXiv preprint arXiv:1804.11286* .

Schwarzschild, K. (1916), Über das Gravitationsfeld eines Massenpunktes nach der Einsteinschen Theorie, *in* 'Sitzungsberichte der Königlich Preußischen Akademie der Wissenschaften zu Berlin, Phys.-Math. Klasse, 189-196 (1916)'.

Seguin, F. H. (1975), 'The stability of nonuniform rotation in relativistic stars', *The Astrophysical Journal* **197**, 745–765.

Semerák, O. (1998), 'Circular orbits in stationary axisymmetric spacetimes', *Gen. Rel. Gravit.* **30**(8), 1203–1215.

Shakura, N. I. & Sunyaev, R. A. (1973), 'Black holes in binary systems. Observational appearance.', *Astronomy and Astrophysics* **24**, 337–355.

Shvartsman, V. (1971), 'Halos around "Black Holes"', *Soviet Astronomy* **15**, 377.

Sikora, M. (1981), 'Superluminous accretion discs', *Monthly Notices of the Royal Astronomical Society* **196**(2), 257–268.

Slanỳ, P. & Stuchlík, Z. (2005), 'Relativistic thick discs in the Kerr–de Sitter backgrounds', *Classical and Quantum Gravity* **22**(17), 3623.

Steinhoff, J. (2011), 'Canonical formulation of spin in general relativity', *Annalen der Physik* **523**(4), 296–353.

Steinhoff, J. & Puetzfeld, D. (2010), 'Multipolar equations of motion for extended test bodies in general relativity', *Physical Review D* **81**(4), 044019.

Stuchlík, Z., Slanỳ, P. & Kovář, J. (2009), 'Pseudo-Newtonian and general relativistic barotropic tori in Schwarzschild–de Sitter spacetimes', *Classical and Quantum Gravity* **26**(21), 215013.

Tanaka, T., Mino, Y., Sasaki, M. & Shibata, M. (1996), 'Gravitational waves from a spinning particle in circular orbits around a rotating black hole', *Physical Review D* **54**(6), 3762.

Taub, A. H. (1951), 'Empty space-times admitting a three parameter group of motions', *Ann. Math.* **53**, 472–490.

Taylor, E. F. & Wheeler, J. A. (2000), *Exploring black holes*, Vol. 98, Addison Wesley Longman San Francisco, CA.

Thorne, K. S. (1974), 'Disk-accretion onto a black hole. II. Evolution of the hole', *The Astrophysical Journal* **191**, 507–520.

Trova, A., Schroven, K., Hackmann, E., Karas, V., Kovár, J. & Slany, P. (2018), 'Equilibrium configurations of charged fluid around Kerr black hole', *arXiv preprint arXiv:1803.02262* .

Tsupko, O. Y., Bisnovatyi-Kogan, G. S. & Jefremov, P. I. (2016), 'Parameters of innermost stable circular orbits of spinning test particles: Numerical and analytical calculations', *Gravitation and Cosmology* **22**(2), 138–147.

Tulczyjew, W. (1959), 'Motion of multipole particles in general relativity theory', *Acta Phys. Pol.* **18**, 393.

Vaidya, P., Patel, L. & Bhatt, P. (1976), 'A Kerr-NUT metric', *General Relativity and Gravitation* **7**(9), 701–708.

Wald, R. M. (1984), *General relativity*, University of Chicago Press.

Witzany, V. & Jefremov, P. (2018), 'New closed analytical solutions for geometrically thick fluid tori around black holes', *Astronomy & Astrophysics* **614**, A75.

Zimmerman, R. L. & Shahir, B. Y. (1989), 'Geodesics for the NUT metric and gravitational monopoles', *General relativity and gravitation* **21**(8), 821–848.

Zurek, W. H. & Benz, W. (1986), 'Redistribution of angular momentum by nonaxisymmetric instabilities in a thick accretion disk', *The astrophysical journal* **308**, 123–133.